DE-NOISING OF MEDICAL IMAGES USING IMAGE FUSION

A THESIS SUBMITTED TO
THE GRADUATE SCHOOL OF NATURAL AND APPLIED SCIENCES
OF
ATILIM UNIVERSITY

BY

OMER SUBHI SIDDIK SIDDIK

IN PARTIAL FULFILLMENT OF THE REQUIREMENTS
FOR
THE DEGREE OF DOCTOR OF PHILOSOPHY
IN
DEPARTMENT OF SOFTWARE ENGINEERING

May, 2020

Approval of the Graduate School of Natural and Applied Sciences, Atilim University.

Prof. Dr. Ali KARA
Director

I certify that this thesis satisfies all the requirements as a thesis for the degree of **Doctor of Philosophy in Department of Software Engineering, Atilim University.**

Prof. Dr. Ali YAZICI
Head of Department

This is to certify that we have read the thesis DE-NOISING OF MEDICAL IMAGES USING IMAGE FUSION submitted by OMER SUBHI SIDDIK SIDDIK and that in our opinion it is fully adequate, in scope and quality, as a thesis for the degree of Doctor of Philosophy.

Asst. Prof. Dr. Erhan GÖKÇAY
Supervisor

Examining Committee Members:

Asst. Prof. Dr. Erhan GÖKÇAY
Department of Software Engineering, Atilim University

Asst. Prof. Dr. Ziya KARAKAYA
Department of Computer Engineering, Atilim University

Asst. Prof. Dr. Çiğdem TURHAN
Department of Software Engineering, Atilim University

Assoc. Prof. Dr. Kasim OZTOPRAK
Department of Computer Engineering, KTO Karatay University

Asst. Prof. Dr. Emre SÜMER
Department of Computer Engineering, Başkent University

Date: 15/05/2020

I hereby declare that all information in this document has been obtained and presented in accordance with academic rules and ethical conduct. I also declare that, as required by these rules and conduct, I have fully cited and referenced all material and results that are not original to this work.

Name, Last Name: Omer Subhi Siddik SIDDIK

Signature:

ABSTRACT

DE-NOISING OF MEDICAL IMAGES USING IMAGE FUSION

SIDDIK, Omer Subhi Siddik

PHD, Department of Software Engineering

Supervisor: Asst. Prof. Dr. Erhan Gökçay

May 2020, 91 pages

Multi-sensor data fusion becomes control to which an ever-increasing number of general conventional answers for a few application cases that requested. Image Fusion is not unlike a system of delivering the main quality image from many accessible images. The most important method is the high-pass filtering method. Later methods are based on Dual-Tree Complex DWT (DTCWT), uniform rational filter bank, and pyramidal techniques. This thesis focuses on image fusion based on Gaussian and Poisson noise removal techniques in cephalometric X-ray images. The digital image applications during the transmission and gathering of the image are tainted from the unbound communication directs and shortcomings in equipment. The different sensors detect the image get damaged with the noise because of unsecured transmission. The resultant images from the denoising procedures will be merged with each other to obtain a resultant image of high-quality resolution. The procedures of merging two or more images to obtain one single image are described as image fusion. The various image fusion algorithm sand (Gaussian and Poisson) noise filter in this thesis were survived. The methodology and results section in chapter four consists of twenty-one methods. The first thirteen methods present the image enhancement methods that have related to our thesis and these methods are used in the steps of our proposed denoising procedure. These methods are presented as follows: The first eight methods were presented the image de-noising using thresholding and Shrinkage methods, then two methods of filters in image filtering, finally three methods of fusing methods. The last

eight methods are consisting of several stages, and each stage of these stages was produced from the best pre-tested method results.

This thesis presents multi-sensor transform based fusion techniques, namely the Dual-Tree Complex Discrete Wavelet Transform and other transforms that are proposed as different models that utilized to the resultant of 400 cephalometric X-ray images. The signal is decomposed into its different frequency sub-bands using the Dual-Tree Complex wavelet transform. The Bilateral filtering method is used to remove the noise of the low approximation sub-bands of both images followed by Bivariate Shrinkage wavelet thresholding being utilized on the high-frequency sub-bands. The de-noised sub-bands are fused using the wavelet transform fusion rule. Trial results show that these fusion algorithms create a high-quality image contrasted with a high-quality de-noised image.

Keywords: Image De-noising, Wavelet Transform, Discrete Wavelet Transform, Dual Tree Complex Wavelet Transform, Thresholding, Wavelet Shrinkage, Image Fusion, Weiner Filter, Bilateral filter.

ÖZET

GÖRÜNTÜ FÜZYONU KULLANARAK TIBBİ GÖRÜNTÜLERDEN GÜRÜLTÜ ARINDIRMA

SIDDIK, Omer Subhi Siddik
Doktora Programı, Yazılım Mühendisliği Bölümü
Danışman: Dr. Öğr. Gör. Erhan Gökçay

Mayıs 2020, 91 sayfa

Görüntü füzyonu birçok erişilebilir görüntüden birinci kalite görüntü alma sistemidir. En önemli yöntem yüksek geçirim filtreleme yöntemidir. Daha sonraki yöntemler Dual-Tree Complex DWT (DTCWT), tek-tip rasyonel filtre bankası ve piramit teknikleri üzerine kuruludur. Bu tez çalışması, sefalometrik röntgen görüntülerinde Gaussian ve Poisson gürültü arındırma yöntemleri üzerinden görüntü birleştirme konusunu ele almaktadır. Görüntünün iletilmesi ve toplanması esnasında hedefsiz haberleşme ve ekipman yetersizliği gibi nedenlerden ötürü dijital görüntü uygulamaları hata vermektedir. Korumasız iletim nedeni ile zarar görmüş görüntüler farklı sensörler aracılığı ile tespit edilir. Gürültü arındırma işlemi sonrasında elde edilen görüntüler, yüksek kalite çözünürlüğe sahip tek bir görüntü elde etmek için birbirleri ile birleştirilirler. Tek bir nihai görüntü elde etmek için iki veya daha fazla görüntünün birleştirilmesi işlemine görüntü füzyonu denilir. Bu tezde farklı görüntü füzyon algoritmaları ve (Gaussian ve Poisson) gürültü filtreleri kullanıldı. 4. bölümde yer alan metodoloji ve sonuç kısmı yirmi bir yöntemden oluşmaktadır. Bu yöntemlerden ilk on üç tanesi bu tez çalışması ile alakalı olan görüntü güçlendirme yöntemlerini içermektedir ve yine bu yöntemler tarafımızca önerilen gürültü arındırma işleminde kullanılmıştır. Bu yöntemler şu şekilde sunulmuştur: Görüntü gürültü arındırma işlemimde ilk sekiz yöntem eşikleme ve küçültme yöntemleri kullanılarak sunulmuş, sonrasında iki adet filtre yöntemi görüntü filtreleme de sunulmuş ve son olarak da üç yöntem füzyon yöntemlerinde kullanılmıştır. Son sekiz yöntem çok sayıda

aşamadan oluşmaktadır ve bu aşamaların her biri önceden test edilmiş olan en iyi sonuçlar ele alınarak gerçekleştirilmiştir. Bu tez çalışmasında, "Dual-Tree Complex Discrete Wavelet Transform" olarak adlandırılan çok sensörlü dönüşüm bazlı füzyon teknolojileri ile birlikte elde edilen 400 sefalometrik röntgen görüntülerini kullanan farklı yöntemler kullanılmıştır. Sinyal, "Dual-Tree Complex Discrete Wavelet Transform" kullanılarak farklı frekans alt bantlarına ayrıştırılmıştır. Düşük frekanslı alt bantlardan gürültüyü arındırmak için iki yanlı filtreleme yöntemi kullanılmış, yüksek frekanslı alt bantlar için ise "Bivariate Shrinkage" dalgacık eşiklemesi kullanılmıştır. Gürültüden arındırılmış alt bantlar, dalgacık dönüşüm füzyon kuralı esas alınarak birleştirilmiştir. Test sonuçları bu birleştirme algoritmalarının yüksek kaliteli bir görüntü ortaya çıkardığını göstermektedir.

Anahtar Kelimeler: Görüntü Gürültü Arındırma, Dalgacık Dönüşümü, Kesikli Dalgacık Dönüşümü, Dual Tree Complex Dalgacık Dönüşümü, Eşikleme, Dalgacık Küçülmesi, Görüntü Füzyonu, Weiner Filtre, İki Yanlı Filtre.

ACKNOWLEDGEMENTS

I would like to take this opportunity to express my most sincere gratitude to my supervisor Asst. Prof. Dr. Erhan GÖKÇAY, for all his help, guidance, and suggestions through the development of this study.

I would like to express my special thanks to my fiancé and my family for their continuous encouragement, understanding, and moral support.

TABLE OF CONTENTS

LIST OF TABELS

TABELS

LIST OF FIGURES

FIGURES

LIST OF ABBREVIATION

DWT	Discrete Wavelet Transform
SWT	Stationary Wavelet Transform
CWT	Complex Wavelet Transform
DTCWT	Dual-Tree Complex Wavelet Transform
PSNR	Peak Signal to Noise Ratio
NIH	National Institutes of Health
SNR	Signal to Noise Ratio
TMJ	Temporomandibular Joint and Muscle Disorders
CCD	Charge Coupled Device
AWGN	Additive White Gaussian Noise
BF	Bilateral Filter
FFT	Fast Fourier Transform
RC	Raised Cosine
NLM	Non-Local Means
SURE	Stein's Unbiased Risk Estimate
MAP	Maximum A Posteriori
PC	Personal Computer
IHS	Intensity Hue Saturation Strategy
HPF	High-Pass Filtering Strategy
PCA	Principal Component Analysis
HRMIs	Human Resource Management System

GUI	Graphical User Interface
PAN	Panchromatic
MS	Multi Spectral
AWA	Adaptive Weight Algorithm
aDWT	advanced Discrete Wavelet Transform
RMS	Root Mean Square
IR	Infrared
SFM	Structure From Motion

CHAPTER 1

INTRODUCTION

Digital images can perform important tasks in everyday life applications, such as geological data frameworks and astronomy. Informational indexes gathered by image sensors are commonly debated by various sorts of noise [1]. Various sources of noise may sully a digital image. It is relative to the presentation time and exceptionally reliant on the sensor temperature. The Poisson dispersion and Shot noise have the same attributes in view of the fact of the quantum vulnerability in photoelectron generation. The general noise qualities in a picture rely upon numerous elements which incorporate sensor types, pixel measurements, temperature, exposure time and ISO speed [2]. Moreover, defective instruments, issues with the information obtaining process, and interrupting common phenomena can completely corrupt the information of intrigue. Additionally, noise may be added through delivery errors and compression [1].

Noise is an additionally channelled subject. Ordinarily, DE mosaicking is utilized to add lost colour elements, thereby implying that the noise will not usually be white. The digital image, when obtaining noise, contains the low-frequency just as high-frequency elements. The greater part of the original images is accepted to have added substance random noise, which is displayed as a Gaussian type. Speckle noise [3] is recognized in ultrasound images, while Rician noise [4] involves MRI images. In this manner, de-noising is frequently an important and initial step to be analysed before the image information is separated. It is important to implement an effective de-noising method to compensate for any information degradation [1]. The objective of de-noising is to remove the commotion while protecting significant image elements however enough could be expected. Linear filtering methods, for example, for this reason, the Wiener filter and match filter utilized for several years. In any case, linear filters may present several issues, such as blurring sharp edges, the destruction of lines and other accurate image features, dropping efficiently to eliminate big-tailed noise. This calls for options, such as nonlinear filtering. Numerous works concerning a signal with noise, there are a few contrasts in the coefficients of the original signal and noise

on account of various characteristics [5], [6]. Basically, if an orthogonal transform with high-energy compaction and de-correlation features is utilized, the greater part of the vitality of the initial signal will be composed within a couple of high extent coefficients [7], [8]. In the event that the image data is damaged by additive white noise, elements that compare to commotion will be dispersed among low greatness high-frequency segments. The greater part of the coefficients of the noise is of lower amplitudes. Therefore, it is sensible to reduce the noise by distinguishing every coefficient and threshold and removing those coefficients with something lower than the threshold values [9], [10].

1.1 Introduction to the Cephalometric X-ray Image

In the previous two decades, the field of dental innovation has developed by a wide margin, making the determination of trauma and the pinpointing of formative concerns substantially more precise than at any other time. One apparatus that can be utilized to aid these undertakings is called Cephalometric Analysis, or a Ceph. Cephalometric Analysis is an X-ray like panoramic X-ray such that it has the capacity of capturing a full perspective of the skull and neck. A distinction is that it is captured utilizing a side-to-side clearing movement rather than the full 360-degree constant movement utilized by panoramic X-rays when complete [11]. The Cleveland Clinic explains that a Cephalometric X-ray image differs from the standard dental X-ray because it is taken extra orally (outside of the mouth) and covers far larger field of view, including the whole side of the head. This kind of image shows the connections the teeth, jaw and profile, which is particularly effective for orthodontists while preparing realignment operations. A Cephalometric X-ray image may not show the kind of detail of the teeth seen on an image taken with film placed inside the mouth, but it is ideal for overall viewing. According to the NIH, while an intraoral (inside the mouth) dental X-ray requires a film or digital sensor to be placed in the mouth, a Cephalometric X-ray image does not require any biting pieces. The process requires only that the technician position the patient properly in front of the imaging equipment. As with all X-rays, the imaging procedure is very quick and painless [12]. Is the Ceph required? All things considered, maybe. It relies upon the types of issues an oral health care professional would be attempting to investigate. It becomes a genuinely standard manner to have in any event a Ceph or all-encompassing X-ray did when orthodontic work. Stunned

outputs in such efforts may likewise be finished relying upon need. Similarly, on the off chance that you play physical games and assume a fault, you may get help by a Ceph. In the event a specialist rather than dental specialist is seen, a scan of the head to analyse any discomfort may be necessary. Cephalometric X-ray image noise that emerges from high-quality lateral skull X-rays is essential for cephalometric X-rays. However, dental X-rays, in general, suffer from random photon noise due to fluctuations in the number of photons recorded by the receptor [13]. Moreover, the signal in a Cephalogram radiograph is disturbed due to noise related to the complexity of the region and different sources of X-rays may cause different disturbances in the X-rays, including:

a. Film-based systems suffering from quantum noise dependent on the film graininess.

b. Additional noise in storage phosphor screens being added due to conversions from light to electron to light; and

c. Lower KV values being used in direct radiography decreasing the SNR.

1.2 What are Ceph X-rays used for?

Ceph X-rays are commonly used to analyse formative matters including the head, neck, and jaw that a dental specialist, orthodontist, or specialist believes might be prevented with received facial and oral progress.

They are usually utilized for:

a. Searching for potential TMJ (Temporomandibular Joint and Muscle Disorders) issues.

b. Determining the causes of extreme tooth misalignment – unusually in situations where an overbite or under bite is available.

c. The diagnosis of suspicious teeth or potential jaw cracks.

d. Capturing exact estimation of teeth including their root structures; and

e. Preparing for orthodontic work.

Cephalometric studies are especially valuable in recognizing the complexities of overbites and under bites on the grounds that the situation or underdevelopment of the jaw allows an important function in these worries. Orthodontists find them to be invaluable in the planning of orthodontic procedures since they have to assess the progress of the teeth, and occasionally the jaw for up to several years. A full image of the Ceph allows them to measure the benefit of an operation and the adjustment of the

body to treatment. Similarly, to different sorts of X-ray devices, Cephalometric can be proceeded as either advanced or film examinations relying upon accessibility inside a dental specialist's office or your decision [14].

1.3 Noise Models

The conceptual origins of noise in digital images emerge during image transmission or through image acquisition. The main point that determines the measure of noise in a medical image is the acquisition of an image with a Charge Coupled Device (CCD) recording visual images, sensor intensity, and amounts of light. Medical images are damaged through delivery from origin to target. The basic purpose is the noise that is overlapping in the path through transmission [15], performing the type of noisy image via:

$$N_r(i,j) = I(i,j) + N(i,j)$$

where $I(i,j)$ is the initial image pixel value, $N(i,j)$ the noise in the image and $N_r(i,j)$ the noise-producing image. The entirety of the introduced technique is given as a flowchart in Figure 1.1.

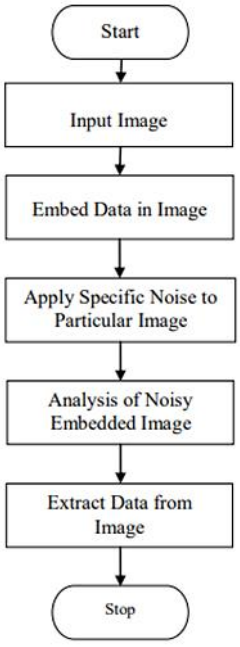

Figure 1.1 Proposed scheme flowchart

Noise is the unwanted impacts created in an image. Through image delivery or procurement, many variables are efficient for presenting noise in an image. Contingent upon the sort of concern, noise can likewise influence the image to an alternate degree.

Various noise types which bring about corrupting image features of the particular methodology are explained as follows.

1.3.1 Poisson Noise

X-ray imaging noise is modelled with Poisson noise [16]. X-ray photons occur on a receptor surface in an arbitrary example and they cannot be forced to be equally distributed over the receptor surface. Individual regions of the receptor surface may gather a larger group of photons than other regions, also already every one of the spots is presented to corresponding average X-Ray intensity. By utilising gamma ray or X-ray photons, the majority of the image noise that is created by the random passage of the photons that are circulated inside the image is identified as quantum noise. The execution of X-ray radiation creates the quantum noise [17]. Poisson noise expulsion methods are somewhat noise created from the nonlinear reaction of identifiers with the Poisson configuration. Image information relies on the location and recording of irregular electron radiation in a circuit or the photon in an optical pattern with Poisson dispersion and the average value is determined. As in the Poisson allocation, the mean is equivalent to the difference and the signal containing the information is totally subject to the regular deviation. Thus, whenever the standard deviation is higher, more noise is added to the signal [18]. The possibility of appropriation of a Poisson random variable X describing the number of achievements occurring in a given time period or in a predetermined part of the period is given as:

$$f(X) = \frac{e^{-\lambda} \times \lambda^{x}}{X!} \tag{1}$$

where X is the specific number of successes, e equals 2.171828, l is the mean number of successes in the given time interval or region and $X!$ is the factorial of X [19]. The sample of decline due to Poisson noise is:

$$u(i,j) = \frac{1}{\lambda}\, Poisson(\lambda \times t(i,j)) \tag{2}$$

where $t(i,j)$ and $u(i,j)$ are the original and noised images, respectively. The contention of the Poisson function is identified with the mean of the Poisson distribution in which the restoration value describes a Poisson random production function dependent on Poisson function amounts. Because the level of degradation depends on the measures of recognized photons, weak photons imply shorter [19]. A few filters are reasonable for Poisson noise reduction. A few obtain visual observation

and others receive appropriate noise concealment or a smoothing capacity. Well-known noise removal filters are shown here, and their related conditions are presented.

1.3.2 Additive White Gaussian Noise (AWGN) Model

Through transmission, a few kinds of noises, for the most part, corrupt the quality of the therapeutic images [20]. White noise is a significant kind of noise which happens in the connection structure. In the communication structure, it is frequently expected that the noise is a stationary Additive White Gaussian Noise (AWGN) including power phantom frequency to such an extent that.

$$G_n(f) = \frac{N_0}{2} \tag{3}$$

where $G_n(f)$ is the spectral density and N_0 the noise frequency according to the possible theory noise can generally be displayed as Gaussian. AWGN is random mathematical noise out of sight of a correspondence channel. The reason for concealing the patient data into the medical image is to data transmission analysis of the patient starting with one centre then onto the next through open systems. Because of transmission within the channel, channel commotion may merge with the inserted image which could impact the Probability Gray Level Salt and Pepper Noise 161 exactness of the restoration of information at the target end [21]. With regard to the impact of channel noise, AWGN noise is created and gathered into the inserted image.

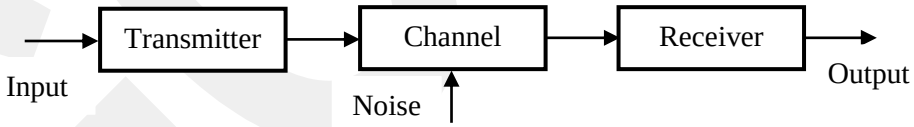

Figure 1.2 Communication channel (AWGN)

1.4 Objectives of the Work

It is the way toward joining important data from at least two images into one image where the subsequent image will be more useful than any of the info image. The subsequent image must be progressively appropriate for visibility, recognition and machine observation or PC preparation. The objective of image fusion is to decrease the vulnerability and limit excess in output just as increasing the important data to implementation or the task [22]. The path to image fusion extends in determining one solid and viable fusion strategy to decide the fusion coefficient [23]. Nowadays, with quick progress in technology, it is presently conceivable to acquire data from multi-

sources of images to create a part of high-quality data from many images. Because of the constrained depth-of-focus of optical focal points in-camera tools, it is generally unrealistic to obtain an image that includes every applicable element. Other than arrangements utilizing specific optics [24], [25] and computational imaging [26], [27] the best approach to handle this issue is multi-focus image fusion, which is defined as a part of image fusion that combines the content of various images against various centre situations in a similar scene into a composite image that contains every element in the centre. The goal of multi-focus image fusion is to deliver an image that includes every single significant element in the centre by separating and manufacturing the engaged objects of the source images.

The fundamental concept in this thesis is fusion and de-noising of high-quality images that are Poisson and Gaussian noise-damaged due to unsafe connections, electromagnetic intervention and implement errors. Image fusion is a significant approach to tackle this issue and it delivers a singular image that processes all important data from a variety of sensors. Including the advancement of various imaging sensors, numerous imaging approaches can be simultaneously envisioned by different sensors. However, there are numerous situations where no sensor can give a total image. There are a few advantages of multi-sensor image fusion, including more extensive spatial and transient inclusion, broadened scope of activity, diminished vulnerability, improved dependability quality, and expanded strength performance execution. Image fusion methods are generally utilised because of capacity and transmission specifications for large numbers of image sets.

1.5 Problem Statement

Until now, numerous multi-sensor image fusion techniques have been created. The simplest fusion technique is to calculate the median of the source image of every pixel but the known strategy is drive unwanted impacts, such as the decrease in the difference of the fused images [28]. In general, the technique for multi-sensor image fusion was ordered to the spatial and transform domains [29]. The strategy for multi-sensor fused image that results in a high-accuracy intertwined image is normally confused and high expending in time, that is of indispensable significance to combination quality. In this thesis, we construct certain methods of multi-sensor image

fusion that are easy and not in any way tedious, which results in a high-quality fused image.

The thesis is structured as follows:

Chapter 2 presents wavelet transforms and filters followed in the second section by image fusion methods. Chapter 3 presents the related work. Chapter 4 presents the different filtering algorithms and image fusion algorithm in addition to experimental results. Finally, Chapter 5 reports the conclusion.

CHAPTER 2

BACKGROUND

2.1 Stationary Wavelet Transform (SWT)

The SWT implies a precisely moved invariant transform, while the DWT, as critically experimented, is not a shift-invariant discrete transform. However, the DT-CWT is around moving invariant also gives directional examination. The wavelets were first demonstrated to be the establishment of an incredible new way to deal with signal processing and an examination known as a multi-resolution theory. They perform by dampening the down-sampling venture of the destroyed method and rather up sampling the channels by embedding zeros into the channel coefficients [30], [31]. In the annihilated algorithm, the channels are utilised first in the rows and afterward in the columns. For this situation, in spite of the fact that the four images created (one estimate and three detailed images) are at a large portion of the goals of the initially, they are a similar size to the initial image. The estimation images from the intact algorithm are subsequently spoken to as levels in a parallelepiped, with the spatial goals becoming coarser with a more significant level and the size continuing as before. Basically, the inverse transform includes the same procedures as the forward transform. In the demolished case, this implies up-examining the approximation and detailed images and applying re-creation filters, which are inverses of the decay scaling and wavelet filters, initially by rows and afterward by columns. For instance, initially, the sections of the Vertical Detail image will be up-sampled and the inverse scaling filter will be applied and at that point, the columns will be up-tested and the inverse wavelet filter will be utilised. The initial image is reproduced by applying the inverse transform to every deconstructed level successively, beginning with the standards on the roughest goals until the initial goals are attained. Rebuilding in the un-decimated issue is equivalent unless that alternatively up-sampling the image, the filters are down-sampled rather than every implementation of the inverse filters. Shift-invariance is essential to analyse and fused the wavelet coefficient images. Instead of shift-invariance, a slight shift in the initial signal in order to submit the types in the wavelet coefficients that may introduce curios in the reduplicate image. Shift variance

is realised by the demolition strategy. Moreover, it can be settled by applying the un-crushed strategy, as seen in Figure 2.1. In any case, the other issue with discrete wavelet transforms is the selective poor direction, which means poor display of highlights with directions which are not horizontal or vertical, being a consequence of independent filtering [32].

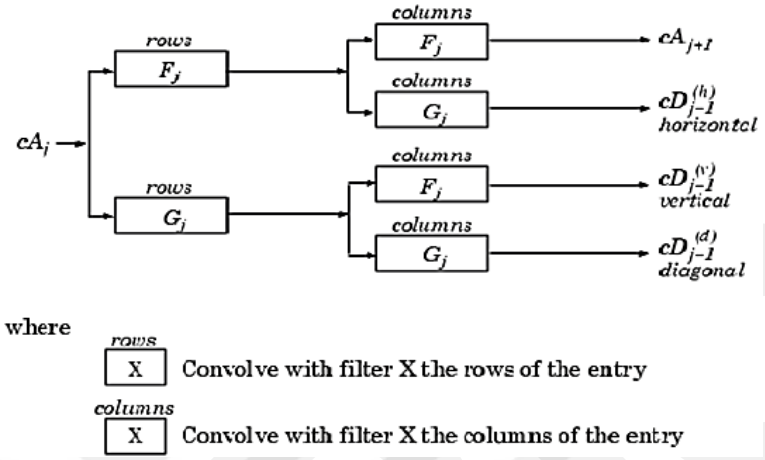

Figure 2.1 Two-dimensional Stationary Wavelet Transform

2.2 Discrete Wavelet Transform (DWT)

Wavelet transforms provide a structure wherein a sign is deteriorated, with every level comparing to more inferior goals. Two principles are gatherings of transforms, continuous and discrete. Discrete transforms remain more usually utilized and can be partitioned into different categories. Despite the survey of the writing providing several strategies for wavelet changes, most can be categorised into one of three classifications: decimated, un-decimated, and non-separated. A continuous wavelet transform is implemented by satisfying an internal item in the signal and wavelet functions. The expansion and interpretation factors are components of the real line [33]. For a certain purpose, dilation a and translation b, the wavelet coefficient $W_f(a,b)$ for a signal f can be computed as:

$$W_f(a,b) = \langle f, \psi_{a,b} \rangle = \int f(x)\psi_{a,b}(x)dx \tag{4}$$

Wavelet coefficients deliver to the data received in a signal at the relating expansion and interpretation. The first signal is produced by implementing the opposite transform:

$$f(x) = \frac{1}{C_w}\int_{-\infty}^{\infty}\int_{-\infty}^{\infty} W_f(a,b)\psi_{a,b}(x)db\frac{da}{a^2} \tag{5}$$

C_ψ is the standardization factor of the source wavelet. Despite the fact that the continuous wavelet transform is easy to depict numerically, the signal and the wavelet function are both more likely than not to be closed structures, making it complicated or unfeasible to apply. The discrete wavelet is applied rather [32].

To simplify the topic further, it will be accepted that the expansion and interpretation factors are selected to have dyadic testing. However, the ideas can be expanded further out to different selections of variables. At particular scale J, to obtain a limited number of scaling and wavelet coefficients, a limited quantity of explanations is utilised in implementing multi-resolution separation. The signal can be executed to as far as these coefficients as:

$$f(x) = \sum_k C_{Jk}\phi_{Jk}(x) + \sum_{j=1}^{J}\sum_k d_{jk}\,\psi_{jk}(x) \quad (6)$$

Where C_{Jk} represent the scaling coefficients and d_{Jk} the wavelet coefficients. The first part in Equation (6) confers the lower solution approximation of the signal and the next phrase confers the detailed data in decisions of the original to the next decision J. The procedure of stratifying the DWT can appear as a group of filters, as shown in Figure 2.2. In the condition of a two-dimensional image, a first-level DWT enables the acquisition of 4 various frequency bands that are low-low, low-high, high-low and high-high sub-bands including an N level decomposition which is produced in 3N+1 in various frequency bands. At every level of decomposition, the image is divided into high-frequency and low-frequency parts. The low-frequency parts for reaching the desired resolution may be additionally decayed [34].

At the point when different degrees of decomposition are utilised, the procedure implies multi-resolution decomposition. Practically speaking, when wavelet decomposition is utilised for image fusion, a single degree of decomposition may be suitable; however, this relies on the proportion of the spatial goals of the images which are fused [35].

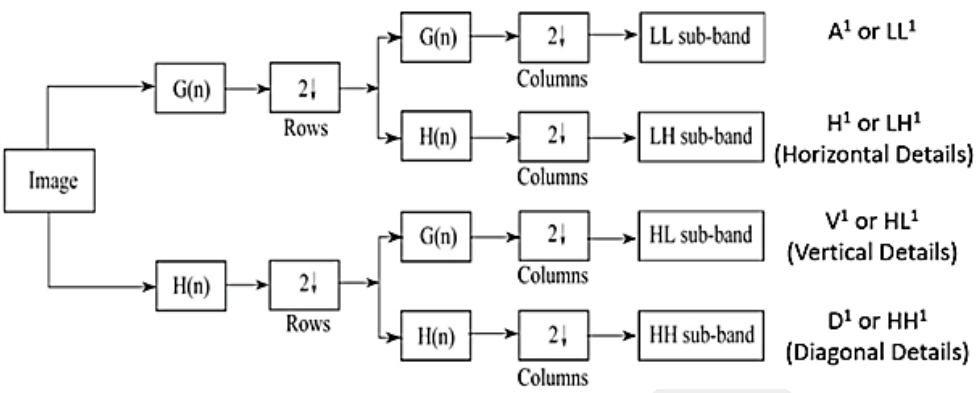

Figure 2.2 Two-dimensional Discrete Wavelet Transform

The ordinary DWT is used to benefit either a decimated or an un-decimated method. In the event that the 2-dimensional image down-sampling is executed by remaining in one out of each row and column, obtaining the transformed image one-fourth of the initial size and half of the initial resolution. Decimals can be calculated, subsequently, be performed visible like a pyramid. Spatial resolution becomes rough as the image size decreases. The decimated calculation is not shift-invariant, which implies that it is sensitive to shifts in the input image. The devastation procedure likewise negatively affects the linear progression of spatial highlights that do not have a horizontal or vertical direction. These two elements will in general present ancient rarities when the calculation is utilised in applications, such as image de-noising [36].

2.3 Dual Tree Complex Wavelet Transform

The Dual-Tree Wavelet Transform (DTWT) overcomes the impediments of DWT as worse directionality and move invariance. It can be utilised to actualise 2D wavelet transforms that are frequently particular concerning direction from the separable 2D DWT. For instance, the 2D DTWT transform obtains six sub-bands at any scale, every one of which is unequivocally situated at unmistakable points. The 2D DTWT transform, specifically, has two variants which are the Dual-Tree Discrete Wavelet Transform (DTDWT) which is 2-expansive times, and the Dual-Tree Complex Wavelet Transform (DTCWT) which is 4-expansive times [35].

2.3.1 Dual-Tree Discrete Wavelet Transform

The DWT of an image is executed utilising two basically sampled separable DWTs in parallel. Here, for every pair of sub-bands, the summation and variance are processed.

The six wavelets accompanying the DTDWT are clarified in Figure 2.3 as grayscale images. We consider that every one of the six wavelets are situated in a particular direction. At variance with the critically-sampled separable DWT, all of the wavelets become liberated from the checkerboard article. Every sub-band of the 2-D dual-tree transform coincides with a particular direction [37].

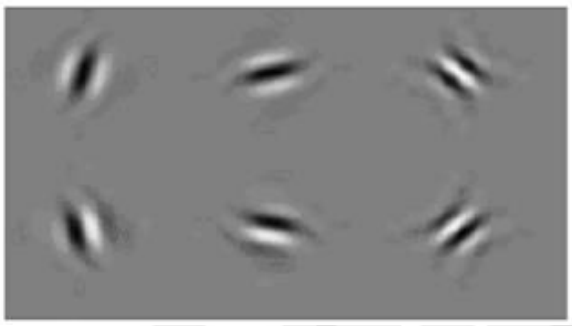

Figure 2.3 Directionality of DTDWT

2.3.2 Dual Tree Complex Wavelet Transform

The DTCWT additionally offers to increase the wavelets in 6 particular directions and 2 wavelets in every direction. Toward every direction, the wavelets are divided into two sections, the first of which will be explained as the real section of a complex-valued wavelet, and the second wavelet as the imaginary section of a complex-valued wavelet. Since the complex model has twice the same number of wavelets as the real model of the transform, the complex model is 4-times expansive [38]. The DTCWT transform is executed as 4 fundamentally sampled separable DWTs working in parallel. In spite of this, various filter combinations are utilised over the rows and columns. As in the real situation, the total and difference of sub-band images are computed to obtain the situated wavelets. The twelve wavelets related to the real 2D Dual-Tree DWT are outlined in Figure 2.4 as grayscale images [39]. The wavelets are arranged in the same six directions as those of the DTDWT. In any case, there are two in every direction. In the event that the six wavelets showing on the main row are explicated as the real part of complex wavelets, at that point, the six wavelets showing on the subsequent row can be explicated as the complex part of the complex wavelets [35].

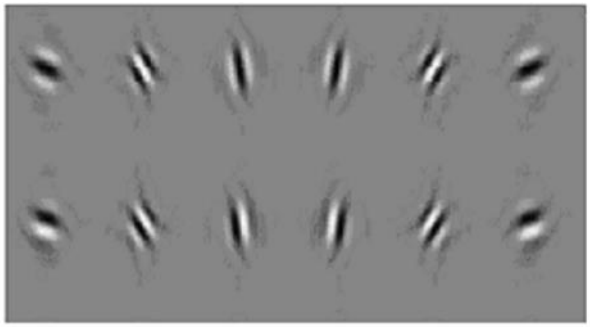

Figure 2.4 Directionality of DTCWT

The filter bank framework of the DTCWT has CWT filters that have complex coefficients and produce complex result samples, as shown in Figure 2.4, in which every block is a complex filter and contains down-sampling by 2 (not shown) in its results. Since the resulting sampling rates are unaltered from the DWT, every example includes a real and imaginary part; a repetition of 2:1 is presented [40]. The complex filters may be planned to such an extent that the sizes of their move reactions differ gradually with input shift just the stages modify rapidly. The real part is odd while the imaginary part is even [41].

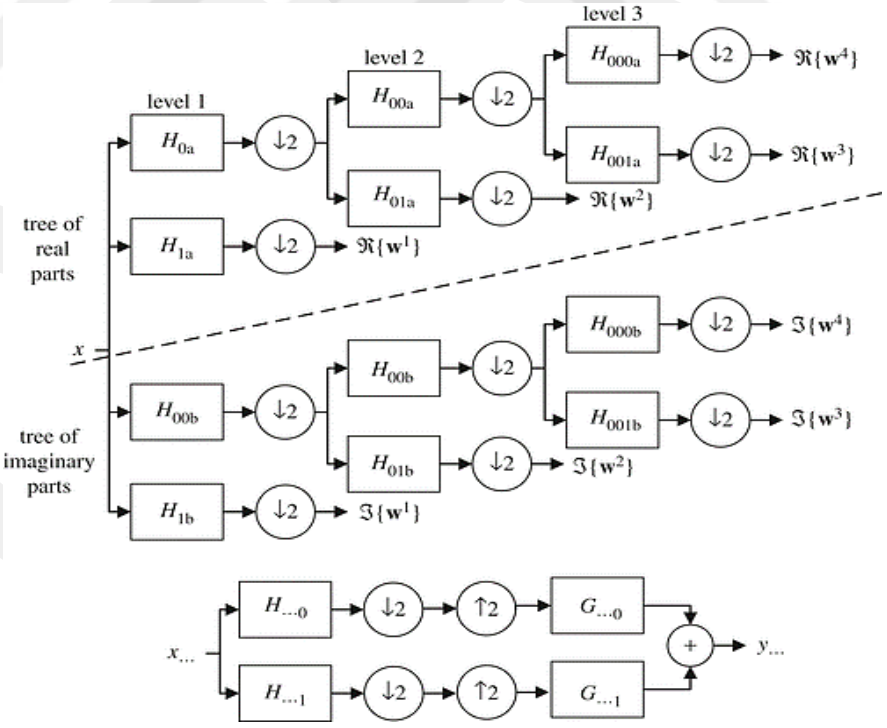

Figure 2.5 3 levels of the Complex Wavelet Tree for a real one-dimensional input signal *x*

The augmentation of complex wavelets to 2-D is accomplished by separable filtering over rows and afterward over columns. However, if the row and column filter both the curbed negative frequencies, at that point only the primary quadrant of the 2-D signal spectrum is kept [42]. The almost mathematically effective approach to obtain the sets of combined filters is to maintain separate imaginary factors, j1 and j2, for the row and column processing, as shown in Figure 2.6. This provides four-element complex vectors which are present as (r, j_1, j_2, j_1j_2) where r is the real part [43]. Complex filters in multiple dimensions give true directional selectivity in spite of being executed as being separable, in light of the fact that they are as yet able to divide all pieces of the *m*-D recurrence space. For example, a two-dimensional DTCWT generates six band pass sub-images of complex coefficients at every level that are strongly directed at angles of ±15°, ±45° and ±75°, represented with the double-headed arrows in Figure 2.4 The DTCWT comprises 2 wavelet transforms performing in parallel on an information signal, as shown in Figure 2.6. We indicate the wavelet related to the initial wavelet filter bank as ψ(t) and the wavelet related to the next filter bank as ψ'(t) [42]. The wavelet ψ(t) is determined by:

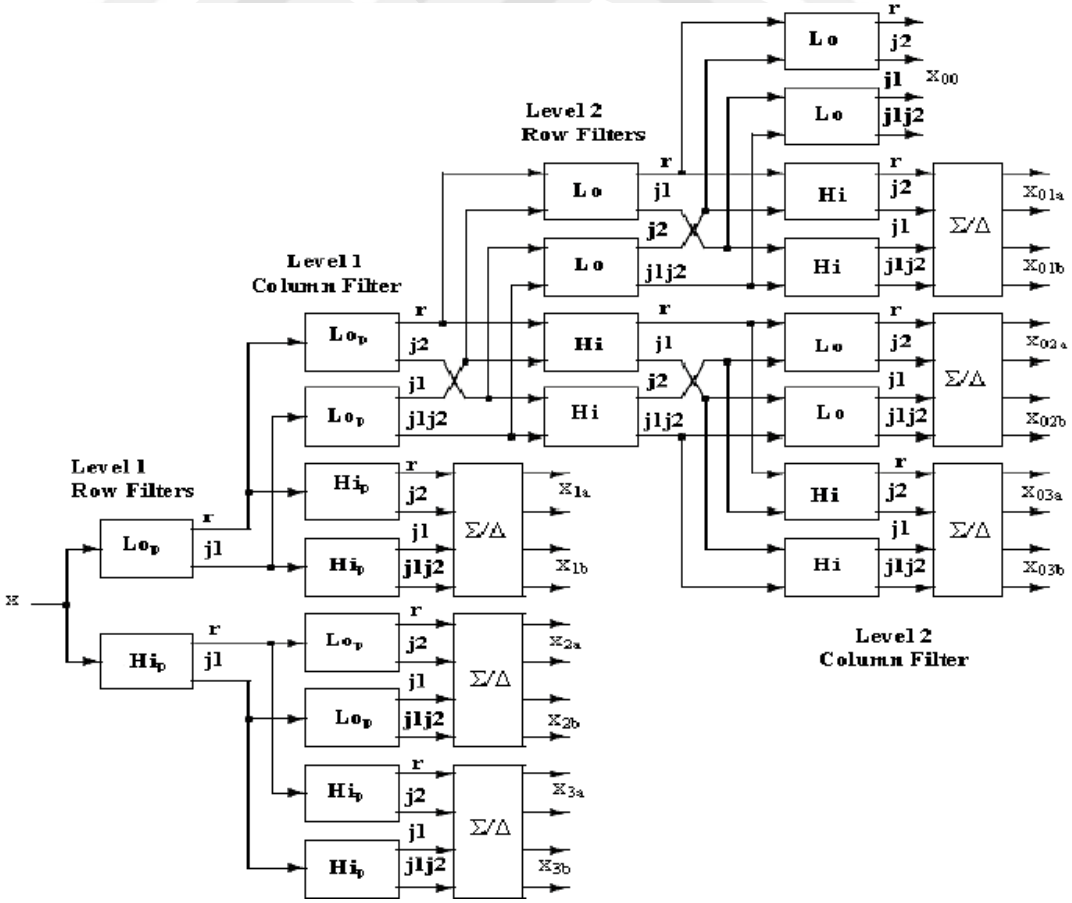

Figure 2.6 2-levels of the Complex Wavelet tree for a real two-dimensional input image *x* presenting six directional bands

$$\psi(t) = \sqrt{2}\sum_n h_1(n)\phi(2t-n) \quad (7)$$

$$\phi(t) = \sqrt{2}\sum_n h_0(n)\psi(2t-n) \quad (8)$$

The second wavelet, $\psi(t)$, is determined likewise in terms of $\{h_0(n), h_1(n)\}$. To obtain a typical DT-CWT, the second wavelet, $\psi(t)$, becomes the Hilbert transform of the first wavelet, $\psi(t)$:

$$\psi'(t) = H\{\psi(t)\} \quad (9)$$

If the low-pass filter $h_0'(n)$ is equivalent to the half-sample delayed version of $h_0(n)$, then the wavelets produced by the DTCWT are achieved as desired. In the event that wavelets $\psi(t)$ and $\psi'(t)$ are orthogonal to an integer change, the later Hilbert relationship is achieved in the condition:

$$H_0'(e^{jw}) = e^{-j0.5w}H_0(e^{jw}) for |w| < \pi \quad (10)$$

For the basis of orthonormal wavelet, the low- and high-pass filters are described essentially as [44]:

$$F_1(e^{jw}) = -e^{-jdw}H_0'(e^{j(w-\pi)}) \quad (11)$$

Equivalently, $h_1(n) = (-1)\, nh_0(d-n)$, where d is an odd integer. For that reason, it results from that during the typical DT-CWT:

$$H_1'(e^{jw}) = -j\, sgn(w)e^{j0.5w}H_1(e^{jw}) for |w| < \pi \quad (12)$$

2.4 Bilateral Filtering

Bilateral filtering smooths images and maintains edges utilising a non-linear collection of nearby image contents. The process is not iterative, local, and simple. It merges grey levels or colours in view of both their geometric closeness, their photometric similarity and favours close to qualities inaccessible to qualities in both their geometric closeness, domain, and range. Filtering is a primary process of the analysis and manipulation of a digitised image, especially in order to improve its quality and computer vision. In the broadest definition of the expression "filtering," the estimation of the filtered image in a specific area is a function of the estimations of the initial image in a small neighbourhood of a similar area. Specifically, Gaussian low-pass

filtering calculates the weighted average of pixel values in the area, while the distance from the neighbourhood leads to decreasing the weights. However, formal and quantitative explanations of weight decreases can be provided [45].

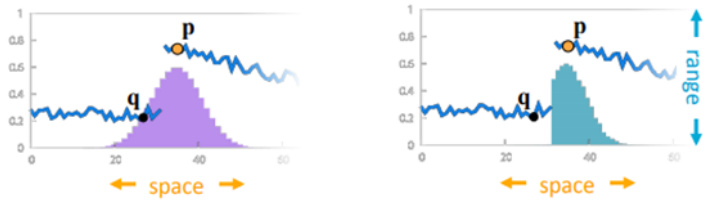

Gaussian blur *Bilateral filter*

Figure 2.7 Gaussian blur and bilateral filter

$$I_p^b = \frac{1}{W_p^b} \sum_{q \in S} G_{\sigma_s}(||p - q||)\, G_{\sigma_r}(|I_p - I_q|)\, I_q \quad (13)$$

The parameter σ_s determining the spatial size is utilised to filter pixels, and σ_r checks that the adjoining pixel is down-weighted due to the intensity variation.

W_p^b normalizes the summation of the weights.

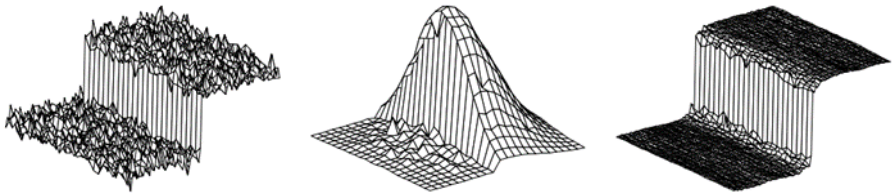

Figure 2.8 Bilateral Filter on a Height Field

Bilateral filters, furthermore, can work on the three groups at one time and can determine which hues are comparable and which are not. Only perceptually comparative colours are then averaged with each other, and the article rarities referenced above disappear. Two pixels can be near each other, that is, including the close spatial location, or they can resemble each other, that is, have close values, potentially in a perceptually significant manner. Closeness implies the region in the area, similarly to the region in the domain. The range filters are non-linear in light of the fact that their weights are based on the image intensity or colour. Mathematically, they are not any more complicated than typical non-separable filters. In particular, they save the edges. The spatial locality is until now a basic notion. Subsequently, we merge the range and domain filtering and show that the merging is more interesting. We refer

to a merged filtering as bilateral filtering. Specifically, bilateral filters can be obtained from colour images simply as they are stratified to black-and-white ones [46]. Therefore, in the event that we utilise this measurement in our bilateral filter, images are smoothed, and edges are saved in a path that is set to human performance. Only perceptually comparative colours are averaged with each other, and only perceptually visible edges are protected.

The Bilateral filtering process is distinct from the suffocation of Gaussian noise. Tomasi and Manduchi [47] suggested that the bilateral filter that leads the Variable intensity shift is dependent on the weighted mean through a local neighbourhood. Elad [48] confirmed that the bilateral filter is a single Jacobian iteration to reduce the least squares. Barash et al. [49] have determined the connection between anisotropic distribution, mean shift strategy, and bilateral filtering [50]. To examine the execution of the bilateral filter, Park et al. [51] extracted a closed-form comparison of bilateral filtering for flat regions and showed that the connection between noise decreases and filtering values. The disadvantage of this filter is that the non-linearity of the bilateral filter denies the use of FFT acceleration-based that makes the usage computationally intensive. Numerous arrangements have been suggested to accelerate bilateral filtering. Porikli [52] suggested a consistent time usage of the bilateral filter (for self-assertive spatial kernels) utilising polynomial range kernels. Durand and Dorsey [53] suggested a piecewise-straight estimate of the bilateral filter obtained by suitable subsampling in the intensity domain [54]. Recently, Chaudhury et al. [55] expanded Porikli's function [52] and suggested a raised-cosine (RC) approach to the Gaussian range part. The RC kernel approximates the Gaussian range part all the more precisely for a similar number of terms than the polynomial approximation [52]. In writing, speculations of the bilateral filter have additionally been created. Buades et al. [56] proposed non-local means (NLM), an expansion of the bilateral filter, with the theory of locality reaching out to the entire image.

Gao et al. [57] extracted an arranged filter by merging the NLM filter and the mean-shift technique. Liu et al. [58] suggested decomposing an image as the summation of geometric structure and wavering style. They utilised the diffusion equation to re-establish the structure part and an NLM filter to de-noise the wavering part of some of the images. Dolui et al. [59] presented a factual structure to determine an all-

inclusive similitude measure, which can be utilised to give the ideal execution of the NLM filter regardless of the noise facts and figures.

Takeda et al. [60] summarised the kernel regression technique and demonstrated that bilateral filtering is a unique case acquired by utilising particular kernel weights and the zeroth-order Taylor series approach. A multi-resolution de-noising procedure utilising transform-domain and spatial-domain de-noising methods together was suggested and tested by Zhang and Günturk [61]. The noisy image was reconstructed utilising DWT and transform the noisy wavelet coefficients in the detail sub-bands are thresholded utilising BayesShrink [62]. The estimated band submitted to BF and filter parameters were elected experimentally as a work of noise variation. Bilateral filtering was likewise offered on the rebuild output at every level of the DWT.

2.5 Wavelet Thresholding

It has been seen that in numerous signals vitality is, for the most part, gathered in a few measurements and the coefficients of these dimensions are generally very large in contrast to different dimensions or to some other signal (particularly noise) that has its vitality spread over innumerable coefficients. Thus, in wavelet thresholding, every coefficient is a thresholder (alcoholic to zero) by contrasting versus a threshold with removed noise, while safeguarding the significant data of the original signal [63]. Generally, two sorts of thresholding methods are utilised:

a. Hard threshold: This thresholding factor is described in Equation (14):

$$D(U,\lambda) = \begin{cases} U, & for\ all\ |U| > \lambda \\ 0, & otherwise \end{cases} \tag{14}$$

Hard thresholding is a “keep or kill” process and is more intuitively obvious. The given transfer function is shown in Figure 2.9.

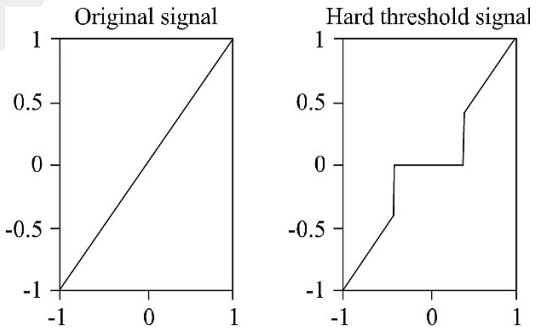

Figure 2.9 Hard Thresholding

b. Soft threshold: This thresholding factor is described in Equation (15):

$$D(U,\lambda) = \begin{cases} (|U-\lambda|, & for\ all\ |U| > \lambda \\ 0, & otherwise \end{cases} \quad (15)$$

The soft threshold shrinks the coefficients on the threshold in absolute value. The given transfer function of itself is shown in Figure 2.10.

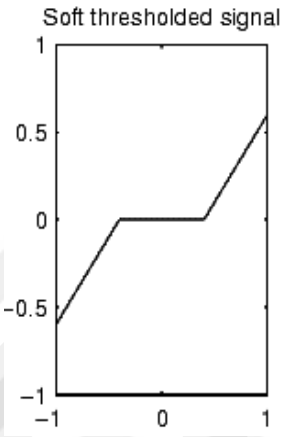

Figure 2.10 Soft Thresholding

2.5.1 Technique of Wavelet Thresholding

The technique of wavelet thresholding can be defined in three stages as below:

1. Compute the wavelet coefficient matrix w by stratifying the wavelet transform W to the data:

$$w = Wg = Wf + Wn \quad (16)$$

2. Thresholding the wavelet coefficients to evaluate the wavelet coefficients of:

$$\widehat{X}: w \rightarrow \hat{X} \quad (17)$$

3. Inverting transforms change coefficients to obtain the de-noised evaluation:

$$\hat{f} = w^{-1}\hat{X} \quad (18)$$

Subsequently, wavelet coefficients are contrasted with a threshold and it decides which coefficients ought to be set to zero. The definition of the value of the threshold is critical as a greater value may result in loss of data while a lower value may permit noise to proceed. The best possible value of the threshold can be defined from multiple perspectives [64]. The various strategies that are utilised for the definition of the threshold value are given as follows:

2.5.1.1 Neigh Shrink Sure

The Neigh Shrink Sure is a square neighbouring window that gets attention to shrink every noisy wavelet coefficient. In sub-band thresholding, the limit and neighbouring window size keep unaltered in all sub-groups. Neigh Shrink Sure has the inconvenience of utilizing each wavelet sub-band by limiting Stein's unbiased risk estimate (SURE). It additionally minimizes the block size inquiry extend.

$$1 \leq L \leq \left[\left(\frac{N}{2^k}\right)^{3/4}\right] \tag{19}$$

Non-ideal all-inclusive limit esteem and the equivalent neighbouring window size in every wavelet sub-bands. It can decide an ideal limit and neighbouring window size for each sub-band by SURE. They consolidate the obscure the coefficients that were not exposed to noise from sub-bands inside the identical one-dimensional vector. To evaluate the ideal threshold and sub-band level is obtained utilizing the accompanying equation:

$$(\lambda^s, L^s) = \arg\min SURE\ (w_s, \lambda, L) \tag{20}$$

The λ^s perform to the ideal threshold for sub-band S, L^s perform to ideal window size for sub-band S that limits SURE (w_s, λ, L). A Sure shrink is a primary aim of presenting sub-band level thresholding [65].

2.5.1.2 VisuShrink

In this procedure, the universal threshold defined by Donoho and Johnstone is utilised. This threshold is described in Equation (19).

$$\lambda_{VISU} = \sigma\sqrt{2logM} \tag{19}$$

where σ is the noise variance and M the number of pixels in the image. Reduced noise from images with this technique outputs in an excessively smooth rating of the image.

2.5.1.3 SURE Shrink

This thresholding technique applies the sub-band adaptive threshold. Stein's Unbiased Estimator based on Risk (SURE) where the method considers the loss in an unbiased version.

The threshold t_S can be obtained with $t_S = argmin_{c \le t \le \sqrt{2logd}} SURE\ (t; X)$. The wavelet coefficients function in the j^{th} sub-band, where $X_i{:}i = 1 \ldots d$. To assess the soft threshold $\hat{X}_i = \eta_i(X_i)$, we have:

$$SURE(t; x) = d - 2\{i{:}\ |X_i| \le t\} + \sum_{i=1}^{d} \min\ (|X|, t) \tag{20}$$

2.5.1.4 Bayes Shrink

This is an adaptive data-based threshold that de-noises the image by utilising the soft threshold strategy. Generalised Gaussian distribution (GGD) is expected for the wavelet coefficients in every sub-band. Here, the threshold T will be discovered, which decreases the Bayesian Risk. In every one of these strategies, the noise variance σ is defined as a parameter. In practice, to obtain a noisy image, the specific noise variance is not recognised. Noise variance can be evaluated with the $j-$robust median estimator.

$$\widehat{\sigma} = \frac{median\ (|Y,j|)}{0.6748}, Y_{ij} \in \text{sub} - \text{band}\ HH_1 \tag{21}$$

There are several implicit disadvantages in the thresholding methods. For example, the evaluated wavelet coefficients following the hard thresholding strategy are not consistent at the threshold λ, and this may drive to the wavering of the restored signal. In the soft thresholding issue, there is variation between the image coefficients and thresholder coefficients that directly impact the precision of the restored signal. Retention of the edges does furthermore an issue here. Distinctive edge detection methods may be utilised to obtain the contour characteristics of cell images. The BF has the benefit of achieving the purpose of edge retention [65].

2.5.1.5 Block Shrink

This is a totally information-driven block thresholding strategy that is also simple to execute. It can determine the ideal block size and the threshold for each wavelet sub-band by decreasing Stein's impartial risk evaluate (SURE). The block thresholding simultaneously keeps or kills each coefficient in groups as opposed to separately. The benefit of this method has various points of benefits through the traditional term separately. The estimation precision increases in black thresholding through the data about the neighbour wavelet coefficients. The local block thresholding strategies most of them own stable block size, threshold, and threshold

base are evaluated for all decision levels in any case of the transmission of the wavelet coefficients [66].

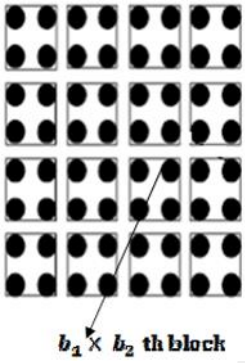

Figure 2.11 2 × 2 block partition for a wavelet sub-band

As shown in Figure 2.11, there are various sub-bands created when we execute wavelet decomposition on an image. For each sub-band, we have to separate it into many square blocks. This type of shrinkage has the ability to select the best block size and the specified sub-band threshold by decreasing Stein's impartial risk assessment. Tested outcomes show that Block Shrink performs better than the traditional Sure Shrink with the term-by-term thresholding and Neigh Shrink with the stable covering block size and threshold proposed by Chen et al. The tested outcomes indicate that the PSNR values in Block Shrink were significantly better than those of Sure Shrink and Neigh Shrink. In fact, Block Shrink receives the benefits of Sure Shrink and Neigh Shrink and gets rid of there [67].

2.5.1.6 Bivariate Shrinkage

A new shrinkage function which relies on both the coefficient and its parent yields better outcomes for wavelet-based image de-noising. The Bayesian estimate has changed the issue to consider the statistical reliance between a coefficient and its parent. Where w_2 introduces the parent of w_1 [68],

$$y_1 = w_1 + n_1 \tag{22}$$

$$y_2 = w_2 + n_2 \tag{23}$$

Let y_1 and y_2 be noisy observations of w_1 and w_2 and let n_1 and n_2 be noise samples:

$$Y = w + n \tag{24}$$

$$y = (y_1, y_2), w = (w_1, w_2) \tag{25}$$

$$n = (n_1, n_2) \tag{26}$$

The standard MAP estimator for given the corrupted observation y is:

$$\widehat{w}(y) = \arg\max p_{w|y}(w|y) \cdot \tag{27}$$

The shrinkage function can be written as:

$$\widehat{w_1} = \frac{(\sqrt{y_1^2+y_2^2} - \frac{\sqrt{3\sigma_n^2}}{\sigma})_+}{\sqrt{y_1^2+y_2^2}} \cdot y_1 \cdot \tag{28}$$

2.6 Image Fusion

Nowadays, numerous criteria that define the properties of a high-quality image, such as sharp focus, being appropriately uncovered, having the right colour parity, and not having an excessive amount of noise, have been introduced and discussed widely in the image processing literature. Image quality has as a lot to proceed with the client implementation and necessities while it appears with visual quality in usual. There are numerous strategies to obtain a decent picture or a high-quality picture. One of these is a picture combination method. Image fusion is a significant research theme in many related fields, such as PC vision, programmed object recognition, and medical imaging [69].

The requirement for image fusion in image processing handling frameworks is expanded for the most part because of the expanded number and assortment of picture procurement systems. Multi-focus image fusion is the path toward consolidating important data from more than two images to a single one image. The recent resultant image will give more data than any of the individual images [70].

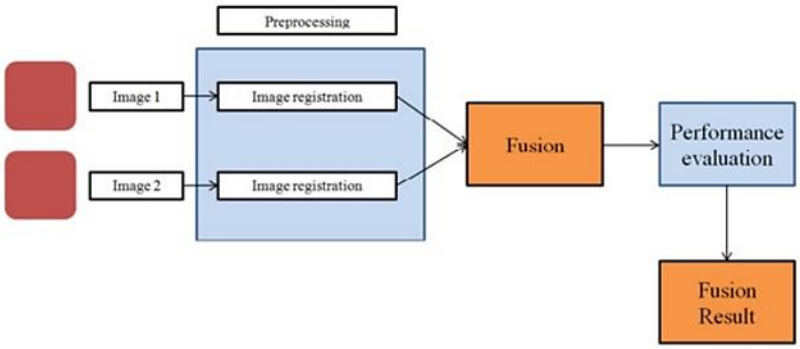

Figure 2.12 Image fusion process

At first, the primary point of fusion was limited to human perception and basic leadership. The principal type of fusion is the average of the pixel; arithmetically, the strategy can express as:

$$f(x,y) = \frac{1}{N}\sum_{i=1}^{N} I_i(x,y) \tag{29}$$

where $f(x,y)$ is a fused image, $I_i(x,y)$ source images, and $i = 1; 2; \dots ; N$. This technique is basic, simple to execute, and computationally requires minimal effort and by utilising this strategy, all data contained inside images are dealt with the equivalent. In any case, the result of this technique is unacceptable as this strategy presents artefacts, causes design dropping and differentiates decreases [71]. In the mid-eighties, Burt and Adelson presented a novel technique for image fusion dependent on progressive image deterioration, specifically the Laplacian Pyramid [72].

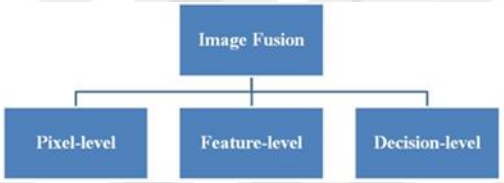

Figure 2.13 Image fusion categorisation

The image fusion procedure is classified into three classes [73]:

• **Pixel-level:** This is the most reduced level of the image fusion procedure. It immediately manages the pixels. The benefits of this level are to identify undesirable noise, to give detailed data, lower the complexity, and simplify the execution. However, these techniques do not deal with miss-registration and can cause a blocking artefact [76].

• **Feature-level:** In the advantage level procedure, advantages are removed from input images. The image is separated in continuous areas and fuses them utilising the fusion rule. The highlights of images, such the size, shape, differentiate, pixel forces, edges and textures [76], are fused.

• **Decision-level:** The decision level comprises combining data at a more elevated level of abstraction and merges the outcomes from different calculations to yield a final fused decision. The initial images are managed severally for data extraction. The gained information is then merged stratifying decision standards to reinforce combined

interpretation. In perspective on the domain, image fusion strategies have two types of domains [74]:

• **Spatial Domain**

The spatial domain proceeds immediately with pixels to combine important data. The spatial domains manage pixels to incorporate important data. A portion of the spatial domain methods incorporate averaging, select maximum/minimum strategy, Bovey transforms, intensity hue saturation strategy (IHS), high-pass filtering strategy (HPF), and Principal Component Analysis strategy (PCA). The disadvantage of spatial domain fusion is that it remembers the spatial distortion for the novel fused image. This spatial deformation issue is handled in the frequency domain [76].

• **Frequency Domain**

An image is converted in the frequency domain and the frequency coefficients are merged to obtain the fused image. Several of the procedures of the transform domain fusion contain DWT and SWT. In view of the input information and the objective [75], image fusion techniques are categorised as:

- **Multi-view fusion**

This merges images that were captured by a sensor from several viewpoints in the same duration of time. Multi-view fusion presents an image with higher accuracy and furthermore reconstitutes the 3D description of a scene.

- **Multi-temporal fusion**

This type of fusion incorporates different images possessed at a different interim effort to recognise changes among them or to deliver exact images of subjects [76].

- **Multi-focus fusion**

An optical lens cannot recognize each of the articles at different central lengths. Multi-focus image fusion combines the images of different central lengths from the imaging tools into a single picture of higher resolution.

- **Multi-modal fusion**

Multi-modal fusion indicates the merging of images from various sensors and is frequently alluded to as multi-sensor fusion which is broadly utilised in applications such as medical diagnosis, security, surveillance, etc. [76].

2.6.1 Multi Scale Fusion

Image fusion is the procedure that fuses data from various images of a similar scene. The result of image fusion is another image that acquires the most attractive data and advantages of every input image [77]. The conventional fusion techniques implement spatially well; however, for the most part, they present spectral noise. To overcome this issue, various multi-scale transform-based fusion projects have been suggested [78]. In this thesis, we focus on the fusion strategies' dependent on the Dual-Tree Complex discrete wavelet transform (DT-CWT) and bilateral filter and threshold methods. Because of the various multiscale transforms, several fusion rules have been suggested for a number of purposes and applications.

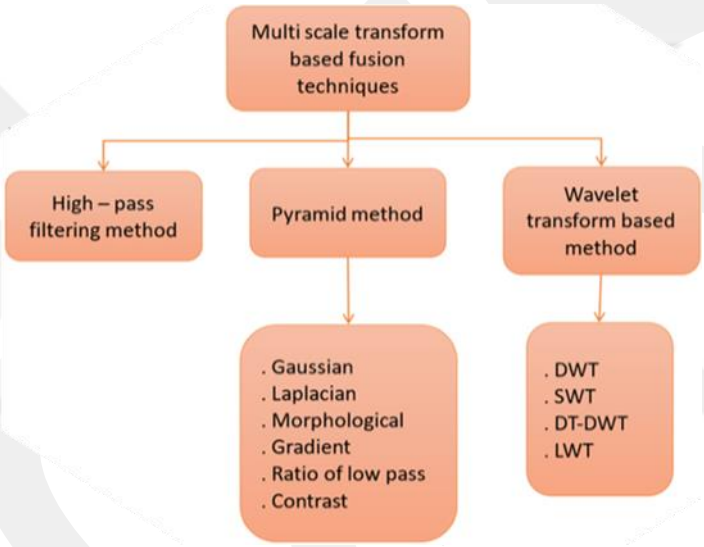

Figure 2.14 Multi Scale Fusion techniques

Figure 2.14 shows the classification of multi-scale transform based fusion techniques. There are three methods available based on multi-scale transform based fusion. Of these three, the first is the high-pass filtering method, the second a pyramid method and the third a wavelet transform based method [79].

2.6.2 Multi-Sensor Fusion

The improvement of various kinds of biosensors progressively of information has become obtainable for technological researches. While the volume of information develops, there is also the need to merge information collected from various sources to obtain the most valuable data. Data fusion is an efficient method for ideal usage of large quantities of information from numerous sources. Multi-sensor data fusion

attempts to merge data from various sensors and sources to obtain inferences which are not practical from a single sensor or source. The fusion of data from sensors with various physical features enhances the comprehension of our environment and gives the foundation of planning, decision-making, as well as control of autonomy and smart machines [80]. In the last few decades, this method has been used in various areas such as pattern recognition, visual upgrades, object detection and regional surveillance [81]. The literature on data fusion in PC vision, machine intelligence and medicinal imaging is fundamental; however, it will not be examined here.

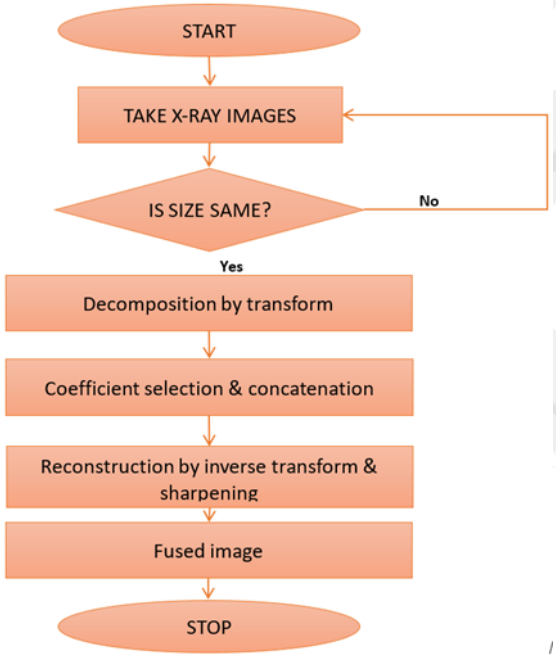

Figure 2.15 The image fusion process

2.7 Image Fusion Strategy

Image fusion strategy is separated into two sections: the spatial domain fusion technique and the transform domain fusion technique.

2.7.1 Spatial Domain Fusion Technique

In spatial domain procedures, we immediately treat with the image pixels. The pixel values impact to perform the ideal result. In the fusion techniques, for example, basic maximum, simple minimum, averaging, principal component analysis (PCA) and IHS based strategies fall within spatial domain technique [82].

a) Average Strategy

In this strategy, the pixel value of the two images is obtained and it locates the average value of that specific pixel. Therefore, resultant images include an average of the pixel gathered from both images.

$$F(i,j) = \frac{(A(i,j) + B(i,j))}{2} \quad (30)$$

The input images are $A(i,j) and\ B(i,j)$ and the fused image is $F(i,j)$; the pixel value is (i,j).

For the weighted average strategy, the equation for this strategy is set as follows:

$$F(i,j) = \sum_{i=0}^{m} \sum_{j=0}^{n} (A(i,j) + B(i,j))/2 \quad (31)$$

The input images are $A(i,j)$, $B(i,j)$ and the fused image is $F(i,j)$.

b) Select Maximum

In the maximum procedure, the resultant combined picture is obtained by selecting the most extreme force of compared pixels from both the info picture pixels.

$$F(i,j) = \sum_{x=0}^{m} \sum_{y=0}^{n} Max(A(i,j) + B(i,j)) \quad (32)$$

The input images are $A(i,j)$, $B(i,j)$ and the fused images are $F(i,j)$ and $F(i,j)$; the pixel value is (x,y).

c) Select Minimum

In this strategy, the resultant fused image is applied by determining the maximum intensity of the identical pixel gathered from both images:

$$F(i,j) = \sum_{x=0}^{m} \sum_{y=0}^{n} Min(A(i,j) + B(i,j)) \quad (33)$$

The input images are $A(i,j)$ and $B(i,j)$ and the fused image is $F(i,j)$.

2.7.2 Image Fusion Algorithm based on Spatial Frequency

This is a parameter that describes the image in detail. As indicated by this parameter, an identical image fusion strategy is suggested. It is expected that two images A and B be fused. Initially, the images are divided into sub-window images $Block_A$ and $Block_B$. At that point, the spatial frequency of the sub-image is determined and the total of the square after convolution is described as the row frequency and the column frequency. With F as the fused image,

$$Block_F(i,j) = \begin{Bmatrix} Block_A(i,j), SF_A > SF_B \\ Block_B(i,j), SF_B > SF_A \end{Bmatrix} \quad (34)$$

In the formula, SFI clarifies the spatial frequency of the sub-image.

2.7.3 Fusion Algorithm based on the Image Pyramid

The pyramid of the image is a multi-resolution test of the structure of the spatial domain. If we need to manufacture a Laplacian pyramid of images, the first step is to create a Gaussian image pyramid structure. According to the rule of the Laplace Pyramid, the Gauss Pyramid image for every layer is calculated and obtained through layers. Finally, the first image can be rebuilt. The image fusion strategy based on the Laplace Pyramid is shown below:

1. Decompose the image to be fused inside the Laplace Pyramid.
2. The first layer image relating to the Laplace Pyramid produces the fused image based on the rule of pixel fusion or region fusion. The novel fusion image is processed as the new first-layer image.
3. The new Laplace image is utilised to extract the pyramid layer by layer, and the last fusion image is reproduced.

At the point when the image pyramid is decomposed, the quantity of information frequently increments. Moreover, there are connections between the pyramid image layers. Consequently, the contrast between the images to be fused is extremely enormous, the calculation depends on the image Pyramid will create unreliability. In addition, the decay of the pyramid needs direction, and the display of the curve will be neither finished nor accurate. Not only do wavelet transforms have the features of multi-resolution examination, they also have the advantages of variable resolution in the course, space and frequency domains. Accordingly, the wavelet-based imaging technology has been introduced with consideration and advancement.

2.8 Image Fusion Schemes

2.8.1 Wavelet Transform

A multi-resolution decomposition of an image is used in a biorthogonal foundation and results in a non-repetitive image exemplification. This fundamental is known as wavelets.

Initially using the wfusimg() function, the images will be converted to the wavelet domain. Then a decision mask is structured in the same manner as described in the Laplacian fusion application. The subsequent stage is performed by developing the fused converted image accompanied by a decision mask. Finally, the fused image is achieved using the inverse wavelet transform [83].

2.8.1.1 Implemented Fusion Rules

Three recent fusion rule plans were actualised utilising DWT use as a basis for image fusion:

- Maximum Selection (MS) plan: This basic plan completely selects the coefficient in every sub-band to the greatest extent.
- Weighted Average (WA) plan: This plan, created by Burt and Kolczynski, utilises a standardised relationship between the two-image sub-bands in a small local area. The resultant coefficient for rebuilding the measurement was determined by the weighted average of the two images.
- Window Based Verification (WBV) plan: This plan creates a binary decision map to select between every couple of coefficients utilising a majority filter.

2.8.1.2 Commands and Syntax Used

The standard of image fusion utilising wavelets is to combine the wavelet decompositions and the pair of initial images utilising fusion techniques applied to approximation coefficients and specific coefficients.

XFUS = wfusimg(A1, A2, WNAME, LEVEL, AFUSMETH, DFUSMETH) restores the fused image XFUS acquired by fusion of the two initial images A1 and A2. Every fusion strategy characterized by AFUSMETH and DFUSMETH combines with a particular path explained below, the decompositions of A1 and A2, at LEVEL and utilizing wavelet WNAME. AFUSMETH and DFUSMETH determine the fusion technique for approximations and details, respectively.

2.8.2 IHS Transform

This method is a typical strategy in image fusion, with the significant constraint that only three groups are included [84]. Initially, it depends on the RGB true colour space and provides the feature that the different channels plot certain colour characteristics, namely intensity (I), hue (H) and saturation (S). This particular colour space is regularly selected on the grounds that the visual cognitive arrangement of individuals will, in general, treat these three segments as generally orthogonal perceptual axes. Therefore, in remote sensing, subjective bands are usually assigned to the RGB channels to deliver false-colour composites for show objective as it were.

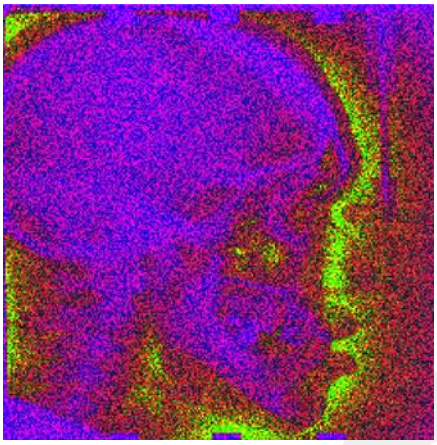

Figure 2.16 IHS image

2.8.2.1 Four stages utilised in IHS

1. Transform the red, green, and blue (RGB) channels (comparing with three multispectral groups) to the IHS parts.
2. Correspond the histogram of the panchromatic picture with the intensity part.
3. Supplant the intensity part with the extended panchromatic picture.
4. Inverse-transform the IHS channels to the RGB channels. The resultant colour composite will at that point have an increased spatial resolution as far as topographic texture data.

2.8.2.2 Advantages of IHS Transformation

1. It does not require radiometric amendments or radiometric improvements.
2. It does not demand the appraisal of practicing areas.
3. It creates a novel data collection where the damaged parts are very much distinguished.
4. It eliminates confusion between damaged parts and other land-cover land-use classes such as shadows, urban zones and water bodies are disposed.

2.8.3 Principal Component Analysis (PCA)

The main head segment image includes the data that is regular to every one of the images utilised as a contribution to PCA, whereas the spectral information that is particular to each of the bands is mapped to different parts. At that point, as in the IHS strategy, the initial principal component (PC1) is exchanged for the HRPI, which is first extended to have a similar mean and difference to PC1. Eventually, the HRMIs are specified by performing the inverse PCA transform [85]. In informational indexes

with numerous factors, groups of factors frequently shift together. One explanation behind this is that more than one variable might be estimating a similar driving standard administering the conduct of the framework. In numerous methods, there are only a couple of such driving impetuses. Therefore, the amount of instrumentation facilitates the measurement of many framework factors. When this occurs, one can exploit this excess of data. One can also extend the issue by changing a group of factors with a single new factor. The primary part examination is a quantitatively thorough technique to achieve this facilitation. The technique produces a novel collection of factors known as principal components. Every PC is a straight set of the original factors. All the PCs are orthogonal to one another, so there is no excessive data. The essential parts all in all structure orthogonal reasons for the space of the information. The limitless number of approaches to develop an orthogonal foundation for a few columns of information [83].

CHAPTER 3

RELATED WORK

One of the most famous methodologies is wavelet thresholding. In this method, a noisy image is first converted to its low-frequency (approximation) and high-frequency (detail) sub-bands. Owing to the fact that the image information is transformed in a small number of large coefficients, the high-frequency sub-bands are modified using soft or hard thresholding operations [86]. The threshold value determination is the critical step in the wavelet thresholding. For this purpose, different threshold determination approaches have been introduced, such as, Sure Shrink [87], Bayes Shrink [88] and Visu Shrink [89]. The Visu Shrink approach uses the minimax error measure to develop a universal threshold which is a function of the noise variance and size of the image. In the Sure Shrink technique, the threshold value is obtained by optimizing Stein's unbiased risk estimator. The Bayes Shrink method models the dissemination of the wavelet coefficients as Gaussian in a Bayesian framework to determine the threshold value. By taking into account the interstate and intractable correlations of the wavelet coefficients, these approaches are later modified [90]. The most widely recognized type of change-type image fusion methods is the wavelet fusion calculation because of its straightforwardness and its capacity to protect the details of the time and frequency of images to be combined.

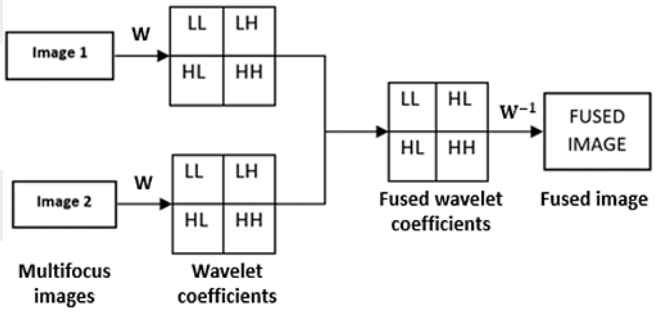

Figure 3.1 Wavelet Transform block diagram

Wavelets are the establishment for speaking to images in different degrees of goals. The wavelets were first demonstrated to be the establishment of an incredible new manner of dealing with signal transformations, and examination is known as a multi-

resolution strategy. This theory is concerned with the portrayal and investigation of images with more than one accuracy [91].

Z. Wang [92] presented the standards of image fusion at the levels of the pixel, feature and decision. The suggested method describes the plan rules and levels of the Graphical User Interface (GUI). The picture combination framework dependent on the GUI is then planned and the framework has numerous capacities.

D. Godse et al [93] proposed a wavelet-based image fusion pixel base most extreme choice guideline algorithm. Two of the same origin pictures are utilized at various points to be broken down in rows and columns by filtering and resulting down and examining at every level. The pixel estimation algorithm on the origin image gives the greatest estimation of the parallel choice guide being mapped and linking the fuse approximation, thereby giving the new coefficient matrix. At that point, the inverse wavelet transform is applied to recreate the resultant image. The wavelet gives a structure wherein an image is decomposed, with every level being compared to a rough resolution set. The wavelet honed images have a generally excellent spectral quality. The wavelet transform is favoured over the Fourier transform and brief timeframe Fourier transforms since it gives multi-resolutions. The spatial quality of the sharpened images differs depending on the information utilized for sharpening. The suggested method has a requirement to examine various mix designs in the wavelet domain to produce the wavelet-based frameworks with increasingly powerful spatial quality.

H. Gao et al. [94] characterized the calculation of image fusion dependent on the wavelet transform. Image fusion technology began to become one of the focuses in remote detection image processing and testing. In remote detection image fusion, the objective is to sharpen the image, to progress the geometric rectification and colour rectification, to progress the distribution of characteristics to produce up lost in a piece of image information, and monitor earth environment changes. These techniques though the fusion procedure does not take part in the combination of image decomposition and transformation; fusion is only achieved at a lower level.

S. Huang [95] suggested a number of various fusion plans of two fusion procedures: the panchromatic (PAN) and multispectral (MS) image fusion and multi-focus image fusion. In the previous procedures, the topic of image fusion produces a novel image featuring the high spatial resolution of the PAN images and the colour data of the MS picture. We have reached up in experimental outcomes that the PCA plan performs

better than the IHS plan while IHS-DWT plan has the best execution since there is very little spectral degradation. A further application and purpose of image fusion is the gathering of every one of the items in the centre from various CCD images of a similar scene. Since input images are grey-level, and consequently only the DWT planner is appropriate. In any case, there are various fusion rules to combine the DWT coefficients of the initial images. A fusion rule contains the decision of an activity-level computation and the decision of a coefficient fusing technique. It has appeared in emulation results that CBA is preferable in activity-level computation, and choose-max (CM) is the best strategy for merging approximation coefficients. However, weighted normal (WA) and adaptive WA (AWA) are powerful strategies in merging detail coefficients.

Dong-Chen He [96] proposed a technique for combination that is able to merge a high-resolution image with a permit resolution image or without spectral connections present between two images by saving the spectral part of the image at low-resolution while merging the spatial data of the image accompanied by the high resolution. The colour image is considered a low-resolution image and it can merge separately every part of the three segments (red, green and blue) with the high-resolution image and afterward obtain another fused colour image. In this manner, the entirety of the images can be merged to low-resolution colour images with a high-resolution image. The novel suggested strategy is an imaginative and unique procedure in its own right and the most generally utilized techniques in these regions are very limited by two obstacles, such as with at least three low-resolution images having to be merged with a high spatial resolution image and the fused images not reliably protecting the colours of the initial images.

Y. Zheng et al. [97] discussed an image fusion strategy, advanced DWT (aDWT), which included Principle Component Analysis (PCA) and morphological preparation into a uniform DWT fusion technique. They contrasted the image fusion execution of six common strategies (five pyramid techniques and a uniform DWT strategy) and our new technique dependent on four significant quantitative measures. In general, over the four various types of measures, the aDWT performance was the best. Several image sources changed significantly in their densities, complexity, noise, and intrinsic qualities; hence, a major challenge for the fusion method is to implement well over an

assortment of image sources. Therefore, a DWT is a committed technique to achieve the objective.

J. Gao et al. [98] presented a combination plan that depends on image improvement and introduces a fusion strategy for wavelet image improvement technology. Initially, they improved the source images as per the wavelet image improvement methods and afterward utilized the proper fusion rule to merge the coefficients of the first image and the improved images. The suggested method was dependent on wavelet improvement having higher values of the fusion image than the common strategy without utilizing wavelet improvement. Entropy and the standard deviation increased, showing that the combination dependent on wavelet improvement can expand the image density distribution, that the amount of data increased, and that it had delve into the unobserved data in the fused image to the maximum range. In spite of the fact that the clearness of the wavelet improved fusion image was not exactly the image acquired without utilizing wavelet improvement, the wavelet improved fusion image generally had a better outcome.

S. Krishnamoorthy et al. [99] explained eleven image fusion methods that were processed utilizing Microsoft Visual C++ 6.0. The fusion was executed on twelve groups of info pairs of medical images. A group of nine image measurements was executed to survey the fused image quality. The fused images of every group were additionally evaluated dependent on their visual quality by ten samples that were randomly selected. The quality appraisal dependent on the image measurement progress and visual recognition was matched with the survey validity of the image measurements. The readings delivered by the nine picture measurements were utilized to evaluate the preferable fusion strategy (as far as the quality of the fused images) utilizing the Pareto optimality technique. DWT with Haar depending on the fusion strategy was surveyed better. The evaluation saw that the fused images delivered by the Morphological Pyramid strategy generally performed modestly in quality. The methods were additionally evaluated dependent on the visual quality of the fused images. Ten individuals were randomly selected for visual evaluation of the fused images delivered in every one of the three sets and these were approached to select the higher and lower quality images they found in every image set. The outcomes here verified the created images were dependent on the image metric readings. DWT with Haar was classified 63.33% of the time, which was a higher rating than other methods.

Moreover, the outcomes were coordinated as Morphological pyramid appraised and second rate in visual quality.

B.Y. Shutao Li [100] proposed techniques depending on a number of numerical changes. At the point when an image is exposed to any change, it deteriorates into its sub-band segments which might be viewed as the frequency domain or wavelet domain. Therefore, this kind of procedure is likewise named 'Multi-resolution analyses. All transform domain systems can be acknowledged by a non-exclusive plan, as shown in Figure 3.2. The result of the change is the coefficients which are to be utilised for combination. For the fusion, a few criteria are fixed, which might be viewed as a 'fusion rule'. This block analyses the coefficients and dependent on the fusion technique, it produces fused coefficients. The inverse transformation is used to acquire manufactured, fused images in the spatial domain. Image fusion in the transform domain demands almost ideal reproduction of the spatial domain data.

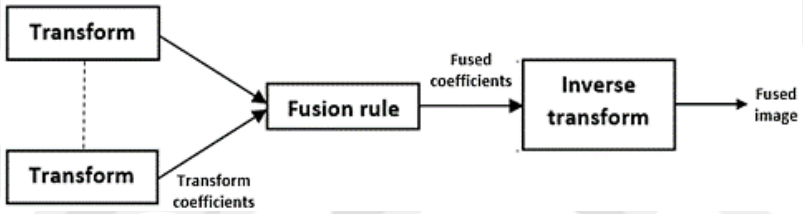

Figure 3.2 Image fusion using the Transform Generic scheme

Wrap up later transform domain strategies confirm effective through the spatial domain techniques. Few estimations of the RMS for the transform domain techniques obviously demonstrates that the fused image is without artefacts. The higher estimation of PSNR indicates that the image is less inclined to noise contrasted with spatial domain strategies. Entropy is roughly the same for every one of the strategies. At the point when the standard deviation estimation of the images of curvelet and wavelet are discussed, the wavelet transform is higher. These show that wavelet transforms are effective in clarifying the contrast data.

F. Sadjadi [101] presents a technique to assess the performance of image merging methods. They represent a collection of proportions of adequacy for performance analysis investigation and afterward utilised them in the results of various utilising methods implemented on a collection of real passive infrared (IR) and visible band imagery. Furthermore, it presumes that the comparative value of every fusion strategy is especially subject to the proportions of the effectiveness being utilised. In any case,

a significant number of the created results of fusion strategies have lower proportions of effectiveness than their information imagery.

S. Udomhusakal [102] proposed a multi-focus image fusion utilising spatial recurrence estimation and wavelet cases. The two arrangements of images were changed and decomposed into 16 sub-bands utilising wavelet parcels. Subsequently, every sub-band was a division in the sub-band division and every sub-band was specified utilising Structure From Motion (SFM). At that point, it located the inverse wavelet transform to reproduce the image. The target execution was measured utilising PSNR and Edge estimation to assess the quality of the fused image. The suggested technique had a preferred position over Structure From Motion (SFM) based strategy that was less than the estimation of the edge estimation higher quality. In the future, the impact of colour data or the chrominance segment to combine an image will be examined so as to obtain higher quality.

C. Lacewells et al. [103] presented a strategy for an exact fuse image utilising the Discrete Wavelet Transform (DWT) to highlight extraction and utilise conventional calculations to obtain an advance image. The proposed fusion was assessed with mutual information (MI) and RMSE. The three arrangements of climate gauging images were utilised to acquire results. The outputs showed that DWT_GA image fusion was better than the earlier strategies. DWT GA is increasingly exact and enhances the downsides of data distortion.

Z. Wu et al. [104] proposed image fusion on the wavelet transform for remote detection of images depending on IHS transformation. To progress, the exhibition of image fusion multispectral images was utilised to obtain I, H and S. The integration of IHS and the wavelet technique has higher retention in the spectral highlights.

S. Vekkot et al. [107] presented an approach with a pixel-based maximum determination rule depending on the combination of the high-frequency wavelet disintegration. The features of pixel and locale-based fusion in a single image had the ability to assist the improvement of refined methods, including upgrading the edges and basic details. The varieties in the execution of combination rules for various test pictures presented the decision of an ideal fusion rule based fundamentally upon the type of images to be utilised and degradation models applied to present noise in the input image. The filter mask hybrid fusion eliminates noise and other artefacts of the image and presents preferable outcomes over pixel combination.

Cui Li et al. [105] suggested a strategy dependent on the multi-scale wavelet deterioration of the image fusion method and a particular examination of the multi-scale image fusion technique dependent on the wavelet domain. The fusion technique for the greatest activity factor was embraced for the sub-images in the low-frequency band. The four presented techniques were compared. The fusion outcomes have a higher quality than the Wavelet Modulus Maxima method dependent on the locale of vitality and present an enhancement in each of the visual and quantitative records in multi-scale wavelet deterioration and provincial vitality image combination.

Mirajkar et al. [106] suggested a wavelet transform method to demonstrate the geometric goals of an image and describe various wavelet-based strategies, such as the main idea of a hybrid design being the wavelet transform in which both pixel and area main standards are incorporated. The SWT and DWT are similar strategies; however, in the stationary wavelet transform procedure, down testing is contained. By contrasting the results of the images, the SWT based image fusion level two strategy presented accurate results.

S. Bedi et al. [108] asserted that wavelets are limited in duration and fluctuating duration functions with zero mean value with limited capacity. They were appropriate for the examination of the transitory signals. The irregularity and great restriction characteristic produced a preferable fundamental for an examination of signals with discontinuities. The correlation and effective utilisation of the considerable number of systems in image quality evaluation is also specified. Appropriate fusion method based on upon the particular application. The spatial domain provides high spatial goals; however, in the spatial domain, spectral distortion is the fundamental disadvantage, and in this manner, transform domain image fusion is terminated. In view of the examination conducted on different transform domain algorithms, it is concluded that every strategy it implied that for a particular usage, one method slightly outperforms the other in terms of specific implementation. The image quality evaluation factors have been checked and decide the job of discrete image quality evaluation factor to determine the quality of the fused image.

CHAPTER 4

METHODOLOGY AND RESULTS

4.1 Dataset

We used one dataset, a dental radiography database (DX) [22]. This database consisted of 400 cephalometric X-ray images gathered from 400 patients at a resolution of 1935 × 2400. Arbitrary images from the dataset are shown in Figure 4.1. The collected dataset DX has a pixel spacing of 0.1 mm and the following data: mean age: 27.0 years; age range: 7-76 years; 235 females, and 165 males. The entire dataset was obtained in TIFF format with a Soredex CRANEXr Excel Ceph machine (Tuusula, Finland) utilising Soredex SorCom software (3.1.5, version 2.0).

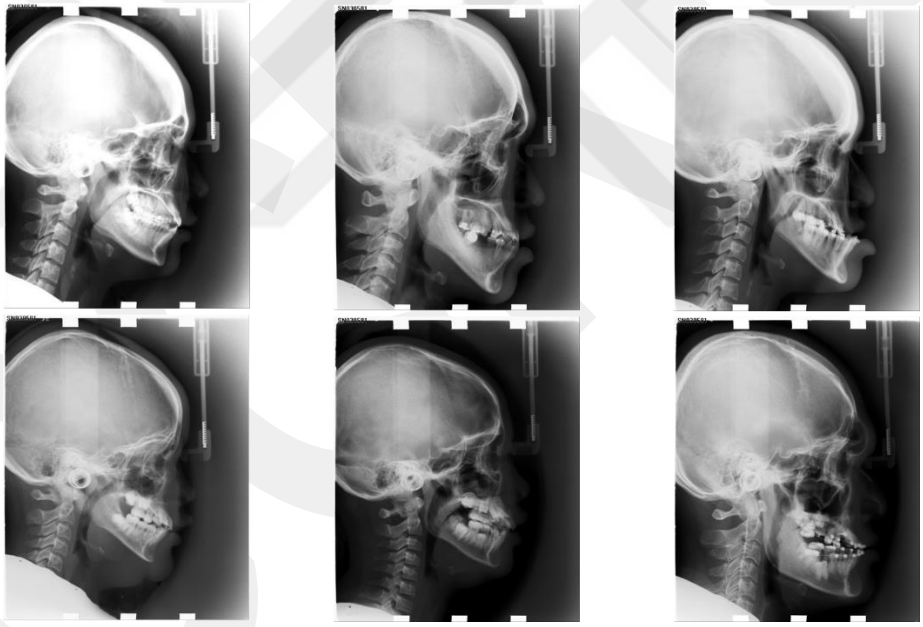

Figure 4.1 Random sample of medical images from dataset DX

4.2 Experimental Setup

Every image was prepared before modelling. Pre-processing comprised resizing every picture to 256 × 256 for arithmetical asset reasons. As various works on image de-noising, the execution process was on grayscale images. In this chapter, we give the results obtained on implementing the proposed method of image de-noising. Every

method was implemented on $MATLAB\ R2017b$. Various parameters described in Table 4.1 were applied for degradation.

4.3 Noise

In the present strategy, the effect of explicit noise on specific cephalometric X-ray images are presented. Various noise types that result in corrupting image quality are considered below. The test proof explains the effect of noise on particular image methodologies. Eventually, the quality of the cephalometric X-ray images modality is measured using $PSNR$. The proposed method was additionally tried for different attacks and results are presented with the assistance of tables and snapshots.

To consider the effect of Poisson noise and Gaussian noise on cephalometric X-ray images, noise is displayed as Poisson and Gaussian noise. With a fixed value of variance, error metrics are measured using Peak Signal-to-Noise Ratio (PSNR) for different capacities of de-noised images in cephalometric X-ray images resized to 256 × 256. The proportion of clarity determined by noise ratio and distortion ratio inside the cephalometric X-ray images and Poisson noise will determine the quality of the image. For a standard examination, images damaged with Poisson noise level ($\lambda = 9LE$ and $\lambda = 10LE$) were applied. To keep a similar sample size for training, we used the 400 images from the datasets.

Here, noise is represented as Gaussian noise to contemplate its impact on the cephalometric X-ray images methodology. The intensity of the noise changes as indicated by the difference utilised in the noise model. With a fixed estimation of difference, error measurements are estimated utilising Peak Signal-to-Noise Ratio ($PSNR$) for different capacity cephalometric X-ray images sized of 256 × 256. For a standard examination, images damaged with Gaussian noise ($p = 0.4$ and $p = 0.6$) were applied. Figure 4.3 shows the effect of Poisson noise and Gaussian noise on cephalometric X-ray images.

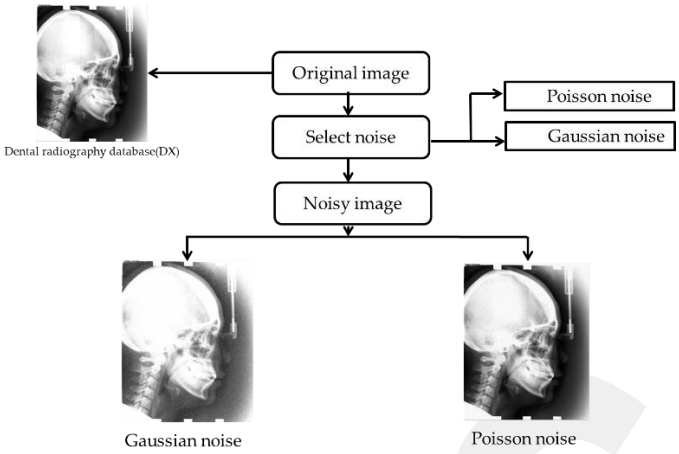

Figure 4.3 Gaussian and Poisson noise

Table 4.1 Poisson noise and Gaussian noise on cephalometric X-ray images

GAUSSIAN NOISE	AVERAGE	MIN	MAX
P= 0.4	28.067511	27.92359	28.4157
P= 0.6	24.627564	24.411487	25.05182
POISSON NOISE	AVERAGE	MIN	MAX
λ = 9 LE	33.228016	35.410826	32.161
λ= 10 LE	23.224866	25.452273	22.10254

4.4 Wavelet Thresholding

Numerous de-noising strategies have been proposed over the years. One of the most popular approaches is wavelet thresholding in which a noisy image initially degrades within its low-frequency (approximation) and high-frequency (detail) sub-bands. Owing to the fact that the image information is transformed in a few large coefficients, the high-frequency sub-bands are modified using soft or hard thresholding operations. The threshold value selection is the critical step in the wavelet thresholding. For this purpose, different threshold determination approaches have been introduced, such as Sure Shrink, Bays Shrink, Bivariate Shrink, Block Shrink, Visu Shrink, Neigh Shrink SURE. The VisuShrink approach uses the minimax error measure to develop a universal threshold which is a function of the noise variance and the size of the image. In the SureShrink technique, the threshold value is obtained by optimizing Stein's unbiased risk estimator. The soft thresholding produces smoother results about examination with the hard thresholding and more visually pleasing images as it is non-stop. Hard thresholding, in any case, gives greater edge protection in correlation

with the soft one, yet here and there, it may be a good idea to apply the soft threshold to a few particular levels.

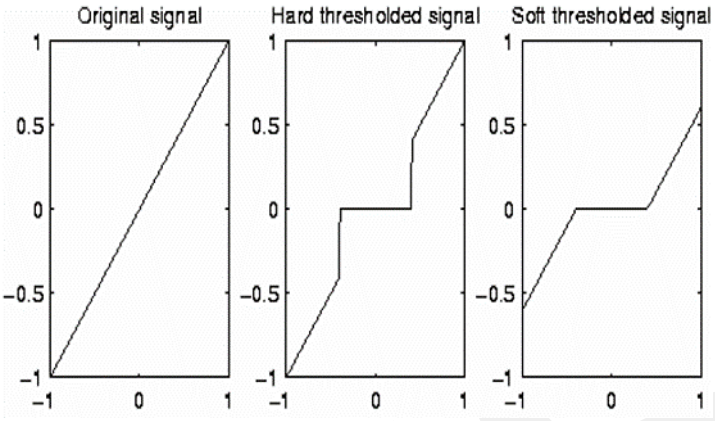

Figure 4.4 Thresholding signals

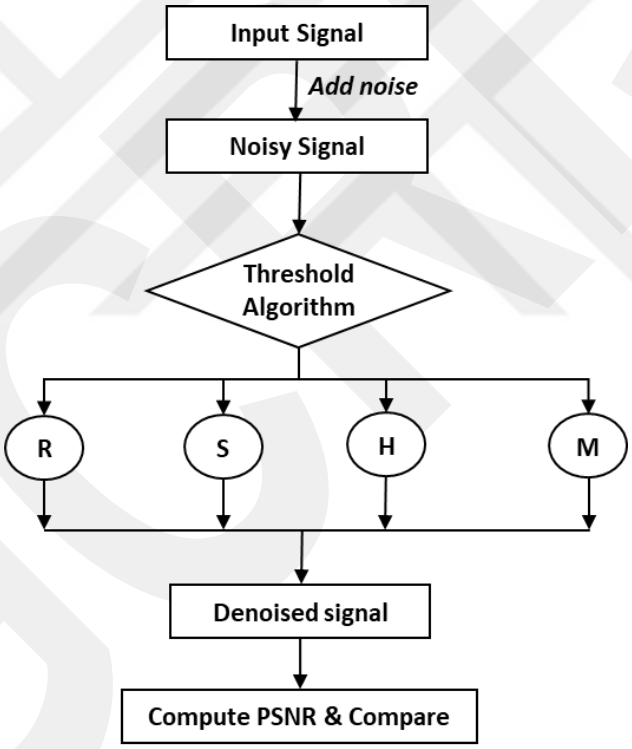

Figure 4.5 De-noising Procedure

This code "Thresholding.m" offers a similar investigation of various wavelet de-noising methods and the achieved results were tested. The de-noising procedure refuses noise by thresholding in the wavelet domain.

A = wthresh(B,sorh,T) produces the soft or hard thresholding, determined by the soft, of the vector or matrix A. T is the threshold value.

It is seen that the 'wthresh' strategy provides an ideal execution. Discrete wavelet transform has the advantage of providing a common time-frequency portrayal of the signal. In addition, it is reasonable for both stationary and non-stationary signals and it is the most fitting framework in the field of signal discovery. The discrete wavelet transform is executed within multiresolution examination and digital filter banks.

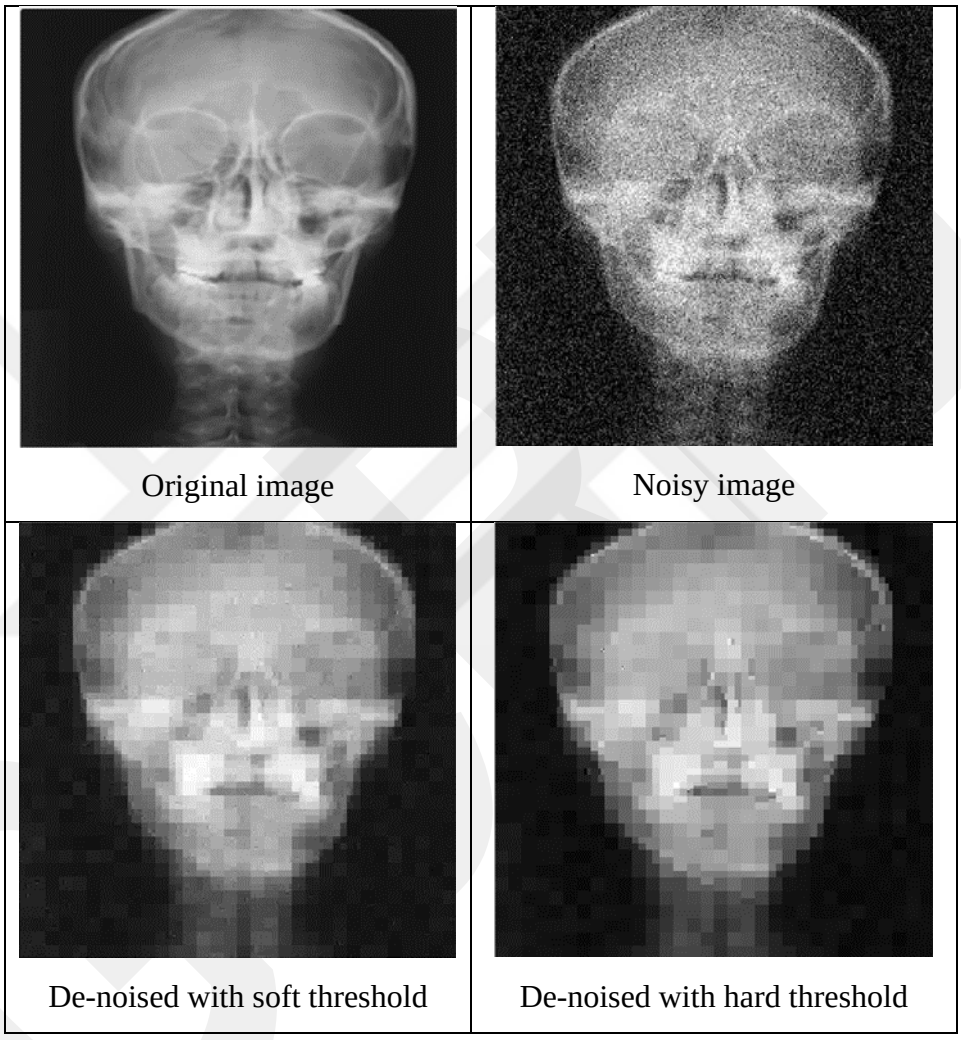

Figure 4.6 Image de-noising using hard and soft thresholding

Table 4.2 Hard threshold test

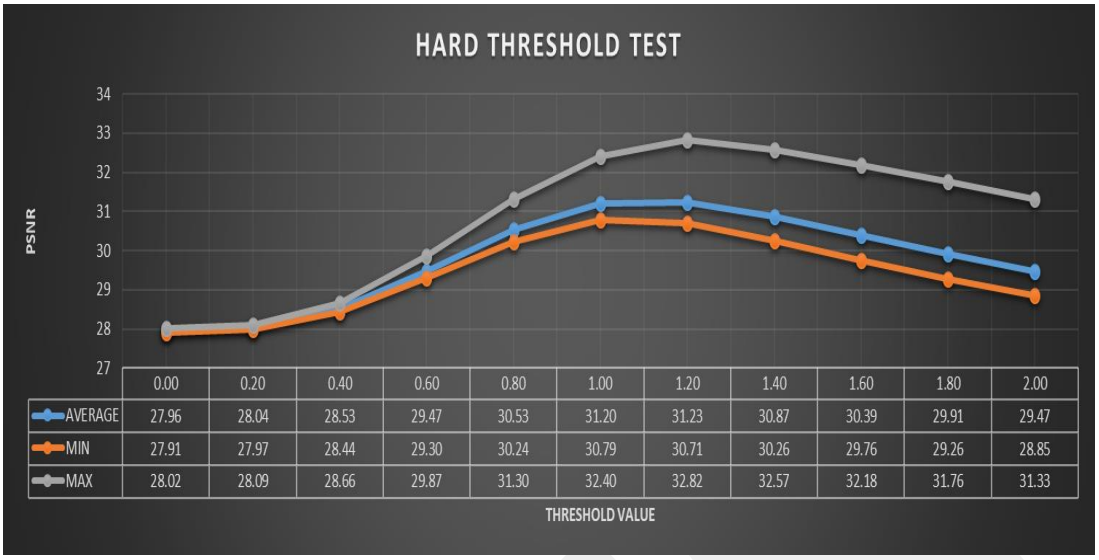

Table 4.3 Soft threshold test

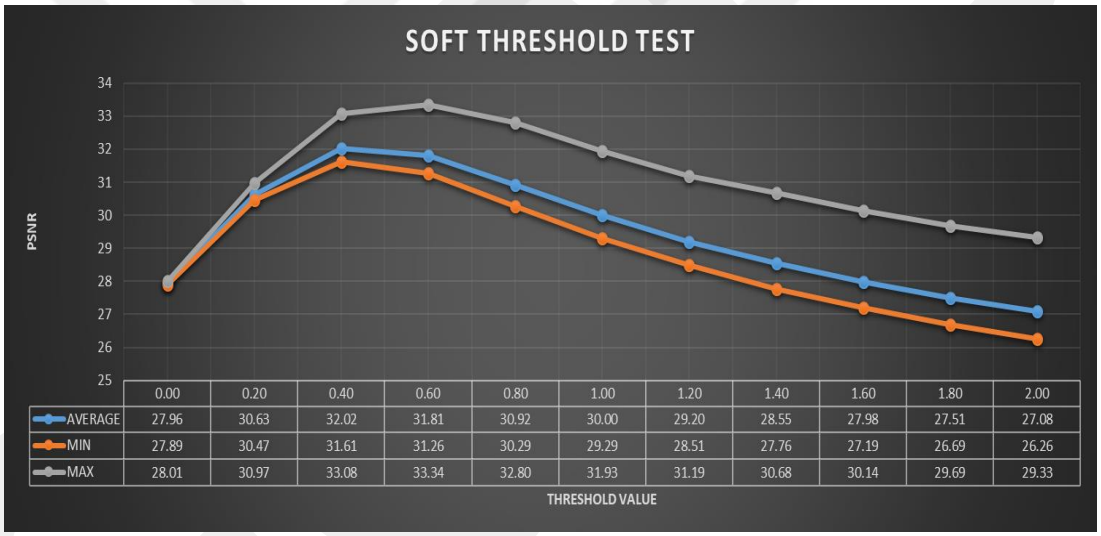

For the first tested code, we used the hard and soft thresholding and tested with more than 11 thresholding starting from 0.00 to 2.00. The best results were as follows:
The best threshold value using hard thresholding tested for 400 cephalometric X-ray images yielded an average PSNR for $T = 1.20$ of +31.23dB. The best threshold value using soft thresholding tested for 400 cephalometric X-ray images yielded an average PSNR for $T = 0.40$ of +32.02dB.

Table 4.4 Wavelet thresholding

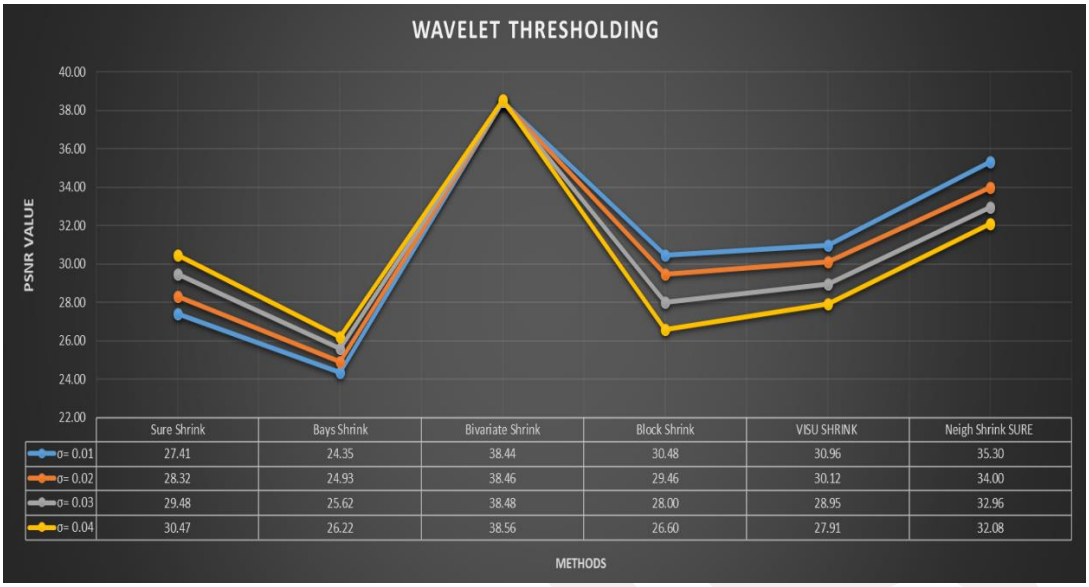

	Sure Shrink	Bays Shrink	Bivariate Shrink	Block Shrink	VISU SHRINK	Neigh Shrink SURE
σ= 0.01	27.41	24.35	38.44	30.48	30.96	35.30
σ= 0.02	28.32	24.93	38.46	29.46	30.12	34.00
σ= 0.03	29.48	25.62	38.48	28.00	28.95	32.96
σ= 0.04	30.47	26.22	38.56	26.60	27.91	32.08

This thesis introduces a close examination of various shrinkages for image de-noising systems utilising wavelet transforms. We examined the image thresholding with six different thresholding techniques using the various noises (Gaussian noise, Poisson noise) and determined the results for 400 cephalometric X-ray test images. Our outcomes were determined using the PSNR. The results for an image that appeared beneath that were influenced by Gaussian noise having various changes are presented in Table 4.4.

The essential strides of wavelet-based image de-noising are:

1. Analysis of corrupted images with noise utilising the wavelet transform.
2. Calculating the threshold in the wavelet domain and applying it to noisy coefficients.
3. Extracting the image using the inverse wavelet transform.

Image de-noising utilising wavelet procedures are successful in view of their capacity to catch the vitality of the signal in a couple of high transform values when a regular image is damaged by Gaussian noise. Out of the different thresholding methods, soft-thresholding is generally mainstream. This theory introduces a relative examination of different image de-noising thresholding methods (Sure Shrink, Bays Shrink, Bivariate Shrink, Block Shrink, Visu Shrink, Neigh Shrink SURE) utilising wavelet transforms. Many blends have been implemented to locate the most suitable technique that can be developed to de-noise intensity images. From the PSNR values as seen in the tables,

without doubt Bivariate Shrinkage presents more suitable results under various noise change conditions for the entirety of the images.

4.5 Wiener Filter

In signal processing, the Wiener filter is a filter applied to provide a measure of the ideal or target irregular process using straight time-invariant filtering of an observed noise execution, allowing for known stationary signal and noise spectra as well as added and additive noise.

X = wiener2(Y,[m n],noise) filters the grayscale image. X processes a pixel-wise adaptive low-pass Wiener filter. The parameter [m n] defines the size ($m \times n$) of the neighborhood utilized to determine the local image mean and standard deviation. The additive noise (Gaussian white noise) power is presumed to be de-noised. The input image has been corrupted by consistent force-added additive noise. 'wiener2' utilizes a pixel-aware adaptive Wiener technique dependent on measurements computed from the local neighborhood of every pixel. The PSNR values are as follows:

	Noisy image	Wiener filter
PSNR	24.62756398	+27.15 dB

4.6 Bilateral Filtering

The idea underlying bilateral filtering is to do in the scope of an image what conventional filters do in its area. Two pixels can be near to each other, that is, involve the nearby spatial areas. Alternatively, they can be like each other, that is, have nearby values, perhaps in a perceptually important design. Proximity regards to region in the area, comparability to the region in the range. Conventional separating is area sifting and requires closeness by gauging pixel esteems with coefficients that tumble off with separation. Essentially, we characterise extent separating, which midpoints image esteems with loads that rot with a uniqueness. Range filters are nonlinear order to loads rely upon image force or colour. Mathematically, they are no more complicated than regular non-separable filters that join the range and domain filtering and confirm that the blend is substantially more interesting. We signify the joined filtering as bilateral filtering.

BFILTER2 is a two-dimensional bilateral filtering method. The function executes 2-D bilateral filtering utilising the algorithm contained in the following:

X = bfilter2(Y, W, SIGMA) implements 2-D bilateral filtering for the grayscale or colour image Y. Y should be a double-precision matrix of size N × M × 1 or N × M × 3 with normalised values in the closed interval [0, 1].

CARTOON Image concept applying bilateral filtering. This function utilises the bilateral filter to extract an image following the strategy laid out as follows:

Z = cartoon (Y) adjusts the shading image Y to have a cartoon-like impression. An absolute necessity is a twofold double-precision matrix of size N × M × 3 with standardized qualities in the closed interval [0, 1]. Virtualization filtering factors are characterized in "Cartoon.m".

The code shows a run of the usage for the bilateral filter executed by BFILTER2. The utilisation of bilateral filtering to image deliberation is shown with the CARTOON function.

Table 4.5 Sigma test with fixed range

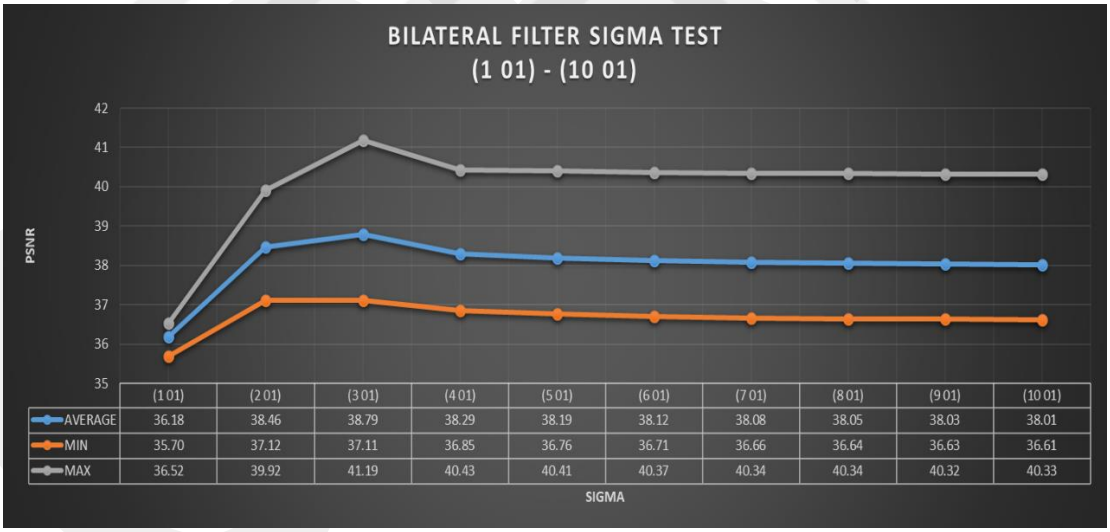

	(1 01)	(2 01)	(3 01)	(4 01)	(5 01)	(6 01)	(7 01)	(8 01)	(9 01)	(10 01)
AVERAGE	36.18	38.46	38.79	38.29	38.19	38.12	38.08	38.05	38.03	38.01
MIN	35.70	37.12	37.11	36.85	36.76	36.71	36.66	36.64	36.63	36.61
MAX	36.52	39.92	41.19	40.43	40.41	40.37	40.34	40.34	40.32	40.33

Only pixels close in the space and in the range and normalise the sum of the weights are considered, and which are present in the sigma parameters [σ_s σ_r]. Our method was tested the value of the sigma to find the best PSNR value. We utilised 10 different sigma parameters by fixing the range $\sigma_r = 0.1$ and change the space parameter σ_s starting from [1 0.1]- [10 0.1]. The highest average PSNR value was sigma = [3

0.1] with PSNR =+ 38.79dB. Our enhanced method was with bilateral filter half-width $w = 4$.

Table 4.6 Sigma test with fixed space

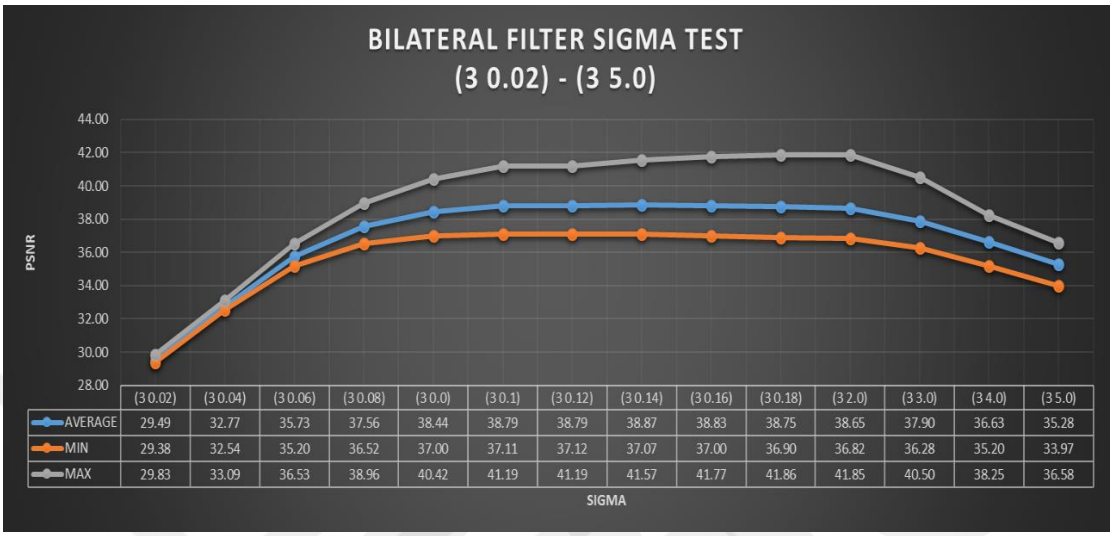

	(3 0.02)	(3 0.04)	(3 0.06)	(3 0.08)	(3 0.0)	(3 0.1)	(3 0.12)	(3 0.14)	(3 0.16)	(3 0.18)	(3 2.0)	(3 3.0)	(3 4.0)	(3 5.0)
AVERAGE	29.49	32.77	35.73	37.56	38.44	38.79	38.79	38.87	38.83	38.75	38.65	37.90	36.63	35.28
MIN	29.38	32.54	35.20	36.52	37.00	37.11	37.12	37.07	37.00	36.90	36.82	36.28	35.20	33.97
MAX	29.83	33.09	36.53	38.96	40.42	41.19	41.19	41.57	41.77	41.86	41.85	40.50	38.25	36.58

In our second proposed method, we utilised these in 14 different range values of sigma parameters by fixing the best average PSNR value of the space parameter in the previous proposed method which was σ_r = 3 and we changed the range parameter σ_s startingfrom [3 0.02]-[3 5.0]. The highest average PSNR value was sigma = [3 0.14] with PSNR =+ 38.87dB. Our enhanced method used the bilateral filter of half-width $w = 4$.

The previous method was $w = 1$ and the $sigma$ = [3 0.1]. Our enhanced method used a bilateral filter half-width $w = 4$ and bilateral filter standard deviations $sigma$ = [3 0.14]. We tested the method and our enhanced method on 400 cephalometric X-ray images. The average of the set bilateral filter parameters was the PSNR values:

	Bilateral Filter	**Proposed Bilateral Filter**
PSNR	**+38.79 dB**	**+38.87 dB**

Original image | De-noised image

Figure 4.7 Image de-noising using the Bilateral Filter

Table 4.7 shows the difference between the Bilateral and Wiener filter in two different noises (Gaussian noise and Poisson noise) with two different values for each noise type. The PSNR values clearly show that the Bilateral Filter has the highest PSNR values.

Table 4.7 Differences between the Bilateral and Wiener filters

Gaussian Noise				Poisson Noise			
p= 0.4	AVERAGE	MAX	MIN	λ= 9	AVERAGE	MAX	MIN
BILATERAL FILTER	38.87	41.57	37.07	BILATERAL FILTER	39.84	43.85	37.79
WIENER FILTER	36.24	37.82	34.61	WIENER FILTER	40.01	43.37	37.63
p= 0.6	AVERAGE	MAX	MIN	λ= 10	AVERAGE	MAX	MIN
BILATERAL FILTER	32.63	36.36	30.70	BILATERAL FILTER	33.35	35.95	31.94
WIENER FILTER	32.33	34.60	30.42	WIENER FILTER	25.11	27.66	23.62

4.7 Fused Rules and Methods

4.7.1 Wavelet Transform

The premise of wavelets is a multi-resolution decomposition of an image in a biorthogonal background and outcomes in non-redundant image impersonation. This premise is return wavelets. Initially, the images are modelled into the wavelet domain using the wfusimg() function, presented as the number of metrics, the wavelet channel, and the edge dealing with are indicated. Later, a decision mask is constructed. The following stage occurs by building the fused transformed image with a given mask. Eventually, the fused image is acquired by computing an inverse wavelet transform.

Wfusimg (Y1,Y2,WNAME,LEVEL,AFUSMETH,DFUSMETH,FLAGPLOT) the rule of image fusion utilising wavelets is to consolidate the wavelet disintegrations of

the two unique images utilising fusion techniques applied to approximation coefficients and subtleties coefficients. Merging the two images from the wavelet disintegrations occurs at level 5 utilising sym4 by taking four diverse fusion strategies. The following are combinations using the average for the two approximations and features: XFUSmean = wfusimg(Y1, Y2, sym4,1,'mean','mean');

Combinations taking the maximum for the approximations and the minimum for the features: XFUSmaxmin = wfusimg(Y1, Y2, sym4,1,'max','min');

A wavelet transform is implemented on the image resulting in a four-component image: a low-resolution approximation component (LL) and three images of horizontal (HL), vertical (LH) and diagonal (HH) wavelet coefficients which include the data of the local spatial feature. The procedure is duplicated for every band and all groups are transformed. A reverse wavelet transform is implemented on the fused elements to create the fused multispectral image. The image fusion technique is shown in Figure 4.8 [21].

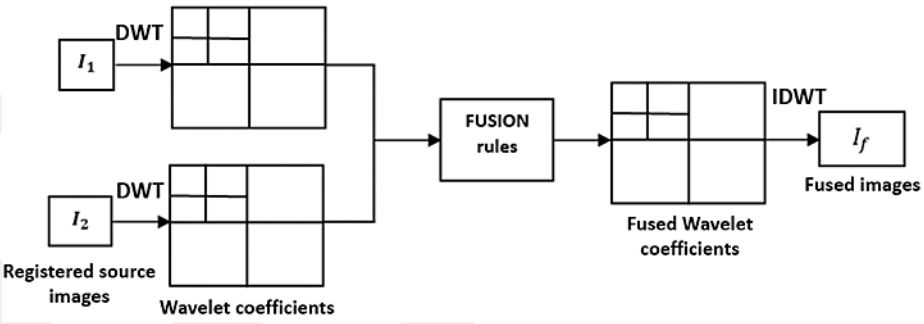

Figure 4.8 Image fusion method

The following procedures are performed:

1- Decompose the source images I_1 and I_2 to the discrete wavelet.

2- The decomposition coefficients are presented as LL (approximations), LH, HL and HH (details) at every level followed by the fusion rules being implemented.

3- The determination map is determined dependent on the fusion rules.

4- The subsequently fused transforms are reproduced into the fused image using the inverse wavelet transformation.

4.7.2 Principal Component Analysis (PCA)

The main head part image includes the data that is regular to every one of the groups obtained as a contribution to the PCA; however, the spectral data which is special to any of the groups is planned for different components. At that point, like the IHS strategy, the main principal component (PC1) was supplanted by the HRPI, which is first submitted to have a similar mean and change as PC1. As the last advance, the HRMIs are dictated by playing out the inverse PCA transform [4]. The strategy produces another arrangement of factors, namely described principal components. Every principal component is a direct mix of the first factors. All the important parts are symmetrical to one another, so there is no repetitive data. There is an unlimited number of approaches to building a symmetrical reason for a few columns of information.

Table 4.8 Fused rules

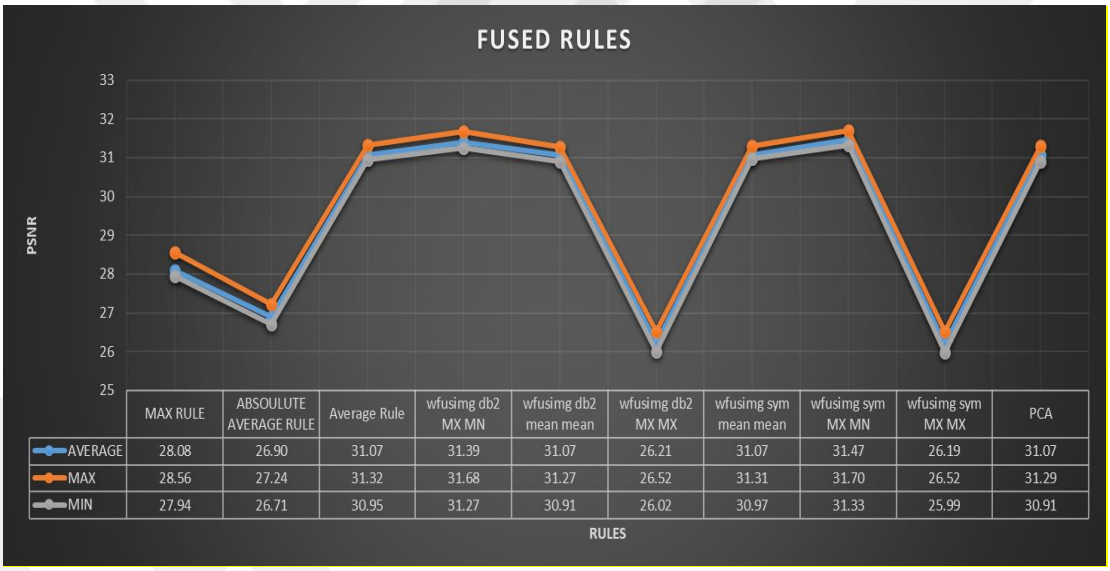

	MAX RULE	ABSOULUTE AVERAGE RULE	Average Rule	wfusimg db2 MX MN	wfusimg db2 mean mean	wfusimg db2 MX MX	wfusimg sym mean mean	wfusimg sym MX MN	wfusimg sym MX MX	PCA
AVERAGE	28.08	26.90	31.07	31.39	31.07	26.21	31.07	31.47	26.19	31.07
MAX	28.56	27.24	31.32	31.68	31.27	26.52	31.31	31.70	26.52	31.29
MIN	27.94	26.71	30.95	31.27	30.91	26.02	30.97	31.33	25.99	30.91

In this part, we examine with five wavelet classes, specifically Haar, Daubechies (db), Symlets, Coiflets and Biorsplines for fusing enhanced methods on 400 cephalometric X-ray images. The Daubechies (db) and Symlets filters, which produced the largest PSNR values, were selected for additional analysis. Diverse fusion rules were utilised in addition to the overall maximum rule, average rule, and absolute average rule. Here, image fusion using the wavelet wfusimg(Y1,Y2,sym4,4,'max','min') gives more efficient results, so this rule is selected.

4.8 Proposed methods and results

4.8.1 Stationary Wavelet Transform (SWT)

The SWT resembles the DWT and unless it is in the SWT, the signal is never sub-sampled but rather, at every level of decomposition, the filters are up sampled. Here we utilized non-linear thresholding strategies in the wavelet domain, such as hard and soft thresholding, using the Stationary Wavelet Transform (SWT) for various wavelets, at various levels, and the Bilateral Filter is proposed to de-noise an image and decide the best one between them.

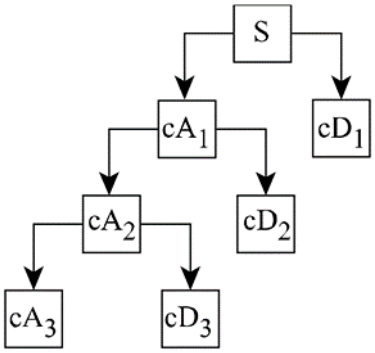

Figure 4.9 Stationary Wavelet Transform

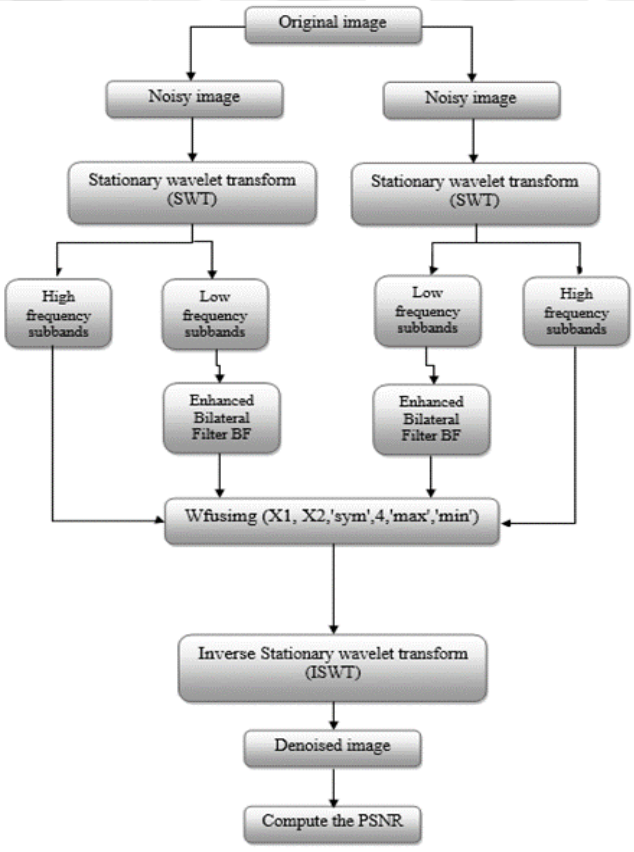

Figure 4.10 Block diagram of the proposed method

Table 4.9 Stationary Wavelet Transform

Stationary Wavelet Transform SWT							
Gaussian Noise	AVERAGE	MAX	MIN	Poisson Noise	AVERAGE	MAX	MIN
p= 0.4	39.47	40.82	38.78	λ= 9	39.10	41.53	37.98
p= 0.6	31.47	32.82	30.78	λ= 10	33.10	35.53	31.98

The proposed method utilised random noise and Gaussian noise with two different parameters of the same image to obtain two different images. We utilised the SWT decomposition on both images and after the decomposition of both images, we apply the enhanced Bilateral filter to the sub-bands of the two images, followed by merging the approximation of them using the Wfusimg(Y1, Y2,'sym4',4,'max','min') fused rule. Finally, we apply the inverse SWT to obtain the fused image.

4.8.2 Discrete Wavelet Transform (DWT)

The DWT includes the multiresolution subdivision property; along these lines, it is generally utilised in image processing. It changes over an image from the spatial domain to the frequency domain. The image decomposes into low- and high-frequency sub-bands using the DWT. The low-frequency sub-bands are compared with the approximation part, which includes the normal data of the whole image. However, the high-frequency sub-bands determine the detailed parts including the sharp information of the images. The particular parts comprise three high-frequency sub-bands (LH, HL and HH), as shown in Figure 4.11 (a). For second level decomposition, only the LL sub-band is moreover degraded into four frequency sub-bands, while the LH, HL and HH sub-bands stay in that capacity, as shown in Figure 4.11 (b). The decomposition levels can be expanded according to necessity.

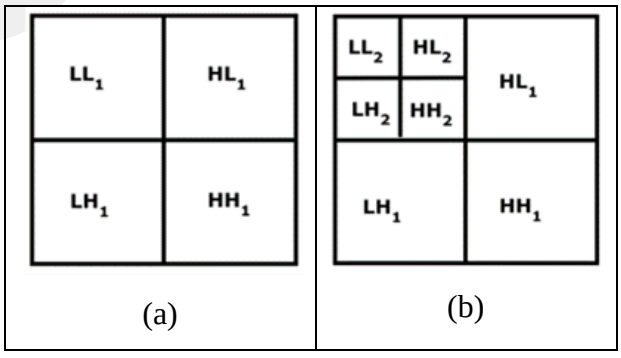

Figure 4.11: (a) First level DWT decomposition; (b) Second level DWT decomposition

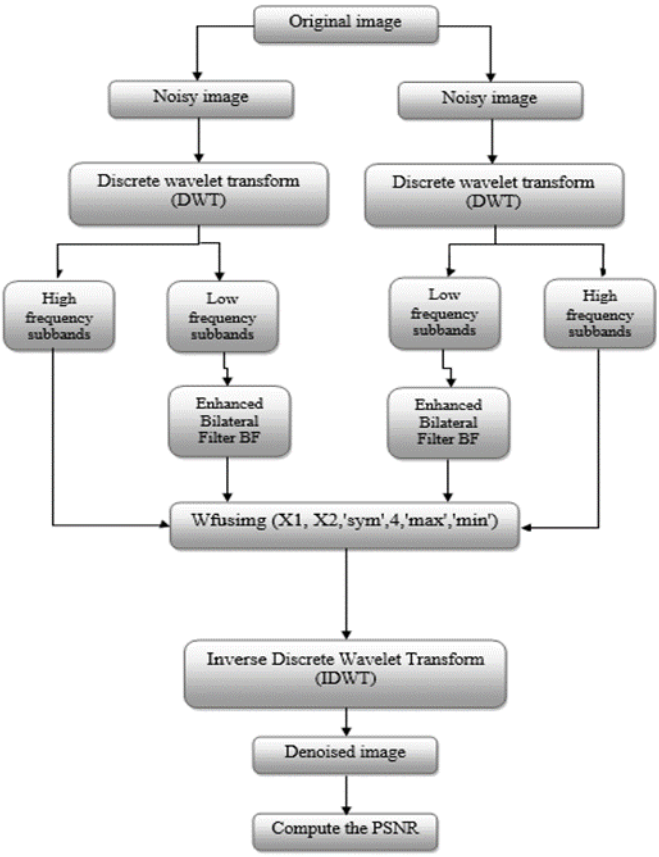

Figure 4.12 Block diagram of de-noising using the Discrete Wavelet Transform based on the fusion method

Table 4.10 Discrete Wavelet Transform

Discrete Wavelet Transform DWT							
Gaussian Noise	AVERAGE	MAX	MIN	Poisson Noise	AVERAGE	MAX	MIN
p= 0.4	40.22	42.56	39.00	λ= 9	40.72	43.12	39.48
p= 0.6	31.61	33.78	30.52	λ= 10	29.61	32.30	28.06

The performance of fusion algorithms was compared in terms of objective and subjective quality. The main findings of this study indicate that wavelet-based fusion generally works better than other image fusion methods and the wavelet transform provides a flexible and efficient framework for image fusion applications and finally, which invariant wavelet transforms, such as the DWT and the SWT, produce the best results.

In this part, novel image fusion techniques established on Discrete Wavelet Transform (DWT) and Stationary wavelet transform (SWT) are used to find the best combination of wavelet transform and bilateral filter (BF), which are proposed. In the suggested structure, noisy images are decomposed into four-level sub-bands (LL, LH, HL and HH) using DWT. The low-frequency sub-bands of the transformed images are filtered using an enhanced bilateral filter for each low sub-band of the image. At the same time, the high-frequency sub-bands of the wavelet transform are fused with the second high-frequency sub-band using the wfusimg(Y1,Y2,'sym4',4,'max','min') fusion rule. The wfusimg wavelet transforms using the Symlets wavelet as a fusion method and 4 levels of decomposition generally produce a technique that offers the best subjective results with noisy data, generating sharp, low-noise fused images.

4.8.3 Dual-Tree Complex Wavelet Transform

4.8.3.1 Introduction

For reasons unknown, for certain uses related to the discrete wavelet transform, upgrades can be obtained by utilising an extensive wavelet transform instead of a critically-sampled one. There are a few types of reaching DWTs, and here we present the Dual-Tree Complex discrete wavelet transform (DTC-DWT). The DTC-DWT of a signal X is actualised utilising two critically-sampled DWTs in parallel on similar information, as shown in Figure 2.5.

The transform is 2-times expansive in order to N-point signal it gives 2N DWT coefficients. No advantage is gained if the filters in the upper and lower DWTs are the same. In any case, if the filters are planned in a special manner, at that point, the sub-band signals of the higher DWT can be described as the real part of a complex wavelet transform, and sub-band signals of the lower DWT can be deciphered as the imaginary part. Equally, for extraordinarily planned arrangements of filters, the wavelet related to the higher-level DWT can be an estimated Hilbert transform of the wavelet connected to the lower DWT. At the point of being structured along these lines, the Dual-Tree Complex DWT is almost moving invariantly and is on the contrary a critically-sampled DWT. Furthermore, the Dual-Tree Complex DWT can be utilised to perform 2D wavelet transforms where every wavelet is situated, which is particularly valuable for image processing. (For the separable 2D DWT, one of the three wavelets do not have a prevailing direction.) The Dual-Tree Complex DWT

outperforms the critically-sampled DWT for use in image de-noising and improvement.

4.8.3.2 MATLAB Implementation

The MATLAB function "DualtreecomplexDWT.m" calculates the J-scale Dual-Tree Complex DWT w of a signal x. The function is extremely comparable to the "2DWT.m" function. It frequently returns the "afb.m" function to perform the test filter bank. The wavelet coefficients are furthermore stacked as a cell array w. "For j = 1.J, w{j}{1}" is the high-frequency sub-band signal generated at stage j in the higher-level DWT, w{j}{2} is the high-frequency sub-band signal generated at stage j in the lower DWT. The "IdualtreecomplexDWT.m" function performs the inverse transform.

4.8.3.3 2-D Dual-Tree Wavelet Transform

The benefits of the Dual-Tree Complex Wavelet transform is can be utilised to execute 2D wavelet transforms that are very specific regarding direction than is the distinguishable 2D DWT. There are two types of the 2D dual-tree wavelet transform: the real 2-D dual-tree DWT is 2-times expansive, and the second type is the complex 2-D dual-tree DWT is 4-times expansive. The two versions have wavelets situated in six particular directions.

4.8.3.4 Real 2-D Dual-tree Wavelet Transform

The real 2-D dual-tree DWT of an image x is performed utilising two critically-sampled separable 2-D DWTs. At this point for each pair of sub-bands, we gather the summation and difference. The "dualtreeDWT2D.m" function evaluates the J-scale real 2-D dual-tree DWT of an image x.

The wavelet coefficients w is stacked as a cell array. For $j = 1.J, k = 1\ldots2, d = 1\ldots3, w\{j\}\{k\}\{d\}$ are the wavelet coefficients created at scale j and orientation (k, d). The image x is recouped from w utilizing the inverse transform, executed using "IdualtreeDWT2D.m". The typical rebuilding feature of the transform is represented in the accompanying code section.

Note that every one of the six wavelets are arranged in a distinct direction. As a different critically-sampled separable DWT, the entirety of the wavelets is liberated

from the checkerboard article. Every sub-band of the 2-D dual-tree transform relates to a particular direction. The figure was delivered with the accompanying MATLAB function ("dualtreeDWT2Dplots.m").

4.8.3.5 Complex 2-D Dual-tree Wavelet Transform

The complex 2-D dual-tree DWT additionally offers to wavelets in six distinct directions, while for this situation, there are two wavelets toward every path as will be delineated below. Toward every path, one of the two wavelets can be explained as the real part of a complex-valued 2D wavelet; however, the latest wavelet can be deciphered as the imaginary part of a complex-valued 2D wavelet. Since the complex version contains twice the same number of wavelets as the real version of the transform, the complex 2-D dual-tree type is 4-times expansive. The complex 2-D dual-tree is executed as four critically-sampled separable 2-D DWTs working equivalently. Because of this, various filter combinations are utilised along the rows and columns. As in the real condition, the summation and difference of sub-band images are executed to obtain the directed wavelets. The complex 2-D dual-tree DWT of an image *x* is computed by the accompanying function, "cplxdualtreeDWT2D.m". The wavelet coefficients *w* is stacked as a cell array. For $j = 1 \dots J, p = 1 \dots 2, k = 1 \dots 2, d = 1 \dots 3, w\{j\}\{p\}\{k\}\{d\}$ are the wavelet coefficients created at scale j and orientation (k, d). With $p = 1$, we obtain the real part and with $p = 2$, we obtain the imaginary part. The image x is taken back from w utilising the inverse transform performed by "IcplxdualtreeDWT2D.m". The ideal reproduction property of the transform is outlined in the accompanying code sample.

4.8.3.5.1 MATLAB Implementation

One procedure for de-noising is wavelet thresholding or wavelet shrinkage. At the point when we decompose information utilizing the wavelet transform, we utilize filters that function as averaging filters, and others that build details. A portion of the subsequent wavelet coefficients compare details in the informational index (high-frequency sub-bands). If the subtleties are small, they may be excluded without the effect of primary highlights of the informational index. The concept of thresholding is to collect all high-frequency sub-band coefficients that are not exactly a specific threshold to zero. After executing the separable DWT, real Dual-Tree DWT, complex

Dual-Tree DWT for 1-D, 2-D and 3-D signals, we can utilize three strategies to expel the noise from an image. The three strategies utilise separable the 2-D DWT "denSDWT2D.m" function, the real 2-D dual-tree DWT "denRDWT2D.m" function, and the complex 2-D dual-tree DWT "denCDWT2D.m" function. Here, these techniques are presented and correlations will be made. The separable 2-D DWT strategy is first presented in the table.

4.8.3.5.2 Review of used and proposed functions

1. "main_dualtreeDWT.m": This function calls the noisy image and loads the de-noising routine.
2. "PSNR.m": This function computes the PSNR value of the de-noised image.
3. "denoise_dualtreeDWT.m": This function calls a number of sub-functions for the determination of the local adaptive image de-noising.
    a. "symmetricext.m": This function is utilised to broaden the noisy image utilising the symmetric extension so as to decrease the limit issue.
    b. "cplxdualtreeDWT2D.m": This function computes the forward Dual-Tree DWT.
    c. "expanded.m": The origin matrix is extended utilizing this function so as to produce a matrix size equivalent to the coefficient matrix.
    d. "BivariateShrinkage.m": It considers the greatness of the complex coefficients. The coefficients are considered utilizing the extents of the complex coefficient.
    e. "bfilter2.m": This function performs 2 D bilateral filtering utilising the strategy, while normalized values in the closed interval [0,1]. The half-size of the Gaussian bilateral filter window is determined by W. The typical deviations of the bilateral filter are designed with SIGMA, while the spatial-domain typical deviation is set with SIGMA (1) and the intensity-domain typical deviation is set by SIGMA (2).
    f. "IcplxdualtreeDWT2D.m": This function computes inverse the wavelet transform.

4.8.3.5.3 Bivariate Shrinkage Functions for Wavelet Based De-noising

We have introduced a simple non-Gaussian bivariate probability distribution function to show the measurements of wavelet coefficients of original images. The method

takes the relationship through a wavelet coefficient and the origin. Utilising the Bayesian evaluation method, we obtain from this a simple non-linear shrinkage function for wavelet de-noising. This popularises the soft thresholding procedure of Donoho and Johnstone. The novel shrinkage function yields increased the issues of the wavelet-based image de-noising.

Let $w2$ perform the origin of $w1$ ($w2$ is the wavelet coefficient at the same spatial position as $w1$, but in the next rough range).

$$y = w + n \tag{34}$$

where $w = (w1, w2)$, $y = (y1, y2)$ and $n = (n1, n2)$. The noise values $n1$, $n2$ are aid zero-mean Gaussian with change sigma_n^2. In view of the exact histograms we have processed, compute the non-Gaussian bivariate:

$$p_{(w)} = \frac{3}{2\pi\sigma^2} . exp\left(-\frac{\sqrt{3}}{\sigma}\sqrt{w_1^2 + w_2^2}\right) \tag{35}$$

At the given, $w1$ and $w2$ are uncorrelated, anyway not free. The MAP estimator of $w1$ yields the accompanying bivariate shrinkage function:

$$\widehat{\omega} = \frac{(\sqrt{y_1^2+y_2^2} - \frac{\sqrt{3\sigma_\eta^2}}{\sigma})}{\sqrt{y_1^2+y_2^2}} . y_1 \tag{36}$$

This has a function of bivariate contraction and the shrinkage increases when the parent value decreases. This is compatible with other types, but here it is determined to utilise a Bayesian evaluation method starting with the novel bivariate non-Gaussian type. The map is shown in the figure below.

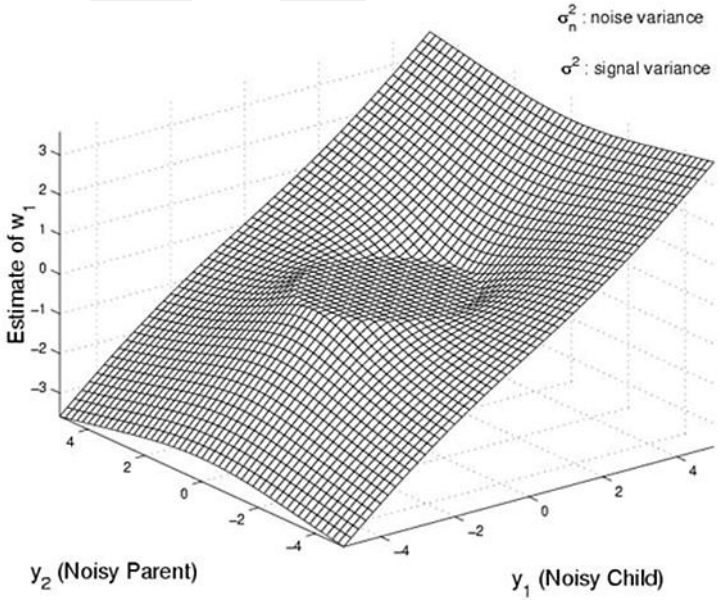

Figure 4.14 A bivariate shrinkage function

The bivariate shrinkage "BivariateShrinkage.m" function is considered as follows:

4.8.3.5.3.1 Local Adaptive Image De-noising

Utilising the bivariate shrinkage function above, we produced an efficient, low complexity, locally adaptive image de-noising method. This shrinkage function needs earlier information on the noise variance and the signal variance for every wavelet coefficient. Subsequently, the method first computes these parameters.

The algorithm is briefly reviewed:

1. Determine the noise variance.
2. For every wavelet coefficient:
    a. Determine the signal difference, and
    b. Evaluate every coefficient utilizing the bivariate shrinkage function.

The following explains the implementation of this method utilising both the separable DWT and the complex Dual-Tree DWT. (Certain applications are implemented).

4.8.4 De-noising using Separable DWT and Dual-Tree DWT with Thresholding

The individual method for de-noising is wavelet thresholding (or "shrinkage"). At the point when we decompose the information utilizing the wavelet transform, we apply filters that go around the averaging filters, and others that provide parts. A portion of the subsequent wavelet coefficients matches with the subtleties in the informational collection (high-frequency sub-bands). If the subtleties are small, they may be rejected without much modification to the fundamental highlights of the informational index. The possibility of thresholding is to set all high-frequency sub-band coefficients that are not exactly a specific threshold to zero. These coefficients are utilized in an inverse wavelet transformation to rebuild the informational index.

After performing the separable DWT, real Dual-Tree DWT, and complex Dual-Tree DWT for 1-D and 2-D signals, we can utilize three different techniques to eliminate the noise from an image. These techniques utilise separable 2-D DWT (code: denSDWT2D.m), real 2-D dual-tree DWT (code: denRDWT2D.m), and complex 2-D dual-tree DWT (code: denCDWT2D.m). In this part, these strategies will be presented and an examination will be given.

The separable 2-D DWT strategy is first presented. This technique consists of two parameters, first of which is for the noise signal and the second for the threshold point. For instance, the noise signal is shown below; dimension of which is 256 × 256. Initially, we take the forward DWT to more than four scales (J = 4). At that point, a de-noising technique, our proposed soft thresholding, is utilized with the wavelet coefficients over all scales and sub-bands. The capacity soft sets coefficients with values not exactly the threshold (T) to zero, and at that point, subtracts T from the non-zero coefficients. After soft thresholding, we take the inverse wavelet transform. The best threshold value for both methods as tested before was T = 0.40. From the resulting table, we can see the de-noising capability of the separable 2-D DWT.

Presently, we need to increase the impact by utilizing a complex 2-D dual-tree DWT. We change the separable 2-D DWT (code: denSDWT2D.m) MATLAB function for a complex 2-D dual-tree DWT (code: denCDWT2D.m). The de-noised results are shown below.

Table 4.11 Separable DWT and Dual-Tree DWT with Thresholding

Separable 2-D DWT with Soft T							
Gaussian Noise	AVERAGE	MAX	MIN	Poisson Noise	AVERAGE	MAX	MIN
p= 0.4	36.82	39.21	31.52	λ= 9	38.76	42.34	37.13
p= 0.6	30.40	33.28	28.85	λ= 10	32.61	35.30	31.06
2-D Dual-Tree DWT with Soft T							
Gaussian Noise	AVERAGE	MAX	MIN	Poisson Noise	AVERAGE	MAX	MIN
p= 0.4	38.97	40.62	37.90	λ= 9	40.10	42.53	38.98
p= 0.6	33.56	35.36	32.51	λ= 10	34.94	38.15	33.33

4.8.5 De-noising using the Separable DWT and the Bivariate Shrinkage Threshold to the magnitudes of the complex coefficients

In our usage, the fundamental function calls the algorithm as a function. In the wake of stacking the input image with the "main_dualtreeDWT.m" function, the determination of the nearby adaptive image de-noising is finished by the MATLAB function "denoise_dualtreeDWT.m".

4.8.5.1 Programs for the De-noising Algorithm

As a first step, we load the noisy image with the "main_dualtreeDWT.m" function. The computation for the local adaptive image de-noising is performed using a

MATLAB function "denoise_dualtreeDWT.m". This function calls many sub-functions. The usage can be summarised as:

1. Insert the window size. The signal difference of a coefficient will be evaluated utilising neighbouring coefficients in a rectangular region of a given window size.
2. Insert the number of stages utilised for the wavelet transform.
3. Submit the noisy image. The noisy image is expanded utilising symmetric extension to obtain the limit issue with the function "symsubmit.m".
4. Compute the forward wavelet transform.
5. Determine the noise variance. The noise difference will be determined to utilise the robust median estimator.
6. Prepare every sub-band independently. We process every sub-band inside a loop until regarding our stocks of wavelet coefficients in a cell array. Initially, the coefficient and the corresponding parent matrices were prepared for every sub-band, and the origin matrix was expanded using the "expanded.m" function so as to obtain the matrix size equivalent to the coefficient matrix.
7. Determine the signal variance and the threshold value: The signal variance for every coefficient is computed utilising the window size and the threshold value for every coefficient will be determined and stacked in a matrix with the same size as the coefficient matrix.
8. Determine the coefficients. The coefficients will be evaluated utilising the noisy coefficient, its parent, and the assessed Bivariate Shrinkage value with the MATLAB function "BivariateShrinkage.m".
9. Compute the opposite wavelet transforms.
10. The de-noised image extraction. The important section of the resultant image is obtained in order to invert the symmetric extension operation.

Table 4.12 Separable DWT and the Bivariate Shrinkage Threshold

Separable DWT and the Bshrink							
Gaussian Noise	AVERAGE	MAX	MIN	Poisson Noise	AVERAGE	MAX	MIN
p= 0.4	40.39	41.28	37.53	λ= 9	44.68	46.80	43.56
p= 0.6	35.30	36.78	30.98	λ= 10	34.62	37.30	33.06

4.8.6 De-noising using the Dual-Tree DWT and the Bivariate Shrinkage Threshold rule with the magnitudes of complex coefficients

The execution of the de-noising algorithm is similar to the separable DWT method. We obtain slight contrasts, which is the Bivariate Shrinkage rule, to the sizes of the complex coefficients. They are about moving invariant, little sign movements don't influence the sizes, and as such, they influence the real and imaginary parts. Subsequently, magnitude data is also more dependable than any real or imaginary parts. The method does not modify the angle. The "main_dualtreeDWT.m" function uploads the noisy image, returns the de-noising routine and calculates the PSNR value of the resultant image.

4.8.6.1 Programs for the De-noising Algorithm

Subsequent to stacking the initial image using the "main_dualtreeDWT.m" function, the computation for of local adaptive image de-noising is finished using the MATLAB function "denoise_dualtreeDWT.m". The function uploads a few sub-functions. The execution can be outlined as:

1. Determine the window size. The signal difference of a coefficient is determined to utilise neighbouring coefficients in a rectangular region of given window size.
2. Set what number of stages will be utilised for the wavelet transform.
3. Submit the noisy image. The noisy image is extended using a symmetric extension in order to improve the boundary problem with the "symmetricext.m" function.
4. Compute the forward dual-tree DWT using "cplxdualtreeDWT2D.m".
5. Set the noise variance. The noise variance is computed utilising the robust median estimator.
6. Determine the signal variance and the threshold value: The signal variance for every coefficient is calculated utilising the window size and the threshold value for every coefficient will be computed and stacked in a matrix the same size as the coefficient matrix.
7. Determine the greatness of the complex coefficients. The coefficients will be assessed utilising the extents of the complex coefficient, its parent and the Bivariate Shrinkage value with a MATLAB function "BivariateShrinkage.m".
8. Compute the opposite wavelet transforms utilizing "IcplxdualtreeDWT2D.m".

9. Extract the image. The necessary section of the final image is obtained in order to invert the symmetric extension operation.

Table 4.13 Dual-Tree DWT and Bivariate Shrinkage

Dual-Tree DWT and Bshrink							
Gaussian Noise	AVERAGE	MAX	MIN	Poisson Noise	AVERAGE	MAX	MIN
p= 0.4	41.62	43.08	37.94	λ= 9	47.23	50.93	40.96
p= 0.6	36.99	39.28	31.59	λ= 10	38.35	41.94	32.12

4.8.7 De-noising using the Dual-Tree Complex DWT combined with the Bivariate Shrinkage and Bilateral Filter to the magnitudes of the complex coefficients

The image is decomposed inside its different frequency sub-bands using a complex wavelet transform. Before the signal is reconstructed [45]. showed that a bilateral filter is very useful for removing the noise of the low-frequency sub-band, while thresholding is a better choice for eliminating high-frequency sub-bands. Using the same strategy, we have proposed a new image de-noising method as illustrated in Figure 4.15. The signal is decomposed into its different frequency sub-bands using the complex wavelet transform. Before the signal is reconstructed, the low-frequency sub-band of the real and imaginary parts are filtered using the bilateral filtering method, which is used to remove the noise of the low approximation sub-bands while the Bivariate Shrinkage thresholding method is used for de-noising the high-frequency sub-bands of the real and imaginary parts. In fact, the proposed image de-noising framework combines bilateral filtering and Bivariate Shrinkage thresholding methods to take advantage of both methods. In this section, we demonstrate that the proposed framework using a Dual-Tree Complex Wavelet Transform (DT-CWT) more efficiently produces results than the one using the conventional wavelet. This result was expected due to the benefits of the complex wavelet transform compared with the conventional wavelet which has more efficient directional selectivity and the shift-invariant property.

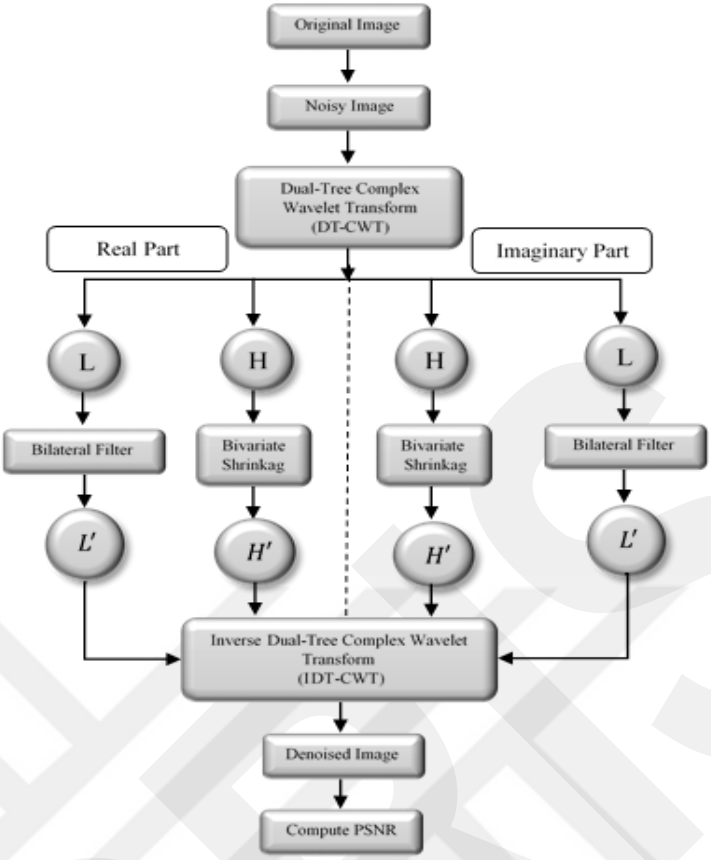

Figure 4.15 Flowchart for de-noising using the Dual-Tree Complex DWT combined with the Bivariate Shrinkage and Bilateral Filter for the magnitudes of the complex coefficients

In order to investigate the performance of the proposed framework both visually and quantitatively, several experiments were performed on 400 cephalometric X-ray images. This section does a quantitative comparison by simulating noisy images. In the simulation, white Gaussian noise and Poisson noise with various standard deviations are added to the standard test images. The de-noising algorithms are used to de-noise the images and the PSNR results are computed. Here, 400 noisy images are simulated by computing the white Gaussian noise and Poisson noise with a standard deviation. The PSNR results for the proposed method are included in Table 4.14. As can be seen from this table, the suggested method has a more efficient performance in terms of PSNR.

Table 4.14 Dual-Tree Complex DWT combined with the Bivariate Shrinkage and Bilateral Filter for the magnitudes of the complex coefficients

Dual-Tree DWT based Bishrink and Bfilter							
Gaussian Noise	AVERAGE	MAX	MIN	Poisson Noise	AVERAGE	MAX	MIN
p= 0.4	42.25	45.86	38.10	λ= 9	47.90	50.95	40.82
p= 0.6	37.46	39.91	31.38	λ= 10	40.18	45.79	32.34

4.8.8 Multi-Sensor images de-noising using wavelet fusion based on the Dual Tree Complex Wavelet Transform (DT-CWT) and Bilateral Filtering

For analysis of the information of images, multi-sensor analysis has been proven to be an effective tool [20-23]. After applying the Dual Tree Complex Wavelet Transform (DT-CWT) "cplxdualtreeDWT2D.m" to both noisy images, the signal variance for each coefficient of each noisy image is determined using the window size, and the threshold value for every coefficient will be computed and kept in a matrix of similar size to the coefficient matrix. The bilateral filtering method is utilized to remove the noise of the low approximation sub-bands of both images and the Bivariate Shrinkage thresholding method is utilized to de-noise the high-frequency sub-bands of real and imaginary parts. The de-noised sub-bands of both the real and imaginary parts are fused using the wavelet transform fusion rule for the real and imaginary parts of both images to obtain one single real and one imaginary part. A multi-sensor decomposition of an image is a biorthogonal basis and results in non-redundant image representation. This basis is called wavelets.

Initially, the images are modelled into the wavelet domain using the wfusimg () function, which is presented as the number of scales, the wavelet channel, and the edge dealing with are indicated. Later, a decision mask is constructed. Computation of the inverse complex wavelet transform of the de-noised sub-bands (high-frequency and low-frequency) to obtain the de-noised image is performed using the "IcplxdualtreeDWT2D.m" function. The fundamental part of the last image is removed to invert the symmetrical extension. De-noising algorithms are used to extract de-noised images and the PSNR results are computed.

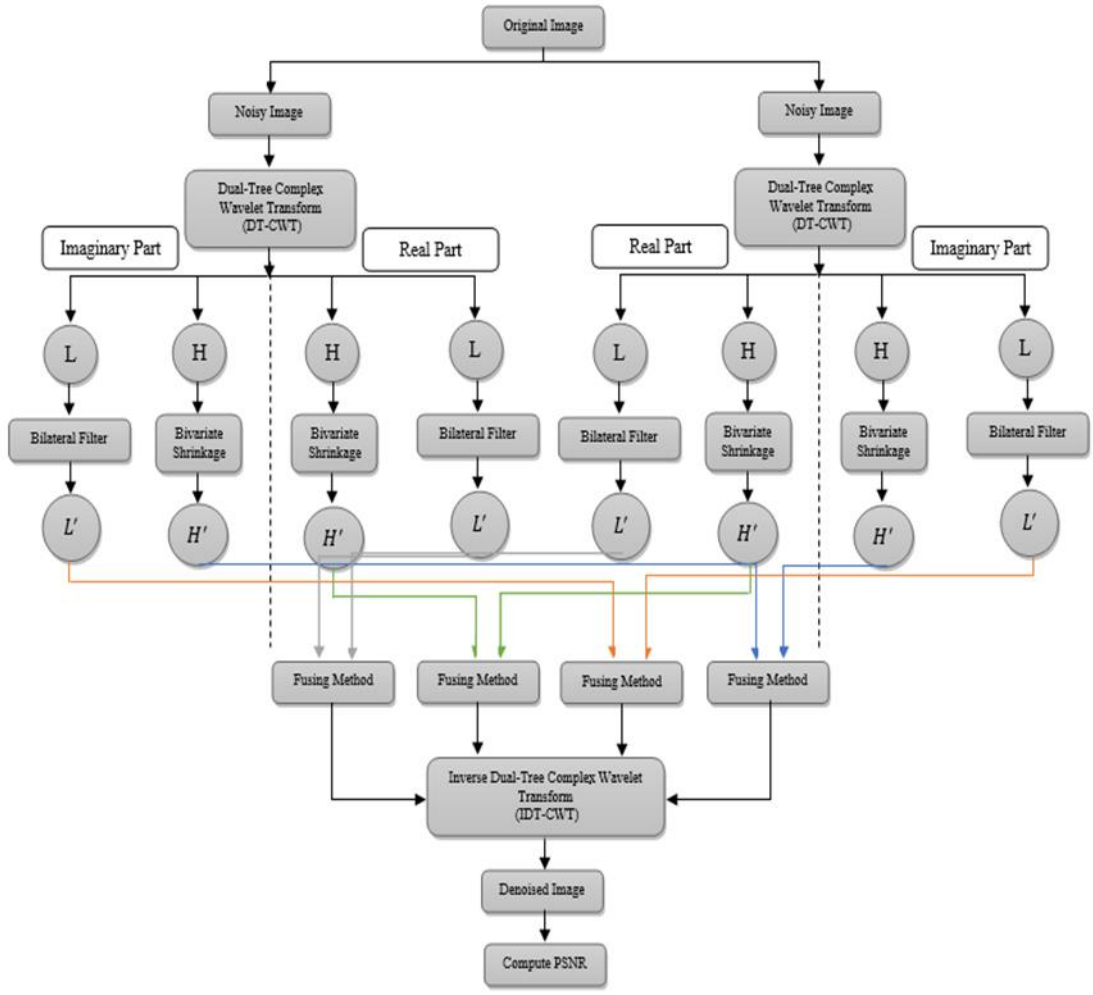

Figure 4.16 Flowchart of fusion based on the Dual Tree Complex Wavelet Transform (DT-CWT) and Bilateral Filtering

In this work, the proposed method is an image fusion method using a combination of Bivariate Shrinkage thresholding and an enhanced Bilateral Filtering method stemming from on the function of the Dual-Tree Complex Wavelet Transform (DT-CWT). The outcome of the examination and tests for 400 cephalometric X-ray images show that the proposed strategy gives better visual and quantitative results in comparison with the other de-noising methods. The fusion of two images is more efficiently done from one of the images de-noising methods. It gives more efficient results than other combinations.

Table 4.15 Fusion based on the Dual-Tree Complex Wavelet Transform (DT-CWT) and Bilateral Filtering

Fused Dual-Tree DWT and the Bishrink and Bfilter							
Gaussian Noise	AVERAGE	MAX	MIN	Poisson Noise	AVERAGE	MAX	MIN
p= 0.4	44.94	47.31	38.96	λ= 9	49.32	53.28	40.95
p= 0.6	38.11	40.70	33.53	λ= 10	41.77	46.08	33.25

For a visual comparison, eight methods were used with two different noise types with two parameters for each, as shown in Tables 4.16, 4.17, 4.18 and 4.19. The PSNR values of the de-noised images for the eight methods are shown in Tables 4.16 and 4.17, which show the de-noising of the Gaussian noise with $p = 0.4$ and $p = 0.6$. The PSNR values of the de-noised images for the eight methods are presented in Tables 4.18 and 4.19, which show the de-noising of the Poisson noise at $\lambda = 9LE$ and $\lambda = 9LE$.

As can be seen from these tables, the proposed methods provide a more efficient visual performance such that the PSNR is higher and the noise is more efficiently attenuated using the proposed method.

Table 4.16 PSNR values of de-noising the eights methods of Gaussian noise with $p = 0.4$

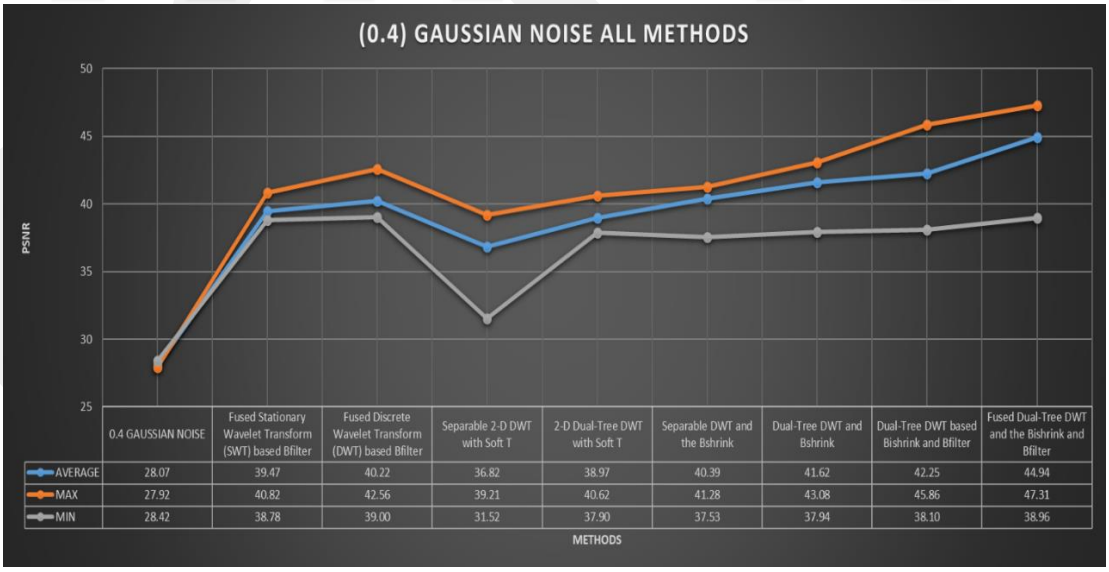

Table 4.17 PSNR values of de-noising the eights methods of Gaussian noise with $p = 0.6$

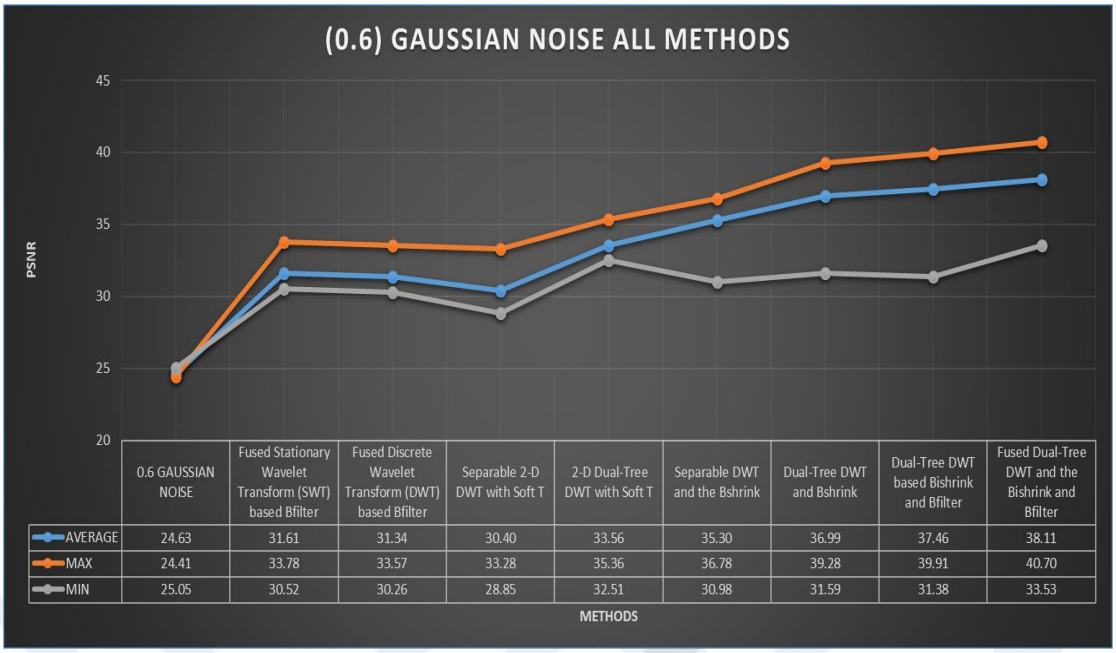

	0.6 GAUSSIAN NOISE	Fused Stationary Wavelet Transform (SWT) based Bfilter	Fused Discrete Wavelet Transform (DWT) based Bfilter	Separable 2-D DWT with Soft T	2-D Dual-Tree DWT with Soft T	Separable DWT and the Bshrink	Dual-Tree DWT and Bshrink	Dual-Tree DWT based Bishrink and Bfilter	Fused Dual-Tree DWT and the Bishrink and Bfilter
AVERAGE	24.63	31.61	31.34	30.40	33.56	35.30	36.99	37.46	38.11
MAX	24.41	33.78	33.57	33.28	35.36	36.78	39.28	39.91	40.70
MIN	25.05	30.52	30.26	28.85	32.51	30.98	31.59	31.38	33.53

Table 4.18 PSNR values of de-noising the eights methods of Poisson noise with $\lambda = 9LE$

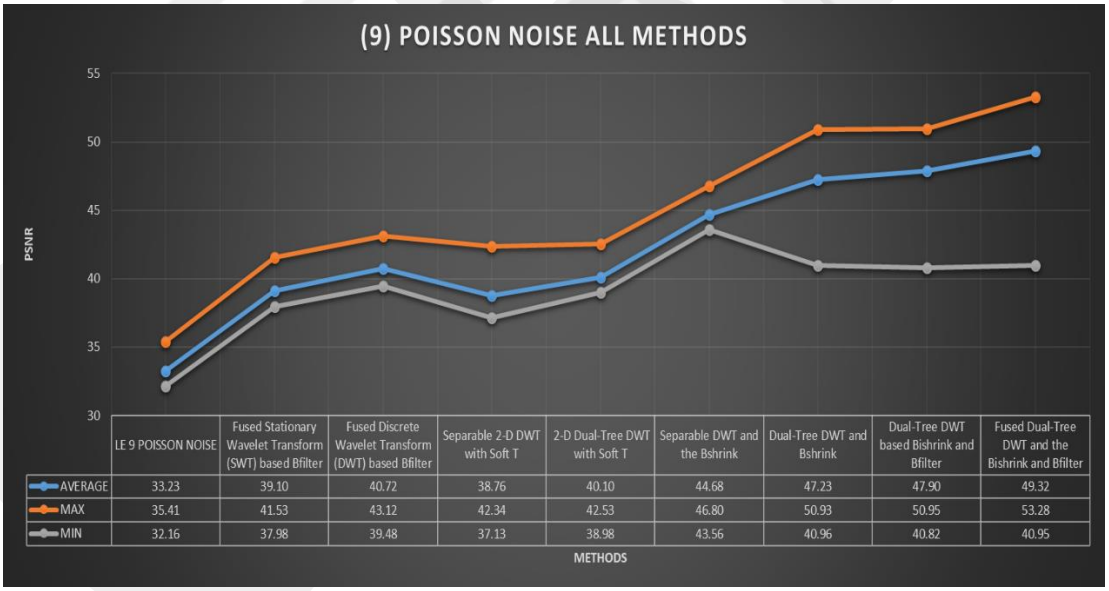

	LE 9 POISSON NOISE	Fused Stationary Wavelet Transform (SWT) based Bfilter	Fused Discrete Wavelet Transform (DWT) based Bfilter	Separable 2-D DWT with Soft T	2-D Dual-Tree DWT with Soft T	Separable DWT and the Bshrink	Dual-Tree DWT and Bshrink	Dual-Tree DWT based Bishrink and Bfilter	Fused Dual-Tree DWT and the Bishrink and Bfilter
AVERAGE	33.23	39.10	40.72	38.76	40.10	44.68	47.23	47.90	49.32
MAX	35.41	41.53	43.12	42.34	42.53	46.80	50.93	50.95	53.28
MIN	32.16	37.98	39.48	37.13	38.98	43.56	40.96	40.82	40.95

Table 4.19 PSNR values of de-noising the eights methods of Poisson noise with $\lambda = 10LE$

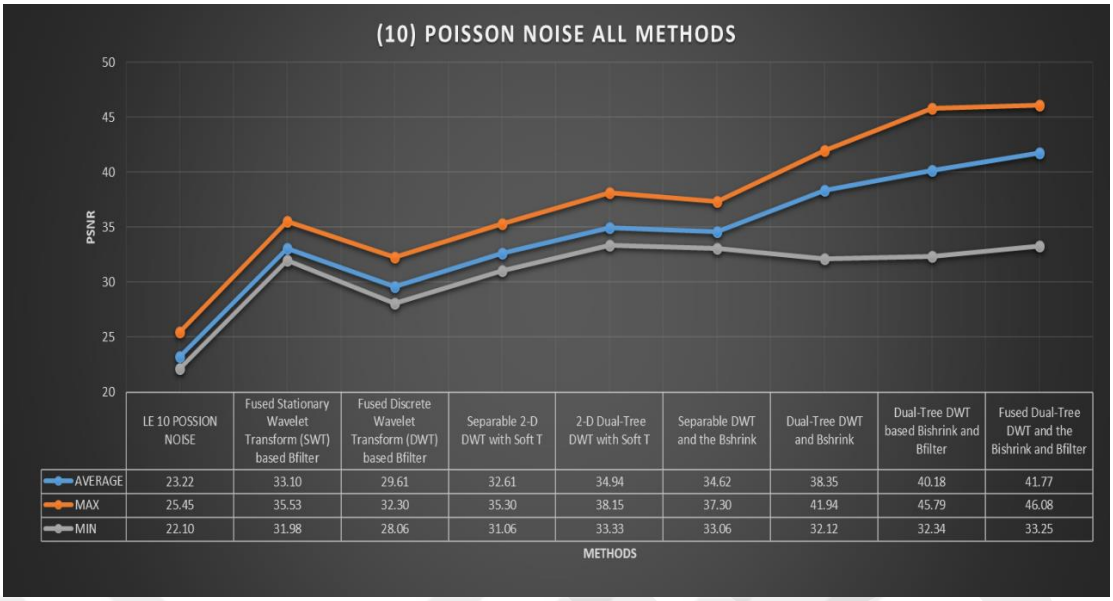

LE 10 POSSION NOISE	Fused Stationary Wavelet Transform (SWT) based Bfilter	Fused Discrete Wavelet Transform (DWT) based Bfilter	Separable 2-D DWT with Soft T	2-D Dual-Tree DWT with Soft T	Separable DWT and the Bshrink	Dual-Tree DWT and Bshrink	Dual-Tree DWT based Bishrink and Bfilter	Fused Dual-Tree DWT and the Bishrink and Bfilter
AVERAGE	23.22	33.10	29.61	32.61	34.94	34.62	38.35	40.18	41.77
MAX	25.45	35.53	32.30	35.30	38.15	37.30	41.94	45.79	46.08
MIN	22.10	31.98	28.06	31.06	33.33	33.06	32.12	32.34	33.25

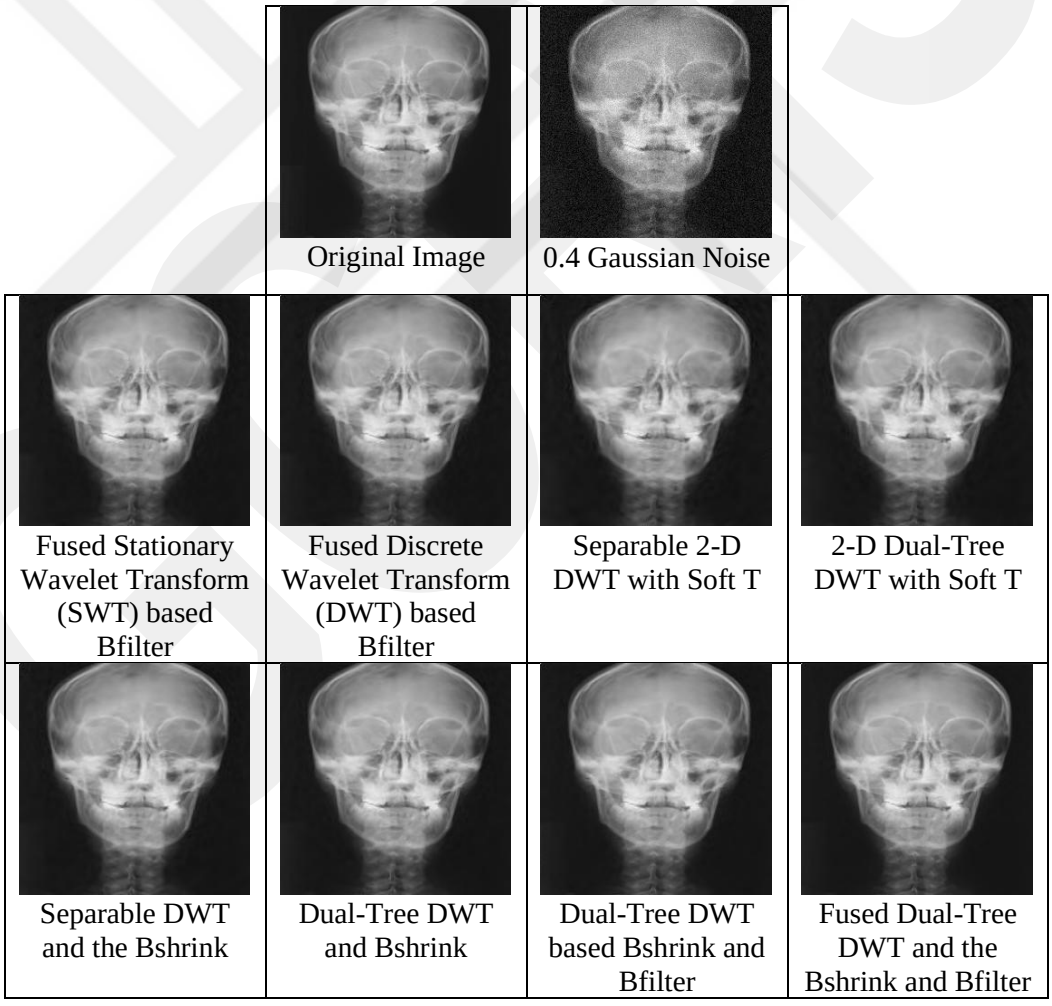

Figure 4.17 Example of image de-noising the eights methods of Gaussian noise with $p = 0.4$

CHAPTER 5

DISCUSSION AND CONCLUSION

5.1 Discussion

There are different existing techniques for denoising images. The significant characteristic of a decent picture denoising method is that it ought to totally expel noise while protecting edges. This proposal presents reviews of some significant works in the field of picture denoising. There have been various methods produced and each technique has its own presumptions, focal points, and restrictions. We took into consideration that there are other additional standards, for instance, enormous estimations of higher subordinates or wavelet coefficients. For commotion expulsion, the fundamental model for picture corruption is an added substance noise type. The reason for this theory is to introduce a review of computerized picture denoising approaches. As pictures are significant in every single field in this way, image denoising is a significant pre-handling task before further preparing pictures in terms of division, include extraction, surface investigation, and so on. The earlier study presents the various models of noises that can degenerate the picture and various kinds of filters which are utilized to improve the corrupted picture. The investigation of different denoising procedures for advanced pictures presents that wavelet transform prevails over the other standard spatial area transform. Spatial transform works by streamlining a fixed window and it produces articles around the target and now and then causes smoothing in this manner causing obscuring of the picture. In this way, the wavelet transform is most appropriate for execution due to its properties like sparsity, multiresolution, and multiscale nature. In the market, we can find some systems for medical image de-noising such as dental radiography image de-noising and de-noising using some of these techniques. But almost none of the available systems still do not include techniques that cover the types of noise that distort cephalometric X-ray images and they do not recognize which types of techniques have the best results and less distortion to the noisy image. Our thesis aims to play a part in the literature with an interest to utilize image denoising techniques to improve dental

image radiography. To test the thesis methods effectiveness, we used a single dataset, which is a dental radiography database (DX). This dataset has 400 cephalometric X-ray images, gathered from 400 patients, with a resolution of 1935×2400 with a pixel spacing of 0.1 mm. For this objective of the study, a GUI was produced utilizing MATLAB and its toolboxes. If we try to explain our thesis briefly, there are twenty-one methods presented in this thesis: The first thirteen methods present the image enhancement methods that are related to our thesis and these methods are used within the stages of our proposed denoising procedure. These methods are presented as follows: The first eight methods are presenting image de-noising action using thresholding and Shrinkage methods, then there are two methods of filters in image filtering, and finally there are three methods of fusing methods. The last eight methods are consisting of several stages, and each one of these stages are produced from the best pre-tested method results. There are some measures taken to reduce the problems. The following action has been considered before considering the effectiveness of Poisson noise and Gaussian noise on the 400 cephalometric X-ray images the whole Cephalometric X-ray images converted from TIFF format to Grayscale image and then we resized the 400 cephalometric X-ray images to 256 x 256 to keep a similar sample size for training. After image denoising and image fusions procedure was complete, objective evaluation results extracted into the possession of and spectral index charts were generated from the fused image bands. The expansion in spatial goals is not just seen by target assessment yet in addition obvious to the unaided eye see when pictures are zoomed in for a closer view as shown for the case study. Picture combination is a significant apparatus for improving the spatial goals of picture information. Regardless of the loss of some target details and ghastly data, better detachment of ground material without utilizing unrivalled warm infrared pictures from different stages and satellites was demonstrated to be conceivable. Image de-noising methodology has the hierarchical shape and contains many phases at each phase that have many technologies, in our thesis firstly we consider each phase separately. In image noising types we considered the types of Cephalometric X-ray image noises and we performed the two effective noise types to discover the actual effectiveness of our proposed methods in de-noising Cephalometric X-ray images. Wavelet coefficients are contrasted with a threshold and it decides which coefficients ought to be set to zero. The definition of the value of the threshold is critical as a greater value may result in

loss of data while a lower value may permit noise to proceed. The best possible parameter of the threshold can be defined from multiple perspectives. In our thesis, we test each type of method or technique with many parameters to set the best and the higher PSNR value which means higher resolution and less image information loss.

In the image filtering process, we have used image filtering and the PSNR values if the Bilateral filtering gives the best results and for the reason of the bilateral filtering is depends on sigma space and sigma range we examine the 11 parameters for each to produce the higher PSNR value. The second style of the image denoising is the image thresholding and in our thesis, we used a number of thresholding types, some of which are hard thresholding and soft thresholding and for each type, we tested them with different parameters to find the pick parameters with higher resolution. As an additional type of thresholding in our thesis, we employ and build a comparison of the six types of wavelet thresholding with different four parameters and the outcomes shows from the PSNR values as seen in the tables, without a doubt, Bivariate Shrinkage presents more suitable results under various noise change conditions for all images. The second part of our thesis was about image fusion and its types were we used our thesis with five fusion rule classes, which are maximum, average rule, absolute average rule, and two wavelet fusions which are Daubechies (db), Symlets implement the methods on 400 cephalometric X-ray images. The Wavelet Transform function at 4 level wavelet decompositions using the 'Symlets' wavelet by taking the maximum for approximations and minimum for details, is producing the best PSNR values. The main part of our thesis is the three wavelet transforms which are the noisy images that are decomposed into high and low sub-bands the main propose of the decomposition is to separate the frequency of the image to produce the process of the denoising methods with minimum information of the details of the original image. The last five proposed methods of our thesis were collected from the best methods results and implement in the steps of decomposition and filtering and shrinking. The last four tables are the comparison of eight proposed methods on 400 real cephalometric X-ray images on two different noises with two different values of noise for each and the PSNR values show the advantage of each method. The denoising using dual-tree complex wavelet transform (DTCWT) has overcome the what happened in the stationary wavelet transform (SWT) and discrete wavelet transform (DWT) and the image sharpness has increased significantly compared to the previous methods. These

methods are accompanied by the assistance of the wavelet fusion function of the image, which aids to obtain better results which are creating a new image that is more suitable for the purposes of human visual perception.

In Discrete Wavelet Transform (DWT) strategies it is simple to execute, diminishes the calculation time and assets required. It gives vitality compaction, bigger SNR, and increasingly exact clinical data for medical determination and assessment. The disadvantage of DWT techniques it presents bad directionality, Shift affectability, Absence of stage data, and nearness of spectral corruption. The Dual-Tree Complex Wavelet Transform (DTCWT) techniques give better picture visual prominence and move invariance include however it has constrained directionality and it presents associating. The combination of Images utilizing their Multiscale edges are reproduced a nearby and outwardly estimate of the information picture additionally it is steady for somewhat altered information pictures. It is conceivable to stifle the nonlinear noise in the picture just as some light surfaces, yet it does not give the specific estimate of the information picture. The Principal Component Analysis (PCA) is a subjective number of groups that can be utilized, and it is a basic calculation likewise it lessens the dimensionality of huge informational indexes. The PCA presents a decent lot of entropy yet it is a pixel-based combination procedure subsequently pictures can be obscured, and the difference of the melded picture is not acceptable. Picture Fusion Based on Multi-Resolution Domain strategies is a combination of pictures that causes it conceivable to advance data to be dealt with and combination to can be viable for specific frameworks of symbolism. The disadvantage of these types of methods is it can prove to be insufficient combination procedures for different frameworks of symbolism. The Complex Wavelet Transform (CWT) techniques are given greatness or stage, move invariant, and free from associating however it is generally costly and computationally concentrated. The Discrete Cosine Transform strategies are easy, quick, and vitality proficient multi-centre picture combination plot likewise gives a good outcome to grayscale pictures. The disadvantage of these types of methods is devouring additional time than the wavelet-based strategy as two diffs multiscale disintegration forms are processed. The Daubechies Discrete (db2) Wavelet Transform strategies can oversee various picture goals and give preferred outcomes over Haar Transform. It offers just the wavelet coefficient worth and unfit to give good outcomes over Shift Invariant Discrete Wavelet Transform for Image Fusion and Redundant

Discrete Wavelet Transform. The Symlet wavelets-based picture combination techniques are a lot of like the Daubechies wavelets except for the main contrast being the disappearing snapshots of the wavelets work. In this way, the wavelet coefficients contrast from that of the Daubechies. The limitation of the Symlets wavelets equivalent to Daubechies Discrete is bad coordination is the main worry on account of Symlets.

The proposed denoising techniques make up for all the impediments of DWT by the usage of improved DT-CWT. It additionally takes out the ringing ancient rarities introduced in the intertwined picture by allocating a reasonable weighting to high pass wavelet coefficients and low pass coefficients independently. The standardized most extreme inclination constructed sharpness model for low-frequency coefficients recover the foundation information just as extends the nature of the obscured territories in the combination result. The most indispensable information substance covered up in the high-recurrence coefficients is likewise expanded up by the doing of bilateral intensity basis. The current work is an early endeavour to investigate various kinds of theories for medical picture denoising under different structures. Beginning from channel draws near, an increasingly refined and new component of fix based denoising is attempted. All strategies proposed are planned as productive as their contemporary techniques, if not better. All tests are executed on cephalometric X-ray pictures datasets; be that as it may, the equivalent is investigated for some genuine datasets as and whenever the situation allows. The combination system utilizing the wavelet transform techniques presents with an increased quality nature of the fusion since the essential combination strategies respected to lose some picture subtleties and significant information during the executing procedure. The wavelet transform combination technique is introduced as the number of scales, the wavelet channel, and the edge managing are shown. The outcomes approved had dependent on picture measurements. Picture combination dependent on wavelet transform and Duel Tree was appraised between 40% to 50% which had a higher rating given from different calculations. The proposed strategy is higher than the other three strategies and it is closest to one which shows a lot of striking data is moved to the intertwined picture. Since DT-CWT permits the parting of rough just as the detail coefficients; naturally, its presentation is better than that of other DT-CWT and different strategies. Along these lines, the proposed strategy delivers the melded picture nearest to those the relating multi-sensors would see at the high-goals level. We have discovered that the

ideal estimation of the reciprocal channel is straight identified with the standard deviation of the commotion. The ideal estimation of the is moderately autonomous of the commotion power. Considering these outcomes, we gauge the noise standard deviation at every degree of the sub-band disintegration and utilize a consistent difference of it for the esteem for respective separating. For the Gray-scale pictures, related wavelet thresholding techniques will even now keep some irregular noises in the picture which can be unmistakably discovered. However, the proposed strategies dependent on the reciprocal channel can evacuate the commotions in the picture well overall. Notwithstanding, the first single-level reciprocal channel has a more grounded power parameter than the staggered multi-level bilateral filter with the end goal that it will lose a few subtleties in the picture. With wavelet thresholding, a multi-level bilateral filter can wipe out the noises in the high-recurrence parts without a clear impact.

Utilizing wavelet thresholding alone is not viable for the genuine loud pictures. The motivation to clarify this can be induced that since wavelet thresholding depends on the powerful middle estimation, the real noise does not have a similar property as the standard irregular commotion so it could not be evaluated accurately. The key factor in the presentation of the proposed technique is the multi-sensor use of the mixing of the bilateral filter and wavelet thresholding. It assisted with wiping out the coarse-grain commotion in pictures. The wavelet thresholding adds capacity to the proposed technique the numerous kinds of noise segments cannot be wiped out with the bilateral filter. The first objective of our proposal was denoising, in which case a little spatial part does the trick, and the remaining of the filter is disposed of as the noise segment. Interestingly, numerous new applications influence the reciprocal transform to make two-scale deteriorations that depend on enormous spatial parts and where the lingering of the filter is saved on the grounds that it is considerably more pertinent to the human visual framework.

5.2 Future Work

With our final words, we accident an outlook into the future. Better image denoising quality impacts any image processing system, like it, is found in digital cameras.

Nowadays, state-of- the-art denoising methods are up to this time too slow for integration into consumer products. Advanced pictures are become bigger by the super pixels and customers request intuitive execution, so far numerous strategies require minutes to process even a little test picture. More straightforward techniques have a favourable position that investigative stunts can prompt execution enhancements. Picture denoising is the beginning stage for some related issues. It ought to be noticed that the Wavelet picture combination can utilize distinctive combination administers other than utilized in this investigation. It might be conceivable to show signs of improvement results from Wavelet change by picking a combination rule fitting for the picture utilized or making an altogether new standard to meet wanted specifications. For future investigations, it is suggested that more picture combination techniques ought to be tried with cephalometric X-ray pictures from various gadgets.

5.3 Conclusion

In this thesis, we presented a new multi-sensor image de-noising framework, taking the benefits of enhanced Bilateral Filtering and complex wavelet thresholding. In the suggested framework, two noisy images are decomposed into low- and high-frequency components using the Dual-Tree Complex wavelet transform, and enhanced Bilateral filtering is utilized in the low-frequency sub-bands. Bivariate Shrinkage wavelet thresholding is utilized on the high-frequency sub-bands. The wavelet fusion method is used in both the low- and high-frequency de-noised sub-bands of the two images to obtain one merged low sub-band and one high sub-band. Then, the inverse complex wavelet transform is utilized in the de-noised sub-bands. In this thesis, twenty-one methods are presented. The first thirteen methods present the image enhancement methods that have related to our thesis and these methods are used in the steps of our proposed denoising procedure. These methods are presented as follows: The first eight methods were presented the image de-noising using thresholding and Shrinkage methods, then two methods of filters in image filtering, finally three methods of fusing methods. The last eight methods are consisting of several stages, and each stage of these stages were produced from the best pre-tested method results. Experiments on 400 real cephalometric X-ray images presented the effectiveness of the given frameworks. This thesis presents a denoising method for enhanced images using

DTCWT and the Bivariate shrinkage threshold based on the bilateral filter. The modified image influences the difference improvement process. Therefore, the denoising procedure will be treated to decrease deformation under the DTCWT domain. At first, noisy image pixels are DE correlated to obtain coarser and better segments, and additional noise details are distorted in the high- frequency sub-bands. In order to decrease the spatial deformation through filtering, the bivariate shrinkage function is utilized in the DTCWT domain. Utilizing spatial filtering and transform domain filtering gives us the ability to minimize the impact of noise in the images. Within the transform domain, the wavelet strategy performs better denoising and simultaneously protect the details of images such as edges. In order to overcome several disadvantages while using the Dual-Tree Complex Wavelet Transform (DTCWT), an ideal reconstruction process occurs that outperforms the conventional wavelet transform.

REFERENCE

[1] M. C. Motwani, M. C. Gadiya, R. C. Motwani, and Jr. F. C. Harris, "Survey of image de-noising techniques", Proceedings of GSPx 2004, Santa Clara Convention Center, CA, USA, Sep 2004.

[2] M. Zhang and B. Gunturk, "A New Image De-noising Method based on the Bilateral Filter", Proceedings of ICASSP, IEEE, pp. 929-932, 2008.

[3] H. Guo, J. E. Odegard, M. Lang, R. A. Gopinath, I.W. Selesnick and C. S. Burrus, "Wavelet based speckle reduction with application to SAR based ATD/R", First International Conference on Image Processing, 1, pp. 75-79, Nov, 1994.

[4] R. D. Nowak, "Wavelet-Based Rician Noise Removal for Magnetic Resonance Imaging", IEEE Transaction on Image Processing, 8(10), pp. 1408-1419, Oct 1999.

[5] A. Chambolle, "Nonlinear wavelet image processing: Variational problems, compression, and noise removal through wavelet shrinkage", IEEE Transaction on Image processing, 7, pp. 319-335, 1998.

[6] G.L Fan, and X.G. Xia, "Image De-noising Using Local Contextual Hidden Markov Model in the Wavelet Domain", IEEE Signal Processing Letters, 8(5), pp. 125-128, May 2001.

[7] I. Daubechies, "Ten Lectures on Wavelets", Society for Industrial and Applied Mathematics3600 University City Science Center Philadelphia, PAUnited States, 1992.

[8] S. Mallat, "Wavelets for Vision", Proceedings of IEEE, 84(4), pp. 604-614, Apr 1996.

[9] D.L. Donoho, I.M. Johnstone, "Ideal spatial adaptation by wavelet shrinkage", Biometrika, 81(3), pp. 425-455, 1994.

[10] D. L. Doiioho, "De-noising by soft thresholding", IEEE Transaction on Information Theory, 41(3), pp. 613-627, May 1995.

[11] A. Kakadiya, R. Tandon, A. Azam, R. Kulshrestha and M. Bhardwaj, "Recent Advancements in Diagnostic Aids in Orthodontics - A Review", Department of Orthodontics and Dentofacial Orthopaedics, Career PG Institute of Dental Sciences, India Sep 05, 2017.

[12] Cda, "Dental Radiographs (X-Rays)", California Dental Association 1201 K Street, Sacramento, CA 95814 800.CDA.SMILE cda.org.

[13] M. B. G. d. Silva, E. F. S. Anna, "The evolution of cephalometric diagnosis in Orthodontics", Dental Press J. Orthod. vol.18 no.3 Maringá May/June 2013.

[14] K. N. Alexander, DDS, "Genetic and Phenotypic Evaluation of the Class Iii Dentofacial Deformity: Comparisons of Three Populations", degree of Master of Science in the School of Dentistry (Orthodontics), Chapel Hill 2007.

[15] A. S. Cohen and A. Lapidoth, "The Gaussian Watermarking Game", IEEE transactions on Information Theory, Vol. 48, No. 6, June 2002.

[16] P. Subbuthai, K. Kavithabharathi, S. Muruganand, "Reduction of types of Noises in dental Images", International Journal of Computer Applications Technology and Research Vol. 2– Issue 4, 436 - 442, 2013.

[17] D. T. Kuan and A. A. Sawchuk, "Adaptive noise smoothing filter for images with signal dependent noise", IEEE Trans. Pattern Anal. Mach. Intell., Vol. PAMI-7, no. 2, pp. 165–177, 1985.

[18] Y. Srinivasan, B. Nutter, S. Mitra, B. Phillips, D. Ferris, "Secure transmission of medical records using high capacity steganography", in Proc. 17th IEEE Symposium on Computer Based Medical Systems, pp.122-127, 2004.

[19] D. Anand, U.C. Niranjan, "Watermarking Medical Images with Patient Information", in Proc. Int. Conf. IEEE-EMBS, pp. 703–706, 1998.

[20] V. Licks and R. Jordan, "Digital Image Watermarking Robust to Geometric Transformations", Proceedings of 2000 International Conference Image Processing (ICIP 2000), Vol. 3, pp. 690-693, 2000.

[21] Ho, A.T.S., Zhu, X., Shen, J., "Authentication of biomedical images based on zero location watermarking", In: Proceedings of Control, Automation, Robotics and Vision Conference, Vol. 2, pp. 973–976.

[22] H-.M. Chao, C-.M. Hsu, S-.G. Miaou, "A data-hiding technique with authentication, integration, and confidentiality for electronic patient records", IEEE Trans. on Information Technology in Biomedicine, Vol.6, No.1, pp.46-53, 2002.

[23] J. Nayak, P.S. Bhat, M.S. Kumar, R. Acharya, "Reliable transmission and storage of medical images with patient information using error control codes", in Proc.IEEE INDICON, pp.147-150, 2004.

[24] N. Nikolaidis, I. Pitas, "Copy right Protection of images using robust digital signatures", in proceeding, IEEE International Conferences on Acoustics, Speech and signal processing, Vol.4, pp. 2168-2171, May 1996.

[25] M. Barni, F. Bartolini, "Data hiding for fighting piracy", IEEE Signal Processing Magazine, Vol. 21, No.2, pp.28–39, 2004.

[26] X. Luo, Q. Chanag, J. Tun, "A Lossless Data Hiding Scheme for Medical Images in Application of e-diagnosis", Proceedings of the 12th Annual International Conference of IEEE EMBS, Cancum, Mexico, September 17-21, 2003.

[27] M. A. H. A. M. El-Bey Bourennane, "A Watermarking of Medical Image: Method Based LSB", Journal of Emerging Trends in Computing and Information Sciences ©2009-2011 CIS Journal. Vol. 2, No. 12, ISSN 2079-8407 all rights reserved, December 2011.

[28] D. Anand, "Compact Storage of Medical Images with Patient Information", IEEE Transaction on Information Technology in Biomedicine, Vol. 5, No. 4, pp. 320-323, December 2001.

[29] B. Ramakrishnan, N. Sriraam, "Internet transmission of DICOM images with effective low bandwidth utilization", Journal of Digital Signal Process, Vol.16, pp. 825–831, 2006.

[30] S. Jadhav, "Image Fusion Based on Wavelet Transform", ISSN: 2319-6890) (online), 2347-5013(print) Volume No.3, Issue No.7, pp: 442-445 .01 July 2014.

[31] S. K. Shah, D.U. Shah, "Comparative Study of Image Fusion Techniques based on Spatial and Transform Domain", International Journal of Innovative Research in Science, Engineering and Technology (An ISO 3297: 2007 Certified Organization) Vol. 3, Issue 3, March 2014.

[32] K. Kannan, S. A. Peruma , K. Arulmozhi, "Area level fusion of Multi-focused Images using Multi-Stationary Wavelet Packet Transform", International Journal of Computer Applications (0975 8887) Volume 2, No.1, May 2010.

[33] A. A. Gurjar, S. M. Patil, S. B. Kasturiwala, "Fusion Technique for Multi-Focused Images using Stationary Wavelet Packet Transform", International Journal of Scientific & Engineering Research Volume 3, Issue 3, March -2012 1 ISSN 2229-5518.

[34] Nandini, S. Manjunath, R. Kumar, "Gait Recognition by Combining Wavelets and Geometrical Features", Conference of 2nd International Conference on Intelligent Agent & Multi-Agent Systems, September 2018.

[35] K. Kannan, S. A. Perumal, K. Arulmozhi, "Performance Comparison of various levels of Fusion of Multi-focused Images using Wavelet Transform", 2010 International Journal of Computer Applications (0975 – 8887) Volume 1 – No. 6.

[36] S. K. Mohideen, "De-nosing of Images Using Complex Wavelet Transform", international journal of advanced scientific and technical research issue2, volume 1 (february 2012) issn: 2249-9954.

[37] D. S. Reddy, S.Varadarajan, M. N. GiriPrasad, "2D-DTDWT Based Image De-noising using Hard and Soft Thresholding", International Journal of Engineering Research and Applications (IJERA) ISSN: 2248-9622 www.ijera.com Vol. 3, Issue 1, January -February 2013, pp.1462-1465.

[38] S. Lal, M. Chandra, "Removal of Additive Gaussian Noise by Complex Double Density Dual Tree Discrete Wavelet Transform", MIT International Journal of Electronics and Communication Engineering Vol. 1, No. 1, Jan. 2011, pp. (8-16) ISSN 2230-7672.

[39] R. K. Sarawale, S. R. Chougule, "Image De-noising using Dual-Tree Complex DWT and Double-Density Dual-Tree Complex DWT", International Journal of

Advanced Research in Computer Engineering & Technology (IJARCET) Volume 2, Issue 6, June 2013 , " ISSN: 2278 – 1323.

[40] Prochazka, A., Kingsbury, N., Payner, P.J.W., Uhlir, J, "Signal Analysis and Prediction", Springer Science, Business Media New York 1998.

[41] Prochazka, A. Kingsbury, N. Payner, P. J. W. Uhlir, "Optimal Decomposition Level of Discrete, Stationary and Dual Tree Complex Wavelet Transform for Pixel based Fusion of Multi-Focused Images", Serbian Journal Of Electrical Engineering Vol. 7, No. 1, May 2010, 81-93 Udk: 004.932.4.

[42] T. Chandrasekhar, C. S. Kumar, "Face Recognition using Fuzzy Neural Network", International Journal on Future Revolution in Computer Science & Communication Engineering, Volume: 3Issue: 8, ISSN: 2454-4248.

[43] S. A. S. Murugan, K. Karthikayan, N. A. Natraj, C. R. Rathish, "Speckle Noise Removal Using Dual Tree Complex Wavelet Transform", International Journal Of Scientific & Technology Research Volume 2, Issue 8, August 2013 Issn 2277-8616.

[44] I. Selesnick, R. Baraniuk, "The Dual-Tree Complex wavelet transform", IEEE Signal Processing Magazine 22(6):123 – 151, December 2005.

[45] S. Bhat, R. C. Lind, "Control-oriented analysis of thermal gradients for a hypersonic vehicle", American Control Conference, June 2009, Pages 2513–2518.

[46] G. Wyszecki and W. S. Styles, "Color Science: Concepts and Methods, Quantitative Data and Formulae", Wiley, New York, NY, 1982.

[47] C. Tomasi and R. Manduchi, "Bilateral filtering for gray and color images", in Proceedings of the IEEE International Conference on Computer Vision, pp. 839–846, 1998.

[48] M. Elad, "Retinex by two bilateral filters", in Proceedings of the Scale-Space conference, pp. 217–229, 2005.

[49] D. Barash, "A fundamental relationship between bilateral filtering, adaptive smoothing and the nonlinear diffusion equation", IEEE Transactions on Pattern Analysis and Machine Intelligence, vol. 24, no. 6, pp. 844–847, 2002.

[50] D. Barash and D. Comaniciu, “A Common framework for nonlinear diffusion, adaptive smoothing, bilateral filtering and mean shift”, Image and Video Computing, vol. 22, no. 1, pp. 73–81, 2004.

[51] J. Park, J.-H. Han, and B.-U. Lee, “Performance of bilateral filtering on Gaussian noise”, J. Electron. Imaging 23, 043024 (2014).

[52] F. M. Porikli, “Constant-time O (1) bilateral filtering”, in Proc. of IEEE Conf. on Computer Vision and Pattern Recognition, pp. 1–8 (2008).

[53] F. Durand and J. Dorsey, “Fast bilateral filtering for the display of high dynamic range images”, ACM Siggraph 21, 257–266 (2002).

[54] Q. Yang, K. H. Tan, and N. Ahuja, “Real-time O (1) bilateral filtering”, in Proc. of IEEE Conf. on Computer Vision and Pattern Recognition, pp. 557–564 (2009).

[55] K. N. Chaudhury, D. Sage, and M. Unser, “Fast O (1) bilateral filtering using trigonometric range kernels”, IEEE Trans. Image Process. 20, 3376–3382 (2011).

[56] A. Buades, B. Coll, and J.-M. Morel, “A non-local algorithm for image de-noising”, in Proc. of IEEE Conf. on Computer Vision and Pattern Recognition, Vol. 2, pp. 60–65 (2005).

[57] Y. GAO, J. Yang, and L. Guo, “Nonlocal oriented method for image de-noising”, Proc. SPIE 50(3), 030502 (2011).

[58] R. Liu, S. Fu, and C. Zhang, “Adaptive mixed image de-noising based on image decomposition”, Proc. SPIE 50(2), 020502 (2011).

[59] S. Dolui, I. C. S. Patarroyo, and O. V. Michailovich, “Generalized nonlocal means filtering for image de-noising”, Proc. SPIE 9019, 90190B (2014).

[60] H. Takeda, S. Farsiu, and P. Milanfar, “Higher order bilateral filters and their properties”, Proc. SPIE 6498, 64980S (2007).

[61] M. Zhang and B. K. Gunturk, "Multiresolution bilateral filtering for image denoising", IEEE Trans. Image Process. 17, 2324–2333 (2008).

[62] Anutam and Rajni, "Performance Analysis of Image De-noising with Wavelet Thresholding Methods for Different Levels of Decomposition", The International Journal of Multimedia & Its Applications (IJMA) Vol.6, No.3, June 2014.

[63] J. Bailia, S. Lahouara, M. Herglia, I. L. Al-Qadic, K. Besbes, "GPR signal denoising by discrete wavelet transform", NDT&E International 42 (2009) 696–703.

[64] S. Ozaydin, I. K. ALAK, "Speech Enhancement using Maximal Overlap Discrete Wavelet Transform", Gazi University, Journal of Science, part a: engineering and innovation, gu j sci, part a, 5(4): 159-171 (2018).

[65] G. Sheng, G. Gao, and B. Zhang, "Application of Improved Wavelet Thresholding Method and an RBF Network in the Error Compensating of a MEMS Gyroscope", Micromachines 2019, 10, 608, doi: 10.3390/mi10090608.

[66] P. Sivamani, V. V. Gowri, S. V. Priyavarshini, N. Revathi, "Image De-noising Using Wavelet Thresholding", International Journal of Advanced Research Trends in Engineering and Technology (IJARTET) Vol. 3, Issue 4, April 2016.

[67] N. Dewangan, A. D. Goswami, "Adaptive Wavelet Thresholding for Image Denoising Using VariousShrinkage Under Different Noise Conditions", International Journal of Engineering Research & Technology (IJERT), Vol. 1 Issue 8, and October – 2012, ISSN: 2278-0181.

[68] S. Khan, A. Jain, A. Khare, "De-noising of Images Based on Different Wavelet Thresholding by Using Various Shrinkage Methods using Basic Noise Conditions", international journal of engineering research & technology, 07-02-2013, issn: 2278-0181.

[69] K. Kalaivani and Y. A. V. Phamila, "Analysis of Image Fusion Techniques based on Quality Assessment Metrics", Indian Journal of Science and Technology, Vol 9(31), pp. 1-8, 2016.

[70] B. M. Latha, B. K. Manjula, S. C. H. Venkata, "Multi Modal Hybrid Image Fusion using Discrete Wavelet and Contourlet Transform", International Journal of

Innovative Technology and Exploring Engineering (IJITEE), ISSN: 2278-3075, Volume-8 Issue-10, August 2019 .

[71] A. O. karali, S. cakir, and T. Aytaç, "Multiscale contrast direction adaptive image fusion technique for MWIR-LWIR image pairs and LWIR multifocus infrared images", 4172 Vol. 54, No. 13 / May 1 2015 / Applied Optics.

[72] Y. Yang, "A Novel DWT Based Multi-focus Image Fusion Method", Procedia Engineering, Volume 24, 2011, Pages 177-181.

[73] G. Kaur and P. Kaur, "Survey on multifocus image fusion techniques", International Conference on Electrical, Electronics, and Optimization Techniques (ICEEOT). pp. 1420-1425, 2016.

[74] M. S. Mahmoud, Y. Xia, "Networked Filtering and Fusion in Wireless Sensor Networks", Published September 18, 2018, Reference - 576 Pages - 178 B/W Illustrations, ISBN 9781138374935 - CAT# K397812.

[75] N. B. Kolekar, R. P. Shelkikar, "A Review on Wavelet transform based image fusion and classification", International Journal of Application or Innovation in Engineering & Management (IJAIEM), Volume 5, Issue 3, March 2016 ISSN 2319 – 4847.

[76] I. S. Wahyuni, "Multi-focus image fusion using local variability", Image Processing [eess.IV]. Université Bourgogne Franche-Comté, 2018. English. ffNNT: 2018UBFCK010ff. fftel-01820628ff.

[77] S. Ibrahim and M. Wirth, "Multiresolution region-based image fusion using the Contourlet Transform", in IEEE TIC-STH, Sept. 2009.

[78] G. kaur, A. K. Mittal, "A New Hybrid Wavelet Based Approach for Image Fusion", International Journal of Innovative Research in Science, Engineering and Technology (An ISO 3297: 2007 Certified Organization) Vol. 4, Issue 1, January 2015.

[79] Komal, R. Dewan, "Energy Based Wavelet Image Fusion", IJIRST–International Journal for Innovative Research in Science & Technology| Volume 1 | Issue 6| November2014ISSN (online):2349-6010.

[80] J. Dong, D. Zhuang, Y. Huang and J. Fu, “Advances in Multi-Sensor Data Fusion: Algorithms and Applications”, Sensors 2009, 9(10), 7771-7784.

[81] Z. Zou, Z. Shi, Y. Guo, and J. Ye, “Object Detection in 20 Years: A Survey”, arXiv:1905.05055v2 [cs.CV] 16 May 2019.

[82] C. Morris, R. S. Rajesh, “Survey of Spatial Domain Image Fusion Techniques”, International Journal of Advanced Research in Computer Science Engineering and Information Technology, Volume: 2 Issue: 3 08-Apr-2014, ISSN_NO: 2321-3337.

[83] A. Singh, M. Saini, P. Nayyer, “Implementation & comparative study of different fusion techniques (Wavelet, Ihs, Pca)”, International Refereed Journal of Engineering and Science (IRJES) ISSN (Online) 2319-183X, (Print) 2319-1821 Volume 1, Issue 4(December 2012), PP.37-41.

[84] B. J. Matuszewski, L. Shark, M. R. Varley, “Region-Based Wavelet Fusion Of Ultrasonic, Radiographic And Shearographyc Non-Destructive Testing Images”, 15th World Conference WCNDT, 15-21 October 2000, Rome.

[85] J. Zhou, D. L. Civco, and J. A. Silander, “A wavelet transform method tomerge Landsat TM and SPOT panchromatic data”, Int. J. Remote Sens,vol. 19, no. 4, pp. 743–757, 1998.

[86] H. R. Shahdoosti and O. Khayat, “Image de-noising using sparse representation classification and non- subsampled shearlet transform”, Signal, Image and Video Processing, vol. 10, no. 6, pp. 1081–1087, September 2016.

[87] D. L. Donoho, I. M. Johnstone, G. Kerkyacharian, and D. Picard, “Wavelet shrinkage: Asymptopia”, J. Roy. Statist.Assoc. B, vol. 57, no. 2, pp. 301–369, 1995.

[88] Z. Xing, P. Carbonetto, M. Stephens, “Flexible Signal Denoising via Flexible Empirical Bayes Shrinkage”, flexible denoising via empirical bayes shrinkage, arXiv: 1605.07787v2, 22 Jan 2019.

[89] S. G. Chang, B. Yu, and M. Vetterli, “Adaptive wavelet thresholding for image de-noising and compression”, IEEE Trans. Image Process., vol. 9, no. 9, pp. 1532–1546, Sep. 2000.

[90] L. Sendur and I. W. Selesnick, “Bivariate shrinkage functions for wavelet-based de-noising exploiting interscale dependency”, IEEE Trans. Signal Process. vol. 50, no. 11, pp. 2744–2756, Nov. 2002.

[91] L. Sendur and I. W. Selesnick, “Bivariate shrinkage with local variance estimation”, IEEE Signal Process. Lett. vol. 9, no. 12, pp. 438–441, Dec. 2002.

[92] V. K. Mishra, S. Kumar and R. K. Gupta, “Design and Implementation of Image Fusion System”, International Journal of Computer Sciences and Engineering, Vol.-2(3), pp (182-186) March 2014, E-ISSN: 2347-269.

[93] D. A. Godse, D. S. Bormane, “Wavelet based image fusion using pixel based maximum selection rule”, International Journal of Engineering Science and Technology (IJEST), Vol.3, No.7, July 2011, ISSN: 0975-5462.

[94] D. A. Godse, D. S. Bormane, “Wavelet based image fusion using pixel based maximum selection rule”, International Journal of Engineering Science and Technology (IJEST), Vol.3, No.7, July 2011, ISSN: 0975-5462.

[95] S. Huang, “Wavelet for Image Fusion”, Graduate Institute of Communication Engineering & Department of Electrical Engineering, National Taiwan University, 2008.

[96] D. He, L. Wang, A. Massalabi, “A new technique for multi-resolution image fusion”, IEEE International Geoscience and Remote Sensing Symposium, 20-24 Sept 2004.

[97] Y. Zheng, E. A. Essock and B. C. Hansen, “An Advanced Image Fusion Algorithm Based on Wavelet Transform Incorporation with PCA and Morphological Processing”, Proc. SPIE 5298, Image Processing: Algorithms and Systems III, May 2004.

[98] J. Gao, B. Li, Y. Bao, and F. Ma, “Wavelet Enhanced Fusion Algorithm for Multisensor Images”, 2011 International Conference on Consumer Electronics, Communications and Networks, 16 May 2011.

[99] S. Krishnamoorthy, K. P. Soman, “Implementation and Comparative Study of Image Fusion Algorithms”, International Journal of Computer Applications (0975 – 8887) Vol. 9, No.2, November 2010.

[100] B. Y. S. Li, “Multifocus image fusion by combining curvelet and wavelet transform”, Pattern Recognition Letters, ELSEVIER, no. 28, p. 1295–1301, 2008.

[101] F. Sadjadi, “Comparative Image Fusion Analysis”, IJITE, Vol.01 Issue-02, June 2013, ISSN: 2321–1776.

[102] S. Udomhunsakul, “Multi-focus image fusion using SFM and Wavelet Packets”, International journal.

[103] C. lacewell, M. Gebril, R. Bauba and A. Homaifai, “Optimization of Image fusion using Genetic Algorith and Descrete Wavelet Transform”, Proceedings of the IEEE 2010 National Aerospace & Electronics Conference, ISSN: 2379-2027, 14 February 2011.

[104] N. D. Rane, B. Kakde, M. Jain, “Comparative study of Image Fusion Methods: A Review”, International Journal of Engineering and Applied Sciences (IJEAS), ISSN: 2394-3661, Volume-4, Issue-10, October 2017.

[105] Jin, H, Liu, F, Jiao, LC, “A method of image fusion based on multiscale contrast pyramid and directional filter banks”, Acta Electron Sinica 2007; 35(7): 1295–1300.

[106] M. Pradnya, S. D. Ruikar, “Image Fusion Based On Stationary Wavelet Transform”, Electronics & Telecommunication Dept. Sinhgad Acadmy of Engg. Pune.

[107] S. Vekkot and P. Shukla, “A NovelArchitecture for Wavelet based Image Fusion”, World Academy of Science, Engineering and Technology, 2009.

[108] S. Bedi, “Image Fusion Techniques and Quality Assessment Parameters for Clinical Diagnosis: A Review”, International Journal of Advanced Research in Computer and Communication Engineering, vol. 2, no. 2, pp. 2319-5940, Feb 2013.